MOLECULAR RECOGNITION RESEARCH UNIT
&
PHARMACEUTICAL CELL BIOLOGY

DEVELOPMENT OF FUNCTIONAL PLASTIBODIES

A thesis submitted in accordance with the conditions governing candidates for the degree of Philosophiae Doctor in the University of Wales.

John Andrew Jones MPharm (Hons)

September 2010

Welsh School of Pharmacy, Cardiff University

Declaration

DECLARATION

This work has not previously been accepted in substance for any degree and is not concurrently submitted in candidature for any degree.

Signed ..... (candidate)

Date .....2/3/11.....

STATEMENT 1

This thesis is being submitted in partial fulfilment of the requirements for the degree of Ph.D.

Signed ..... (candidate)

Date .....2/3/11.....

STATEMENT 2

This thesis is the result of my own independent work/investigation, except where otherwise stated.
Other sources are acknowledged by explicit references.

Signed ..... (candidate)

Date .....2/3/11.....

STATEMENT 3

I hereby give consent for my thesis, if accepted, to be available for photocopying and for inter-library loan, and for the title and summary to be made available to outside organisations.

Signed ..... (candidate)

Date .....2/3/11.....

For Angharad,

Without you, nothing is possible.

Acknowledgements

"At times our own light goes out and is rekindled by a spark from another person."

Albert Schweitzer

My thanks go to Dr. Mark Gumbleton and Dr. Chris Allender for their support and encouragement throughout, and indeed the Welsh School of Pharmacy for funding this project. My thanks also go to Dr Jimmy Hedin-Dahlström, Jenna Bowen and Marc Kelly for plenty of chemistry; to Mathew Smith and Chris Morris for phage and peptides; to Ghaith Al-Jayoussi for some good games of chess, to Danielle Francombe and Dr. Lee Campbell for many imaginative philosophical debates, to Deri Burgess for some truly remarkable Java programming, and to Claire Gilvear who very kindly read this work.

My gratitude extends to my parents, my parents-in-law, my sisters Laura and Jennifer, Clare Baker, Gareth Jones, Keng Ng, Liam Ip, Michaela Cassemis, Nicola Joseph, Phillip Haines, Rhian Cosslett, Richard Haines, Shelley Jenkins, and Wing Lau who have provided much-needed motivation, ranting, and coffee along the way.

Also, I appreciate many insightful scientific and abstract conversations with a small-ish dog.

Abstract

For many years, molecularly imprinted polymers (MIPs) have been described as "plastic antibodies", yet even some modern examples cannot approach the true binding affinity and specificity of monoclonal antibodies. This project sought to include within the imprinted site a short peptide sequence isolated from a phage display library with high affinity and specificity. A system is hypothesised in which synergism between the robust nature of the polymer and the binding affinity and specificity of the peptide may be exploited.

Peptide phage display is a technique that can rapidly enrich binding peptides from a combinatorial library of over 10^9 unique moieties. Initial studies attempted to isolate peptides with high affinity and specificity to propranolol from this library. However, when several methodologies failed to demonstrate any binding effect, a peptide was selected from the literature that had been found to bind the fluorophore Texas Red. The peptide was immobilised to a Merrifield Resin support, its binding properties thoroughly assessed, and a polymerisation protocol was developed using living radical polymerisation.

Preliminary studies suggested that when peptide-functionalised resin was washed in ethanol, no binding to Texas Red was evident, whereas

once a protective polymer shell was formed, the peptide retained a binding conformation and affinity for Texas Red was slightly increased. This was, however, at the expense of binding capacity, which fell dramatically. Whilst the evidence presented here is by no means complete, it provides proof-of-principle for a functional peptide-molecularly-imprinted polymer. Further work in this area may lead to the development of a truly biomimetic artificial antibody: the plastibody.

Contents

Declaration i

Acknowledgements iii

Abstract iv

Contents vi

Figures xiv

Abbreviations xxv

Chapter 1 1

1.1 The Molecularly Imprinted Polymer 1

1.1.1 Methods of Imprinting 4

1.1.1.1 Covalent Imprinting 5

1.1.1.2 Semi-covalent Imprinting 6

1.1.1.3 Non-covalent Imprinting 7

1.1.2 Components of an Imprinted Polymer 8

1.1.2.1 Functional Monomers 9

1.1.3 Methods of Polymerisation 10

1.1.3.1 Bulk Polymerisation 11

1.1.3.2 Precipitation Polymerisation 11

1.1.3.3 Emulsion/Suspension Polymerisation 12

1.1.3.5 Surface Grafting 13

1.1.3.6 Hierarchical Imprinting 16

1.1.4 Biological Molecules and MIPs 17

1.1.5 Peptides and Polymers 18

1.1.6 Current Applications 19

1.2 Phage Display 20

1.2.1 Surface Display 20

1.2.2 The M13 Phage 22

1.2.3 Mechanism of Phage Infection and Replication 23

1.2.4 Construction of a Phage Display Library 26

1.2.5 Utility of Phage Display 27

1.2.5.1 Protein Conformation 27

1.2.5.2 Immunological Properties 28

1.2.5.3 Medicine 30

1.2.5.4 Low Molecular Weight Compounds 32

1.3 Functional Plastibodies – Aims and Objectives 34

Chapter 2 36

2.1 Introduction 36

2.2 Materials and Methods 41

2.2.1 Media and Solutions 41

2.2.2 Phage Amplification Procedure 43

2.2.2.1 First Centrifugation Step 44

2.2.2.2 Second Centrifugation Step 44

2.2.3 Gene Sequencing of Identified Phage Clones 45
2.2.4 Panning Against Propranolol 46
2.2.4.1 Panning Against Propranolol Free-Base as Suspension .. 46
2.2.4.2 Panning Against Propranolol Covalently Bound to Glass Beads 48
2.2.5 Determination of Binding Effect 50
2.2.5.1 Franz Diffusion Cell Assay 50
2.2.5.2 Side-by-Side Franz Cell Study 51
2.2.5.3 MDCK-1 Transport Study 52
2.2.5.4 Filter Centrifugation 53
2.2.5.5 Propranolol Affinity for Experimental Materials 53
2.2.5.6 Microcentrifuge Tube Equilibrium Dialysis 54
2.3 Results and Discussion 56
2.3.1 Panning Against Propranolol 56
2.3.2 Demonstration of Binding 58
2.3.2.1 Franz Diffusion Cell Assay 58
2.3.2.2 Side-by-Side Franz Cell Study 62
2.3.2.3 MDCK-1 Transport Study 64
2.3.2.4 Filter Centrifugation 71
2.3.2.5 Propranolol Affinity for Experimental Materials 73
2.3.2.6 Microcentrifuge Tube Equilibrium Dialysis 75
2.4 Further Discussion 77

2.5 Conclusions 79

Chapter 3 80

3.1 Introduction 80

3.2 Materials and Methods 87

3.2.1 Linking chemistry 87

3.2.1.1 Solution Chemistry – 1 87

3.2.1.2 Solution Chemistry – 2 88

3.2.1.3 Peptide attachment to Merrifield Resin 89

3.2.2 Development of Binding Assay Protocol 90

3.2.2.1 Calibration using polypropylene plates 90

3.2.2.2 Excitation and emission scans of sulforhodamine 101 90

3.2.2.3 Fluorescence Titration 91

3.2.2.4 Merrifield Resin Titration 92

3.2.2.5 Effect of Incubation Time on Binding 93

3.2.3 Final Titration Protocol and Binding Assays 93

3.3 Results and Discussion 96

3.3.1 Linking Chemistry 96

3.3.1.1 Solution Chemistry – 1 96

3.3.1.2 Solution Chemistry – 2 97

3.3.1.3 Peptide attachment to Merrifield Resin 98

3.3.2 Development of Binding Assay Protocol 98

3.3.2.1 Calibration using polypropylene plates 98

3.3.2.2 Excitation and emission scans of sulforhodamine 101 ... 100

3.3.2.3 Fluorescence Titration ... 101

3.3.2.4 Merrifield Resin Titration ... 102

3.3.2.5 Effect of Incubation Time on Binding ... 103

3.3.3 Binding Assays ... 104

3.4 Further Discussion ... 107

3.5 Conclusions ... 108

Chapter 4 ... 109

4.1 Introduction ... 109

4.2 Methods ... 112

4.2.1 Functionalisation of Resin ... 112

4.2.1.1 Attachment of Iniferter ... 112

4.2.1.2 Attachment of Peptide, TR401 ... 112

4.2.2 Peptide Exposure to Monomers ... 113

4.2.3 Ethanol as Eluent ... 113

4.2.3.1 Effect of Ethanol on MR ... 113

4.2.3.2 Effect of Ethanol on Peptide ... 114

4.2.4 Polymerisation ... 115

4.3 Results and Discussion ... 116

4.3.1 Functionalisation of Resin ... 116

4.3.1.1 Attachment of Iniferter ... 116

4.3.1.2 Attachment of Peptide, TR401 ... 118

4.3.2 Peptide Exposure to Monomers 120
4.3.3 Ethanol as Eluent 121
4.3.3.1 Effect of Ethanol on MR 121
4.3.3.2 Effect of Ethanol on Peptide 122
4.3.4 Polymerisation 124
4.3.4.1 Key Observations 125
4.4 Further Discussion 130
4.5 Conclusions 132
Chapter 5 134
5.1 Phage Display 134
5.2 TR401 139
5.3 Peptide-Molecular Imprinted Polymers 141
5.4 Future Work 143
5.5 Conclusions 144
References 146
Appendix 1 158
Peptide Sequences Isolated from Phage Display Against Propranolol 158
Peptide 1 - EMTSTRA 158
Peptide 2 - NANNRLY 159
Peptide 3 - PAQDPRY 160
Peptide 4 - QIKHRHM 162

Appendix 2 164

Fluorescent Properties of Sulforhodamine 164

A2.1 Introduction 164

A2.2 Methods 164

A2.2.1 Detection limit of Sulforhodamine 101 using FLUOstar OPTIMA 164

A2.2.2 Effect of "Gain" on Sulforhodamine Calibration Linearity 165

A2.2.3 Influence of Plate Colour and Filter 165

A2.2.4 Binding of Sulforhodamine to Experimental Materials 165

A2.2.5 Repeated readings and binding to polystyrene plates 166

A2.3 Results 167

A2.3.1 Detection limit of Sulforhodamine 101 using FluoSTAR OPTIMA 167

A2.3.2 Effect of "Gain" on Sulforhodamine Calibration Linearity 168

A2.3.3 Influence of Plate Colour and Filter 169

A2.3.4 Binding to Experimental Materials 173

A2.3.5 Repeated readings versus binding to polystyrene plates 174

Appendix 3 176

Preparation of Glass Surfaces Prior to Immobilisation of TR401 176

A3.1 Introduction 176

A3.2 Methods 176

A3.2.1 Surface Functionalisation 176

A.3.2.2 Confirmation of surface alteration 178

A3.3 Results..... 179

Linking Chemistry – AFM and contact angles..... 179

Appendix 4 184

A4.1 Introduction..... 184

A4.2 Methods..... 185

A4.3 Results..... 185

Appendix 5 190

Peptide TR401 Stability..... 190

Appendix 6 194

Polymerisation data 194

Figures

Figure 1: Basic concept of the imprinted polymer: a template is exposed to functional monomers (1) which are known to interact (2), an excess of cross-linking monomer, and conditions to provoke polymerisation (3), resulting in imprinted binding pocket (4). 1

Figure 2: Schematic representation of the preparation of MIP to theophylline using methacrylic acid functional monomer, adapted from (Vlatakis et al., 1993). 3

Figure 3: Covalent imprinting of dopamine adapted from (Takeuchi et al., 2006), including the structure of dopamine (inset) 6

Figure 4: Methacrylic acid (MAA) 8

Figure 5: 2,2'-azobisisobutyronitrile (AIBN). 9

Figure 6: MIP beads approx 5μm diameter formed via precipitation polymerisation (SEM micrograph) (Wang et al., 2003). 11

Figure 7: Schematic representation of chloromethylated polystyrene beads with dithiocarbamate iniferter-mediated polymerisation using lysozyme as template, adapted from Qin et al (Qin et al., 2009), showing functionalisation of chloromethylated resin with a dithiocarbamate iniferter (1), subsequent activation of the iniferter with UV (2), and the resulting molecularly imprinted system (3). 14

Figure 8: Illustration of diethyldithiocarbamate iniferter, showing iniferter-functionalised moiety (A), the more reactive radical species (B),

and the less reactive (C)..... 15

Figure 9: β-cyclodextrin. 18

Figure 10: Representation of the "Plastibody". In this situation, a peptide which has been found to bind with high affinity and specificity to a template molecule is imprinted in its binding conformation, producing a robust, highly specialised binding site. 34

Figure 11: Template phage displayed peptide structure from Ph.D-C7C Library..... 37

Figure 12: Propranolol falls into the therapeutic category of antihypertensive. Its mechanism of action is through the blockade of beta-adrenergic receptors (beta blocker), thereby reducing sympathetic stimulation. 38

Figure 13: Nabumetone is a non-selective non-steroidal anti-inflammatory drug (NSAID). 38

Figure 14: Atenolol [A] and sotalol [B]. Both compounds fall into the therapeutic category of "beta-blocker"..... 39

Figure 15: Reaction scheme for the coupling of propranolol to glass beads. Ref: J. Hedin-Dahlström (MRRU, WSP, Cardiff University) – personal communication..... 43

Figure 16: The passage of phage from library to output through various biopanning strategies. 49

Figure 17: "Side-by-side" Franz cell setup..... 52

Figure 18: Basic microcentrifuge dialysis setup..... 54

Figure 19: Number of plaque forming units recovered from each elution

with glycine buffer pH 2.2 over three rounds of panning against propranolol free base as precipitate. 57

Figure 20: Franz cell diffusion pattern of 3H-propranolol through polycarbonate membrane (n=4±SD). 60

Figure 21: Franz cell diffusion pattern of 3H-propranolol through viskin dialysis membrane (n=4±SD). 61

Figure 22: Diffusion of ^{3}H-propranolol from the donor chamber of a side-by-side Franz cell setup (n=4 ±SD). 63

Figure 23: Total amount of 3H-propranolol diffused into receiving chamber when exposed to phage expressing the sequence EMTSTRA (n=4±SD). 64

Figure 24: Total amount of 3H-propranolol diffused into receiving chamber when exposed to phage expressing the sequence EMTSTRA (n=4±SD). First four points only. 65

Figure 25: Total amount of 3H-propranolol diffused into receiving chamber when exposed to phage expressing the sequence PAQDPRY (n=4±SD). 66

Figure 26: Total amount of 3H-propranolol diffused into receiving chamber when exposed to phage expressing the sequence PAQDPRY (n=4±SD). First four points only. 67

Figure 27: Total amount of 13C-mannitol diffused into receiving chamber when exposed to phage expressing the sequence PAQDPRY; mean and standard deviation shown (n=4±SD). 68

Figure 28: Amount of 3H-propranolol diffused across the Transwell©

polycarbonate insert without the presence of MDCK cells..... 70

Figure 29: Propranolol (DPM) liberated by filter under each treatment (n=4±SD). 71

Figure 30: 3H-propranolol liberated via centrifuge filter. Four-fold excess of propranolol to phage was used (n=4±SD). 72

Figure 31: Percentage of the original 3H-propranolol dose recovered from solution after 60 minutes incubation with various materials..... 73

Figure 32: Depletion of 3H-propranolol from solution after 60 minutes incubation with Viskin dialysis membrane..... 74

Figure 33: Diffusion of 3H-propranolol molecules in the presence of 1:1 ratio of phage particles, n=4±SD. 75

Figure 34: Proportion of 3H-propranolol found in the phage-containing chamber after 24 hours (1:1 ratio of phage particles to propranolol molecules). Polycarbonate membrane is included to demonstrate the effect of binding propranolol, n=4±SD. 75

Figure 35: Twelve further clones examined using the microcentrifuge tube dialysis method using viskin dialysis membrane, (n=4±SD). 76

Figure 36: Sulforhodamine 101 acid chloride (Texas Red) (A), and sulforhodamine 101 (B). 81

Figure 37: Structure of TR401 (KHVQYWTQMFYS) with the addition of three glycine and one cysteine residues to the C-terminus. 82

Figure 38: Merrifield Resin. 83

Figure 39: Sulfosuccinimidyl-4-[N]maleimidomethyl] cyclohexane-1-carboxylate (Sulfo-SMCC)..... 84

Figure 40: Naphthyl ethylenediamine (NED). 85

Figure 41: Rhodamine 6G (A), rhodamine 123 (B), and fluorescein (C). 86

Figure 42: APTES (A) and MPTES (B). 87

Figure 43: Ninhydrin (2,2-Dihydroxyindane-1,3-dione). 88

Figure 44: Ellman's reagent, (5,5'-dithiobis-(2-nitrobenzoic acid)) 88

Figure 45: Conjugated product of NED with Sulfo-SMCC. 89

Figure 46: APTES reaction with ninhydrin (A) compared with APTES-Sulfo-SMCC product reacted with ninhydrin (B). 96

Figure 47: MPTES reaction with Ellman's (A) compared with MPTES-Sulfo-SMCC product reacted with Ellman's (B). 96

Figure 48: Spectral shifts observed when comparing untreated NED with NED-Sulfo-SMCC conjugate. 97

Figure 49: The fluorescence associated with solutions of sulforhodamine 101 in water. Filters used were Excitation at 544nm and Emission at 590nm. Each point is an individual sample. 99

Figure 50: Excitation and emission spectra of sulforhodamine 101 in water. 100

Figure 51: Fluorescence intensity and maximum emission wavelength change as peptide to SR ratio increases. 101

Figure 52: Amount of sulforhodamine 101 bound from aqueous solution upon exposure to increasing amounts of Merrifield Resin. 102

Figure 53: Fluorescence associated with sulforhodamine 101 free in solution after contact with functionalised Merrifield resin over time; n=1.

..... 103

Figure 54: Amount of sulforhodamine 101 bound from aqueous solution by 25μg of TR401-functonalised Merrifield Resin (n=4±SD)..... 104

Figure 55: Amount of sulforhodamine 101 bound from TBS by 25μg of TR401-functonalised Merrifield Resin (n=4±SD). 105

Figure 56: Raw data of fluorescence associated with sulforhodamine 101 remaining free in aqueous solution upon exposure to 25μg of resin at various concentrations..... 107

Figure 57: Dithiocarboxysarcosine (DTCS). 110

Figure 58: Methylene bisacrylamine (MBA).....110

Figure 59: Reaction of bifunctionalised MR with DTCS to produce iniferter-functionalised resin..... 111

Figure 60: Petri dish with drilled hole with coverslips above and below creating a space for an ethanolic suspension of resin. 113

Figure 61: FTIR spectra of untreated MR (A), DTCS-coupled MR (B), and DTCS-coupled MR exposed to acrylamide under UV for 24 hours (C). FTIR experiments were performed by J. Bowen and M. Kelly. 117

Figure 62: Sulforhodamine binding assay performed with Bifunctionalised Merrifield resin to which TR401 has been linked alongside iniferter. K_D = 2.14nM, Bmax = 3.47pmoles (n=4±SD) 118

Figure 63: Sulforhodamine binding assays performed with peptide-functionalised resin which has either been incubated with MBA solution or with water, then washed either once or three times (n=4±SD). 120

Figure 64: Example image from the sequence of Merrifield resin

exposure to ethanol. No size changes were visible of the duration of the experiment (10 minutes). (Scale bar = 65μm) 121

Figure 65: Malvern Mastersizer data comparing particle sizes of Merrifield resin after incubation in water or ethanol. 122

Figure 66: Binding assay performed using resin functionalised with peptide which had been dissolved in ethanol prior to its immobilisation (n=4±SD). 123

Figure 67: Sulforhodamine binding assay at optimal polymerisation time for P-NIP (n=4±SD). 126

Figure 68: Sulforhodamine binding assay at optimal polymerisation time for P-MIP (n=4±SD). 127

Figure 69: Sulforhodamine binding to Peptide-functionalised, iniferter-derivatised Merrifield resin. K_D 370.0nM, Bmax 286.4pmoles (n=4±SD). 128

Figure 70: Peptide-functionalised, iniferter-derivatised Merrifield resin washed in ethanol (n=4±SD). 129

Figure 71: Reaction scheme showing the production of TR401-DTCS bi-functionalised Merrifield Resin. 132

Figure 72: Paracetamol (A), dexamethasone (B), and methotrexate (C). 136

Figure 73: Propranolol. 137

Figure 74: Sotalol. 139

Figure 75: Sequence 1: EMTSTRA (Glutamic acid–Methionine–Threonine–Serine–Threonine–Arginine–Alanine). 158

Figure 76: Sequence 2: NANNRLY (Asparagine-Alanine-Asparagine-Asparagine-Arginine-Leucine-Tyrosine). 159

Figure 77: Sequence 3: PAQDPRY (Proline-Alanine-Glutamine-Aspartate-Proline-Arginine-Tyrosine)..... 160

Figure 78: Sequence 4: QIKHRHM (Glutamine-Isoleucine-Lysine-Histidine-Arginine-Histidine-Methionine)..... 162

Figure 79: The fluorescence associated with low concentrations of sulforhodamine 101. Mean and standard deviation are shown, n=4. Ex 544nm, Em 590nm. 167

Figure 80: The fluorescence associated with low concentrations of sulforhodamine 101. Mean and standard deviation are shown (n=4). In graph A, the sensitivity of the plate-reader is given as 2476. In graph B, the sensitivity is increased to 3141. In each case the instrument settings were determined automatically to place the highest data point at 90% of the capacity of the instrument..... 168

Figure 81: The fluorescence associated with solutions of sulforhodamine 101 in water – in black plates. Filters used were Excitation 544nm and Emission 590nm in A; Excitation 580nm and Emission 610nm in B. Graphs shown mean and standard deviation (n=4)..... 169

Figure 82: The fluorescence associated with solutions of sulforhodamine 101 in water – in black plates. Filters used were Excitation 544nm and Emission 610nm. Graph shows mean and standard deviation (n=4)..... 170

Figure 83: The fluorescence associated with solutions of sulforhodamine 101 in water – in white plates. Filters used were Excitation 544nm and Emission 590nm in A; Excitation 580nm and Emission 610nm in B. Graphs shown mean and standard deviation (n=4). 171

Figure 84: The fluorescence associated with solutions of sulforhodamine 101 in water after incubation with a range of materials. Filters used were Excitation 544nm and Emission 590nm. Graphs shown mean and standard deviation (n=4). 173

Figure 85: The fluorescence associated with sulforhodamine 101 solutions in water upon repeated reading over time (A) and single readings with incubation time alone (B). Filters used were Excitation 544nm and Emission 590nm. 174

Figure 86: Layout of the evaporation process, showing the glass coverslips arranged around the upturned microcentrifuge tube lid, encased within a Petri dish. 177

Figure 87: Peptide-functionalised resin: Unexposed resin (A), exposed to sulforhodamine (B), sonicated in arginine buffer (C), re-exposed to sulforhodamine (D) observed under Leica SP5 confocal laser-scanning microscope. 186

Figure 88: Non-functionalised resin: Unexposed resin (A), exposed to sulforhodamine (B), sonicated in Arginine buffer (C), re-exposed to sulforhodamine (D) observed under Leica SP5 confocal laser-scanning microscope. 187

Figure 89: Peptide-functionalised resin: unexposed resin (A), exposed to sulforhodamine (B), sonicated in ethanol (C), re-exposed to sulforhodamine (D) observed under Leica SP5 confocal laser-scanning microscope. 188

Figure 90: Non-functionalised resin: unexposed resin (A), exposed to sulforhodamine (B), sonicated in ethanol (C), re-exposed to sulforhodamine (D) observed under Leica SP5 confocal laser-scanning microscope. 189

Figure 91: MALDI-TOF scan of TR401 as supplied by Severn Biotech. 190

Figure 92: MALDI-TOF scan of TR401 after three freeze-drying cycles. 191

Figure 93: HPLC trace of TR401 from C18 column using gradient mobile phase H_2O + 0.1% trifluoroacetic acid (TFA) and acetonitrile (MeCN) + 0.1%TFA, initially 95:5 for 35 minutes, and then 0:100 until 50 minutes. 192

Figure 94: Sulforhodamine-binding assay performed using Peptide-functionalised, non-imprinted polymer (P-NIP) – Polymerisation times ranging from 0 to 15 minutes. 195

Figure 95: Sulforhodamine-binding assay performed using Peptide-functionalised, non-imprinted polymer (P-NIP) – Polymerisation times ranging from 20 minutes to 120 minutes. TR401-functionalised resin with no polymerisation is included for reference. 196

Figure 96: Sulforhodamine-binding assay performed using Peptide-

functionalised molecularly imprinted polymer (P-MIP) – Polymerisation times ranging from 0 to 15 minutes. 197

Figure 97: Sulforhodamine-binding assay performed using Peptide-functionalised molecularly imprinted polymer (P-MIP) – Polymerisation times ranging from 20 minutes to 120 minutes. TR401-functionalised resin with no polymerisation is included for reference. 198

Figure 98: Sulforhodamine-binding assay performed using Molecularly Imprinted Polymer (MIP) *[No peptide]* – Polymerisation times ranging from 0 to 15 minutes. 199

Figure 99: Sulforhodamine-binding assay performed using Molecularly Imprinted Polymer (MIP) *[No peptide]* – Polymerisation times ranging from 20 minutes to 120 minutes. TR401-functionalised resin with no polymerisation is included for reference. 200

Figure 100: Sulforhodamine-binding assay performed using Non-imprinted Polymer (NIP) *[No peptide, no template]* – Polymerisation times ranging from 0 to 15 minutes. 201

Figure 101: Sulforhodamine-binding assay performed using Non-imprinted Polymer (NIP) [No peptide, no template] – Polymerisation times ranging from 20 minutes to 120 minutes. TR401-functionalised resin with no polymerisation is included for reference. 202

Abbreviations

AFM – Atomic Force Microscopy

AIBN – 2,2'azobisisobutyronitrile

AMA – Apical Membrane Antigen

ANOVA – Analysis of Variance

APTES – (3-Aminopropyl)Triethoxysilane

BSA – Bovine Serum Albumin

CD – Circular Dichroism

cDNA – Complementary DNA

Da – Dalton

DEVPA – N,N'diethyl(4-vinylphenyl)amidine

DMEM – Dulbecco's Modified Eagle's Medium

DMF – Dimethylformamide

DNA – Deoxyribonucleic Acid

DNT – Dinitrotoluene

DPM – Decompositions Per Minute

DPP – Diphenylphosphate

dsDNA – Double-stranded DNA

DTCS – Dithiocarboxysarcosine

EDMA – Ethylenedimethacrylate

EDTA – Ethylenediaminetetraacetic acid

FTIR – Fourier-Transform Infrared Spectroscopy

HIV – Human Immunodeficiency Virus

HPLC – High-Performance Liquid Chromatography

IPTG – Isopropyl beta-D-1-thiogalactopyranoside

IVT – *In Vitro* Time

K_D – Dissociation Constant

LB – Lysogeny Broth

MAA – Methacrylic Acid

MAb – Monoclonal Antibody

MALDI-TOF MS – Matrix-Assisted Laser Desorption/Ionisation-Time of Flight Mass Spectrometry

MBA – Methylene bisacrylamide

MDCK – Madin-Derby Canine Kidney Cells

MeCN - Acetonitrile

MIP – Molecularly Imprinted Polymer

MPTES – (3-Mercaptopropyl)Triethoxysilane

MR – Merrifield Resin

NED – Naphthyl ethylenediamine

NHS – N-Hydroxysuccinimide

NIP – Non-Imprinted Polymer

NMR – Nuclear Magnetic Resonance

P-MIP – Peptide-containing Molecularly Imprinted Polymer

P-NIP – Peptide-containing Non-Imprinted Polymer

PEG – Polyethylene Glycol

PFU – Plaque-Forming Unit

QCM – Quartz Crystal Microbalance

SD – Standard Deviation

SPR – Surface Plasmon Resonance

SR – Sulforhodamine 101

ssDNA – Single-stranded DNA

Sulfo-SMCC – Sulfosuccinimidyl 4-[*N*-maleimidomethyl]cyclohexane-1-carboxylate)

TBS – Tris-Buffered Saline

TBST – TBS with 1% Tween-20

TER – Transepithelial Electrical Resistance

TFA – Trifluoroacetic Acid

TNT – Trinitrotoluene

UV – Ultraviolet

Xgal – 5-bromo-4-chloro-3-indolyl-beta-D-galactopyranoside

Chapter 1

General Introduction

"Take the first step in faith.
You don't have to see the whole staircase,
just take the first step."

Dr. Martin Luther King Jr.

1.1 The Molecularly Imprinted Polymer

The concept of the molecularly imprinted polymer (MIP) is the creation of a plastic cast of a given target molecule. Functional monomers with complementary functionality are selected that should interact with functional groups on the target molecule. Following the addition of a cross-linkable monomer, the mixture is polymerised. The resulting polymer has a binding pocket that will recognise the target to which the MIP was initially created. While the aim is for absolute specificity to the target molecule, the MIP will also

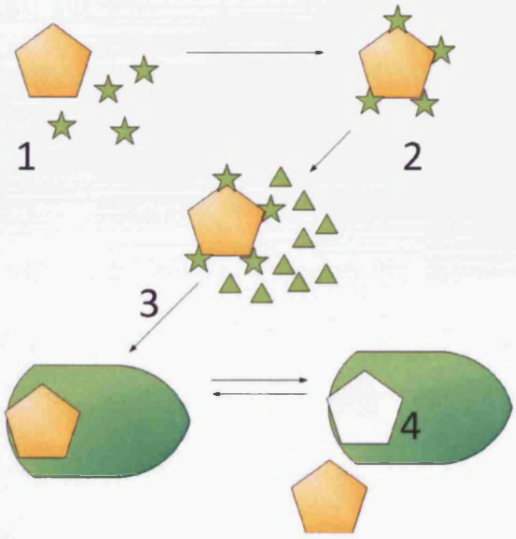

Figure 1: Basic concept of the imprinted polymer: a template is exposed to functional monomers (1) which are known to interact (2), an excess of cross-linking monomer, and conditions to provoke polymerisation (3), resulting in imprinted binding pocket (4).

recognise certain related compounds (reviewed in (Alexander et al., 2006, Haupt and Mosbach, 1999, Hillberg et al., 2005, Ansell, 2005)).

The concept of the molecular imprint is not new technology. Initial reports in the 1930s were made (Polyakov, 1931) when silica gels were cast in the presence or absence of other molecules in solution. The resulting gels were found to have higher affinity for solutes that had been present during casting, compared to solutes that had not been previously exposed to the silica gels.

These early examples were inorganic systems. The first example of an imprinted organic polymer was presented in the early 1970s (Wulff et al., 1973) using a covalent imprinting approach. This paved the way for the first demonstration of what is now termed non-covalent imprinting in an organic polymer (Arshady and Mosbach, 1981), although the term used at the time was "host-guest" polymerisation.

An example in which the synthetic polymer was used to replace antibodies in a ligand binding assay was presented in the early 1990s (Vlatakis et al., 1993) in which MIPs were created with theophylline or diazepam as templates. These polymers showed strong binding in a radio-labelled ligand-binding assay and were sufficient to measure drug levels in human serum. MIP formation schematic is shown in Figure 2.

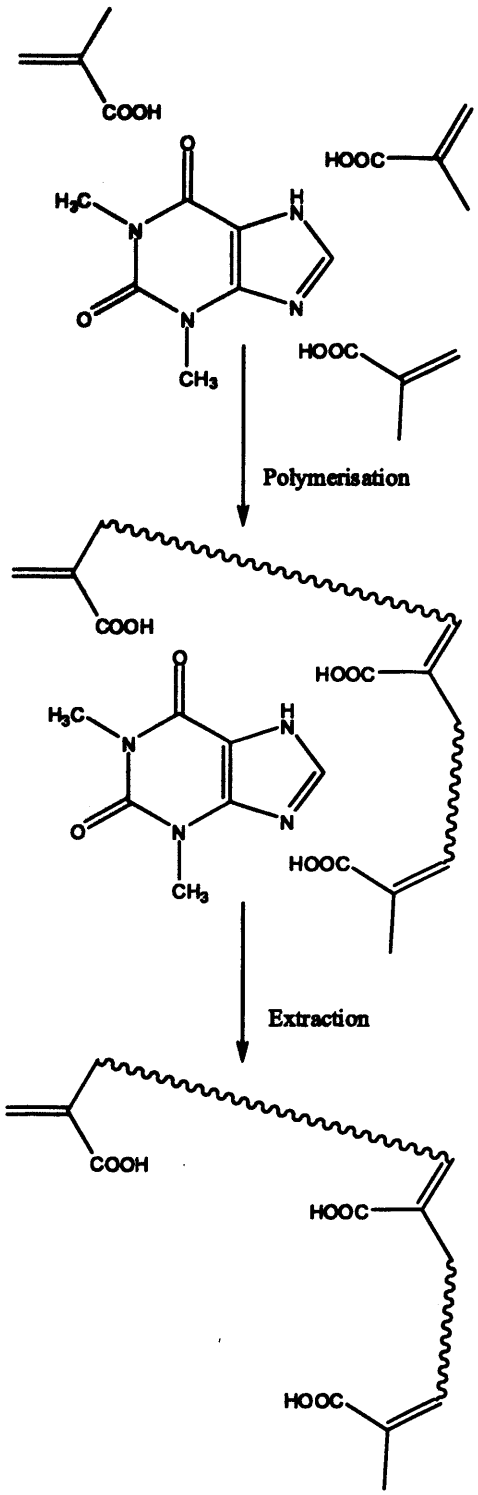

Figure 2: Schematic representation of the preparation of MIP to theophylline using methacrylic acid functional monomer, adapted from (Vlatakis et al., 1993).

In a more recent example (Busi et al., 2004), an acrylic resin was imprinted with a transition state analogue for the Diels-Alder reaction (an organic chemical reaction – specifically cycloaddition). The authors showed that the MIP or "plastic antibody" was able to catalyse this reaction with an efficiency comparable to that of a monoclonal antibody which has been recently developed (Haupt and Mosbach, 2000) to catalyse this same reaction; this example highlights the potential of plastic enzymes.

As the field developed, the concept of this "plastic antibody" has become ever more achievable. Recent advances in imprinting technology include the immobilization of MIP particles/beads on the sensor chips of a quartz crystal microbalance (QCM), producing piezoelectric sensors (Uludag et al., 2007). Two further reports have also demonstrated MIPs raised against glucose (Seong et al., 2002) and nateglinide (Yin et al., 2005), to display dissociation constants (K_D) at millimolar concentrations (1.6mM and 7.4mM respectively). Physiologically safe nanoparticles have even been tested *in vivo* showing high affinity for a component of bee venom (Hoshino et al., 2010).

1.1.1 Methods of Imprinting

In general, there are two main forms of the molecular imprinting process: covalent and non-covalent imprinting. However, an

amalgamation of the two has also been demonstrated in the semi-covalent approach.

1.1.1.1 Covalent Imprinting

When this method is employed, the goal is to control the arrangement of functional groups within the binding cavity to best effect, thus ensuring the tightest fit of target structure in the binding site.

The earliest example (Wulff et al., 1973) involved the imprinting of functional monomers with boronic acid functional groups. Boronic acid undergoes rapid and reversible reaction with diols, therefore once the template is recognised it is covalently attached to the polymer until the system is washed with either water or methanol to detach the template.

A more recent example, illustrated in Figure 3, shows the covalent imprinting of a dopamine analogue, which after hydrolysis of the esters and reduction of the disulfide bond resulted in a binding site for dopamine.

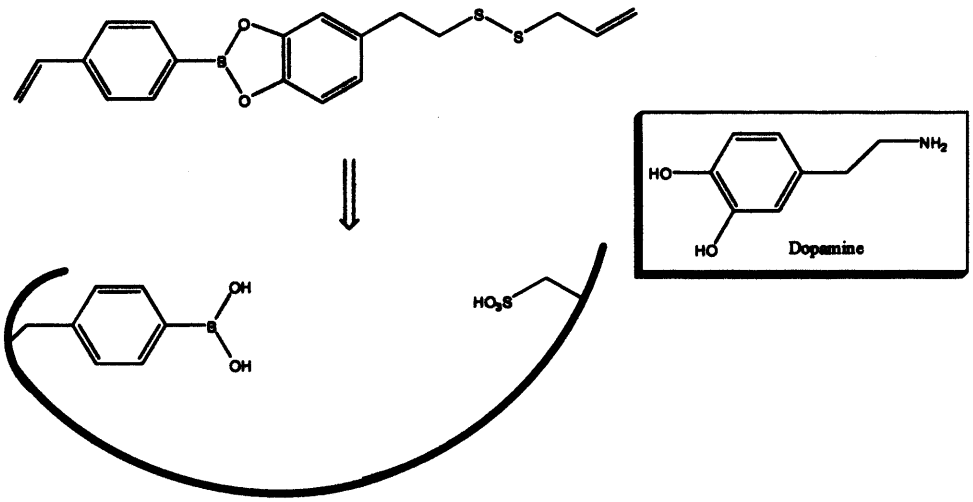

Figure 3: Covalent imprinting of dopamine adapted from (Takeuchi et al., 2006), including the structure of dopamine (inset)

Using a covalent imprinting technique can place functional groups so accurately within a binding site that two or more templates can be recognised simultaneously, indeed they may even interact. In a recent example (Carlson et al., 2006) a chemical sensor for fluorene was produced such that the binding pocket of the MIP could covalently bind to a fluorophore which underwent alterations in spectroscopic properties when in close proximity to fluorene.

Rebinding to this type of polymer can either be through the reformation of a covalent bond, or can be non-covalent. This non-covalent binding to a covalently imprinted polymer is sometimes referred to as the semi-covalent approach (Alexander et al., 2006).

1.1.1.2 Semi-covalent Imprinting

When the semi-covalent approach is undertaken, the template is

covalently attached to a polymerisable group as in the covalent strategy, with binding becoming available after cleavage of the template. There are two variations on this method: template and monomer are directly connected (Caro et al., 2002), or the template and monomer are connected via a spacer group (Whitcombe et al., 1995).

This sacrificial-spacer method provides more space within the imprinted recognition site than previous methods, allowing for greater diffusion into and out of the binding sites. Imprinting using this method has been applied in several studies (Hwang and Lee, 2002, Percival et al., 2002, Petcu et al., 2001) and is still in use today (Qi et al., 2010).

1.1.1.3 Non-covalent Imprinting

The basic drive behind imprinted polymer science has always been the pursuit of a material that mimics natural antibodies whilst being constructed artificially. When the antibody binds to its target molecule, or "template", covalent bonds are not formed; instead the binding is via a series of non-covalent interactions. With this in mind, the non-covalent imprinting approach, in which binding can nevertheless be specific yet reversible, becomes an obvious choice for the production of MIPs (Caro et al., 2002) as the interactions between the template and the functional monomers are the same as those between the final polymer and the template when re-binding, pioneered by the Mosbach group (Arshady and Mosbach, 1981). The non-covalent approach was shown briefly in

Figure 2.

The quality of the final MIP hinges upon the quality of the complexes formed in the pre-polymerisation solution, and therefore the strength of the template-monomer interaction (Chianella et al., 2002, Karim et al., 2005).

1.1.2 Components of an Imprinted Polymer

When constructing a polymer several components are essential. Firstly, there must be a functional monomer. This is a compound which, while showing some level of interaction with the template (ionic, hydrogen-bonds, van der Waals), should also have a separate function group capable of supporting polymerisation. An example would be methacrylic acid (MAA) which is used extensively in imprinting science (Dai et al., 2010, Liu et al., 2010).

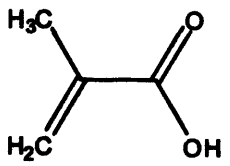

Figure 4: Methacrylic acid (MAA).

The template molecule and the monomer of choice must then be dispersed in a solvent. It is this dispersion in a porogenic solvent that should result in the macroporous structure of the final polymer allowing

elution of the template and indeed rebinding. The correct choice of porogen is essential to producing the intended quality of polymer (pore size distribution, structure, swelling properties) (Haginaka et al., 2008).

Polymerisation initiators can take several forms, most commonly activated by either heat or UV light (O'Shannessy et al., 1989). An example of a widely used polymerisation initiator is 2,2'azobisisobutyronitrile (AIBN) which generates free radicals upon exposure to UV light (Urraca et al., 2008).

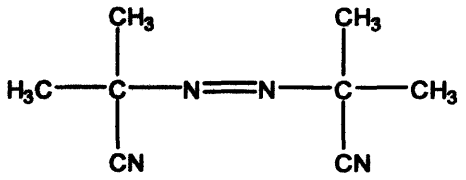

Figure 5: 2,2'-azobisisobutyronitrile (AIBN).

1.1.2.1 Functional Monomers

While it is relatively easy to predict molecular interactions in terms of hydrogen bonding or pi-pi stacking, the three-dimensional, constantly shifting solution complexation can be a far more complicated issue, although, one which can be simulated using molecular dynamics studies (Karlsson et al., 2009). Whilst recent developments suggest a computational approach to the design of an imprinted polymer may soon be practical (Dong et al., 2009), often the design of MIPs necessitates the performing of a series of explorative experiments in which a range of monomers are tested against the desired template at a

range of monomer-to-template ratios whilst observing for some change in the system indicative of some form of interaction occurring (Lulinski and Maciejewska, 2009, Feas et al., 2009).

In the case of molecules that fluoresce (whether intended as the template or as a functional monomer leading to a fluorescent MIP), simply a shift in the peak fluorescence, or indeed fluorescence quenching may be enough to indicate interaction with the fluorophore (Rathbone and Bains, 2005). Other methods to determine complexation include via NMR titration (Athikomrattanakul et al., 2009, Takeuchi et al., 2000) and UV spectroscopy (Svenson et al., 1998). Essentially, the hydrogen atoms responsible for hydrogen bond donation should shift on an NMR spectrum as nearby structures cause a change in resonance; likewise, hydrogens neighbouring carbonyl groups, for example, may also shift as hydrogen bonds are accepted. With this in mind, a range of monomer-to-template ratios can be examined in search of a combination which results in the greatest spectroscopic shift.

1.1.3 Methods of Polymerisation

A number of approaches have been used to prepare MIPs. These include bulk polymerisation, suspension polymerisation, precipitation, emulsion, and surface grafting, which would include living systems such as iniferter-mediated polymerisation (Fairhurst et al., 2004, Alexander et al., 2006).

1.1.3.1 Bulk Polymerisation

When Polyakov (Polyakov, 1931) first stumbled across the imprinting phenomenon, he was casting silica gels. Therefore, the structure of the system was one, large, single, inorganic unit. When this concept was followed up by other researchers, a similar bulk-production method was employed with grinding and sieving of the block polymer down to smaller units which could be assessed for their binding affinity (Leonhardt and Mosbach, 1987).

1.1.3.2 Precipitation Polymerisation

In this type of system, a polymer is formed which is insoluble in the pre-polymerisation mixture. An example of beads produced by precipitation polymerisation is shown in Figure 6 (Wang et al., 2003) in which approximately 5μm MIP beads were produced which selectively bound theophylline.

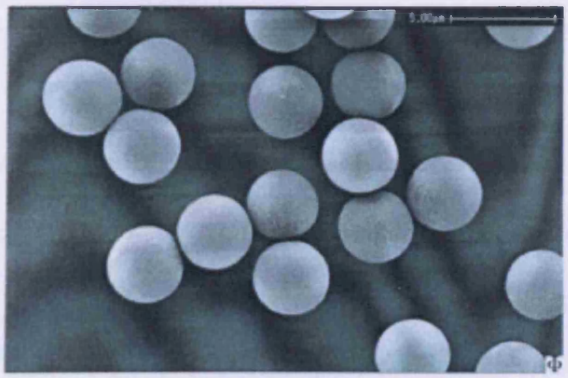

Figure 6: MIP beads approx 5μm diameter formed via precipitation polymerisation (SEM micrograph) (Wang et al., 2003).

1.1.3.3 Emulsion/Suspension Polymerisation

Emulsion polymerisation can be advantageous in generating polymer beads of uniform size. In this instance the pre-polymerisation mixture is an emulsion with small droplets of monomer (usually the oil phase) suspended throughout the solvent (usually aqueous) (Vaihinger et al., 2002), although there are examples of the inverse (Mayes and Mosbach, 1996), termed suspension polymerisation.

One of the overriding issues with the older bulk polymerisation method is the loss of binding sites, both in terms of restricted access to those sites within the solid construct, and damage to binding sites when the polymer is processed (e.g. milling). Whilst suspension or precipitation polymerisation protocols go some way toward resolving this, provided the resultant beads are sufficiently porous, some binding sites will remain relatively inaccessible (Wei and Mizaikoff, 2007).

Bulk or suspension polymers as catalytic agents were compared (Strikovsky et al., 2000) in which polymerisation mixtures were identical (ethylenedimethacrylate (EDMA), methyl methacrylate (MMA), N,N'-diethyl(4-vinylphenyl)amidine (DEVPA), and diphenylphosphate (DPP) as template, with acetonitrile (MeCN), cyclohexanol-n-dodecanol, or toluene as porogen) yet the product was either monodisperse beads or a block polymer requiring grinding and sieving. Assessment of both polymers gave comparable binding and catalytic effects.

1.1.3.5 Surface Grafting

As the technology advances, a further option available to the imprinting polymer chemist is that of grafting polymers onto solid supports. MIPs can be generated from silica supports with free-radical initiators immobilised to the surface, thus producing controllable thin films of polymer (Sulitzky et al., 2001). A further advancement of this was seen in which a dithiocarbamate iniferter was grafted to a polystyrene bead (Qin et al., 2009), shown in Figure 7.

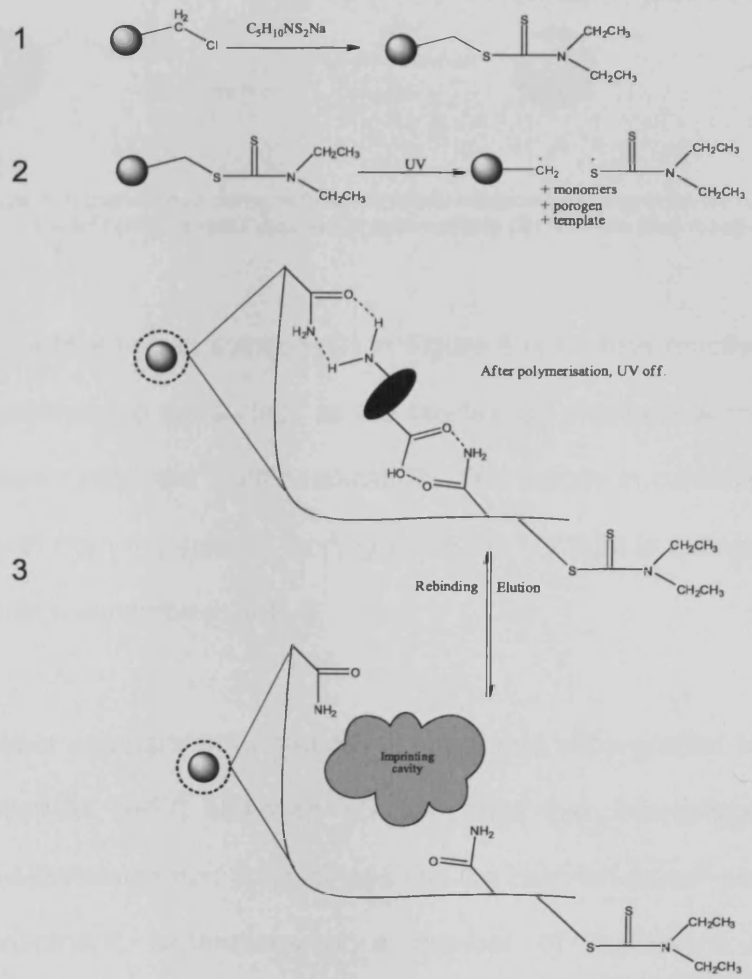

Figure 7: Schematic representation of chloromethylated polystyrene beads with dithiocarbamate iniferter-mediated polymerisation using lysozyme as template, adapted from Qin et al (Qin et al., 2009), showing functionalisation of chloromethylated resin with a dithiocarbamate iniferter (1), subsequent activation of the iniferter with UV (2), and the resulting molecularly imprinted system (3).

The principle concept of the iniferter is that a single molecular species may initiate free-radical polymerisation, transfer the radical through the growing polymer, and subsequently terminate polymerisation (Otsu et al., 1989).

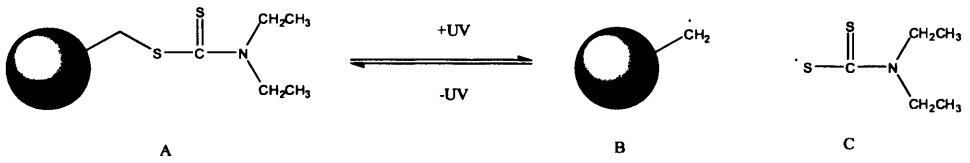

Figure 8: Illustration of diethyldithiocarbamate iniferter, showing iniferter-functionalised moiety (A), the more reactive radical species (B), and the less reactive (C).

The radical free in solution (C) in Figure 8 is far less reactive than that immobilised to the surface as the radical can distribute across the CS_2 system, unlike the methyl radical (B). This results in controlled polymer growth from the surface, ending when the UV light is extinguished and radical C recombines with B.

A direct comparison of ground, beaded, and silica-grafted MIPs, when applied as HPLC stationary phases found that, interestingly, "ground monolithic imprinted polymer was still the best "all-round" performer for enantiomeric separations of a number of β-blockers by HPLC" (Fairhurst et al., 2004), although the beaded material was the most efficient to synthesise and gave improved peak shape. In the same study the authors also produced silica-grafted material, which, whilst taking the longest to manufacture, and not allowing enantiomeric separation of four of the nine compounds tested, allowed higher resolution of more strongly retained compounds in a relatively short period of time.

An important distinction must be made between surface-initiated

polymerisation, which results in very thin films grown from the surface, and solution-initiated polymerisation, in which the polymer can be grafted to a surface (Kato et al., 2003). The latter can often result in very thick polymer layers.

1.1.3.6 Hierarchical Imprinting

The fundamental concept of the hierarchical imprint is to immobilise the template on a support that can subsequently be degraded, perform polymerisation, and then remove the support-template complex (Titirici and Sellergren, 2004). In this situation it is possible to control to some degree the spacing of functional binding pockets in the finished polymer (Wu et al., 2008). A typical example in which multiple types of binding site were produced hierarchically within a single polymer is presented by (Dai, 2001) in which metal ions were imprinted along with surfactant micelles. This resulted in imprints of different sizes and functions within a single silica matrix.

Another approach makes use of porous silica particles containing immobilised templates. The pores are filled with the polymerisation mixture, polymerised, and the silica moulds dissolved. This results in a porous spherical MIP bead with recognition sites throughout (Titirici and Sellergren, 2004).

1.1.4 Biological Molecules and MIPs

More recently, researchers in molecularly imprinted polymer science have found interest in the application of these systems to biological molecules such as peptides (Yoshimatsu et al., 2009, Papaioannou et al., 2008) including synthetic peptide receptors incorporating metal ions into the binding matrix (Hart and Shea, 2001), proteins (Hansen, 2007), and even viruses (Bolisay et al., 2007).

Larger proteins present a problem to the current systems for molecular imprinting, however, one method (termed the "epitope approach") (Nishino et al., 2006) allows imprinting of short peptide constituents of the protein with a view toward recognising the protein as a whole after polymerisation.

A further study was produced recently (Hoshino et al., 2010) in which melittin (a component of bee venom) was imprinted into polymer nanoparticles which were then injected into living mice. When the mice were then inoculated with melittin, mortality and peripheral toxicity symptoms were greatly reduced, demonstrating that the MIP nanoparticles were capable of capturing and facilitating the clearance of melittin from the bloodstream.

Another interesting project which may have direct relevance here was the construction of a molecularly imprinted polymer using β-cyclodextrin

as a functional monomer (Ng and Narayanaswamy, 2009). This represents a step toward natural compounds as recognition elements in an imprinted system, rather than merely conjugated to polymer supports.

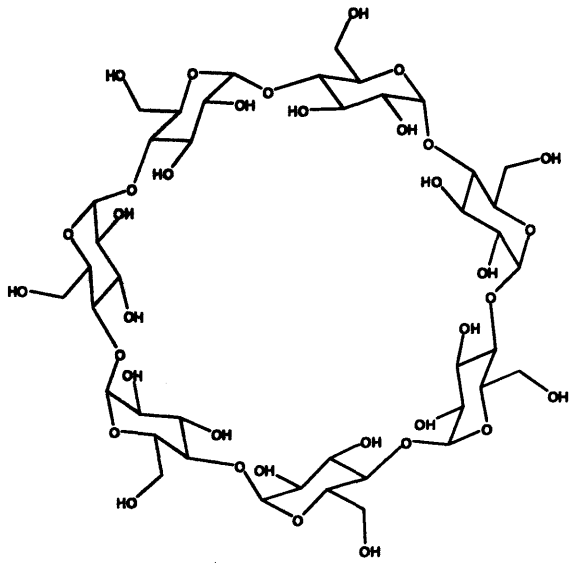

Figure 9: β-cyclodextrin.

1.1.5 Peptides and Polymers

Several projects have made use of the conjugation of peptides with polymers, including an example in which phage display was used to obtain peptides that bound trinitrotoluene (TNT) that were then supported on a polymer scaffold and used to detect explosives in water (Cerruti et al., 2009). This system was able to differentiate between the target TNT and dinitrotoluene (DNT) yielding undetectable levels of binding to the latter.

This is an interesting first step. However, in this system the polymer was present purely for support and to attach the peptide to the sensor grid. There was no imprinting action from the polymer, and no intention for it to take part in the binding process itself.

1.1.6 Current Applications

Of course, imprinted polymers can potentially find application wherever there is a need for reliable detection or perhaps even differentiation of one compound over another. However, current commercial applications are limited, although, there are many laboratory-scale examples of MIPs as chromatographic stationary phases (Ansell and Kuah, 2005, Boyd et al., 2007, Wistuba and Schurig, 2000, Liu et al., 2004) and solid-phase extraction aids (Baggiani et al., 2007, Pereira and Rath, 2009, Sharma et al., 2007).

MIPs as solid phase extraction materials are currently commercially available, until recently only for a limited number of compounds, and from a single manufacturer (SupelMIP® by Sigma-Aldrich). A greater range of polymers is now available through Biotage (AFFINILUTE™) for a wider range of compounds, yet still only as solid-phase extraction materials. Although marketed applications appear somewhat limited, the potential applications of imprinting science are put forward and eagerly anticipated in several recent reviews on imprinted drug delivery systems and therapeutic implications of imprinted polymer sensors (Cunliffe et

al., 2005, Hillberg et al., 2005, Sellergren and Allender, 2005).

With regard to the potential use of MIPs in sensing, the electroconductive qualities of certain modern polymers may be worth some consideration. There are many examples in the literature of polymers which modulate their conductive properties in response to their immediate environment, whether it is changes in pH (Pei and Qian, 1991), inorganic ions (Liu et al., 2001), or organic molecules (Shoji and Freund, 2002). A molecularly imprinted conducting polymer has been produced that was applied for detection of paracetamol binding to polypyrrole film (Özcan and Sahin, 2007). Conducting polymers are reviewed further in (Lange et al., 2008).

1.2 Phage Display

Phage display, first conceived over 20 years ago (Smith, 1985), allows the selection of ligands which bind to a given target with very high affinity, often very rapidly. The use of a combinatorial library of, in this case, short peptides displayed on M13 bacteriophage allows for consecutive rounds of biopanning to be amplified easily in *Escherichia coli* allowing enrichment of binding clones over several rounds.

1.2.1 Surface Display

Small molecules can be expressed on a variety of cell surfaces, most

utilised is the display of peptides or antibodies on the surface of a bacteriophage or "phage". These expressed, or "displayed", molecules most commonly exist as simple peptides comprising as few as seven amino acid residues or larger proteins such as antibody fragments (Ascione et al., 2005). Other displayed molecules have included fragments of cDNA (Hufton et al., 1999), and even synthetic compounds (Woiwode et al., 2003). The common theme between these methods is the subsequent identification of the displayed moiety by sequencing the DNA of the displaying organism.

The phage display process requires a biopanning step during which the vast library of surface-displayed moieties, in the magnitude of 10^9 or up to 10^{11} different units, is allowed the opportunity to bind to an immobilized target. Any unbound phage are easily washed away along with any loosely bound particles, leaving only those phage displaying peptides which are tightly associated with the target. The tightly bound peptide-vectors can then be eluted with either a compound that is known to demonstrate greater affinity for the target molecule, or by non-specific disruption of protein binding by, for example, lowering the pH with a glycine buffer.

After the selection of phage-peptide clones in the first biopanning round, those that show greater affinity for the target are then used in a further round of panning to enrich binding clones. After several rounds of

panning, the harvested phage-peptide clones that display the highest binding are subject to DNA sequencing to elucidate the primary structure of the peptide which had been expressed on the surface (Azzazy and Highsmith, 2002).

1.2.2 The M13 Phage

The M13 is a filamentous bacteriophage, approximately 930nm in length and 6nm in diameter. If this was to be scaled up keeping the correct proportions, we would witness a structure the width of a pencil which is approximately four feet in length (Kehoe and Kay, 2005). The M13 bacteriophage lends itself well to the technology of phage-display for several reasons. Firstly, the single-stranded circular DNA has been sequenced in its entirety thus allowing substitution to predictably alter various phenotypic characteristics (van Wezenbeek et al., 1980). Also, the M13 phage is non-lytic, which therefore allows rapid and continuous amplification of the phage particles in host bacteria, whilst not depleting bacterial load, merely increasing generation time (Stegen and Hofschneider, 1970).

The main component of the phage structure is the genetic material, which consists of 6,407 bases. This phagemid is encapsulated within a shell composed of approximately 2,700 copies of the major coat protein pVIII. One end of the phage is capped with five copies each of pVII and pIX, while the other end contains five copies each of pIII and pVI

(Sidhu, 2001).

1.2.3 Mechanism of Phage Infection and Replication

The minor coat protein pIII is instrumental in the recognition and subsequent penetration of the host cell. The pIII unit itself is divisible into three subsections: two N-terminus portions and one C-terminus portion. The C-terminus portion is anchored in the phage coat and has a role in the assembly and ejection of the new phage particles at the membrane of the host cell. The first of the N-terminus regions is responsible for the recognition of the F-pilus on the male *E. coli* cells, while the second is thought to mediate the withdrawal of the F-pilus into the periplasm, resulting in internalization of the phage genetic material (Kehoe and Kay, 2005).

Once the phage genetic material is internalized, the single-stranded DNA is converted into double-stranded DNA by bacterial enzymes and the synthesis of the phage proteins begins. The phage assembly commences as the proteins and ssDNA accumulate within the infected bacterium. The structural proteins (pVIII, pVII, pIX, pVI, and pIII) are inserted into the inner bacterial membrane awaiting sufficient production of the phage genome.

Newly synthesized ssDNA - comprising the phage genome - is coated by pV to prevent its conversion to dsDNA, with the exception of a small

packaging signal which is left free of pV. This packaging signal is captured by a complex composed of the proteins pIV, pXI, and pI, which form an opening in the host cell membrane (Stassen et al., 1994). The phage particle is concurrently assembled and extruded from the bacterium at this complex, which is often described as a membrane pore (Yang et al., 2004). During construction, pV is removed from the ssDNA and the phage genome is coated with pVIII; five copies each of pVII and pIX are then placed at the end of the phage that contains the packaging signal.

In general, increases in supernatant phage in a culture of susceptible host bacteria are not seen until a period of 30-40 minutes has elapsed at 37°C. This would be the amount of time required for assembly of the new phage to begin. When host cell densities are very low it has been observed that a longer delay occurs before phage numbers increase. This has been referred to as a "replication threshold" (Wiggins and Alexander, 1985) or a "proliferation threshold" (Payne and Jansen, 2002). Wiggins and Alexander report this density to be around 10^4 cells per millilitre for the phage-host combinations tested.

Bacteria are able to monitor their local population density through autoinducers or quorum factors that they secrete into the environment, thereby altering the expression of many genes and regulating the metabolic state of the sensing bacteria when concentrations are

sufficient. Therefore, one explanation for the additional time required for phage replication to begin in lower population densities of host bacteria is that certain metabolic states are required for phage infection to occur (de Kievit and Iglewski, 2000).

The replication threshold density phenomenon can be extracted from a mathematical model (Schlesinger, 1932), which relies on the assumption that phage rely entirely on chance encounters with their hosts and that their ability to infect and reproduce in liquid culture can therefore be predicted by the equations that describe the movements and irreversible binding of inert particles under the influence of Brownian motion. This model states that:

$$P/P_0 = e^{-kCt}$$

where P/P_0 is the fraction of phage that remains unbound at time *t* (minutes), *C* is the concentration of host cells per cubic centimetre (which remains constant at time *t*), and *k* is an adsorption rate constant in cubic centimetres per minute that can be determined experimentally for a given phage-host system. This rate constant accounts for variations between systems including the number of binding sites per cell and the efficiency with which collisions actually result in infection. For example, the T4 phage can use several hundred binding sites per cell, whereas the M13 phage has only two or three binding sites per cell, so the *k* values for these two phages would be in the region of 2.4 x 10^{-9} cm^3min^{-1} (Stent, 1963) and 3 x 10^{-11} cm^3min^{-1} (Tzagoloff and

Pratt, 1964), respectively.

It follows from the equation above that if the concentration of host cells in culture (C) is lower, with all other parameters remaining equal, a larger proportion of phage will remain unbound at any given time (*t*). In a study which puts this equation under closer scrutiny (Kasman et al., 2002), it was discovered that the host cell density itself determines the phage infection rate, irrespective of the presence of quorum factors. This was tested by comparing phage proliferation rates in known low populations of host bacteria and populations with the addition of media conditioned with quorum factors. Concentrating the same quantity of both phage and host bacteria into a smaller volume of the same media improved efficiency of infection three- to five-fold. The data presented suggested that phage infection can happen at any concentration of host cell providing there is sufficient presence of phage to ensure that contact is made and maintained.

1.2.4 Construction of a Phage Display Library

The majority of researchers who use phage display have very little to do with the manufacture of the library. For the manufacture of the complete library, a knowledge of the construction of DNA libraries is of greater importance (Kehoe and Kay, 2005). A technique still in common use to generate this effect is base substitution mutagenesis by terminal transferase, first described by (Snow et al., 1987). The commercially

available Ph.D-C7C M13 phage display library is a construction based upon random mutations of the gIII gene, which codes for the surface protein pIII.

Thomas Kunkel demonstrated in 1985 that single-base substitution mutations were possible to introduce into the *lacZ*$_\alpha$ gene in M13mp2 (Kunkel, 1985). He was able to induce these mutations in a rapid procedure with 40-60% efficiency. Using two simple additional treatments of the DNA prior to transfection, it was possible to produce a site-specific mutation frequency approaching 100%. This high efficiency was obtained by using a DNA template containing several uracil residues in place of thymine. The template was found to have normal coding potential for the *in vitro* reactions typical of site-directed mutagenesis protocols, but was not biologically active upon transfection into wild-type *E. coli* cells. Therefore, expression of the desired change, present in the newly synthesised non-uracil-containing covalently closed circular complementary strand, was strongly favoured.

1.2.5 Utility of Phage Display

1.2.5.1 Protein Conformation

The technology of phage display has met many applications in recent years. In one study (Bai and Feng, 2004), proteins were selected that fold in only stable conformations. The authors suggest two basic

biophysical issues in protein design. One is to find mutations that make proteins thermodynamically more stable; the other is to find an amino acid sequence for a polypeptide chain that will fold to a target structure. They suggest that the second issue is more critical for testing the principles of protein folding.

To learn the factors that stabilise the proteins, researchers have become interested in studying the proteins from thermophilic organisms. These proteins are stable at very high temperatures. It is therefore hoped that the rules for stabilising proteins may be revealed after comparing the thermophilic proteins with mesophilic proteins. In this study (Bai and Feng, 2004), phage display and proteolysis were used to select stably folded proteins in which the DNA encoding the N-terminal half of the beta barrel domain (from cold shock protein CspA) was substituted with fragmented genomic *E. coli* DNA. The phage library was then challenged by several proteases. The authors isolated four proteins selected from library which were soluble and characterised them using NMR, CD spectroscopy and amide hydrogen exchange. The CD spectra indicated formation of the beta sheet structure consistent with the segment from the CspA.

1.2.5.2 Immunological Properties

Phage display libraries have also found their use in the selection of internalising antibodies. In a study (Becerril et al., 1999), an antibody library (scFv) based on the fd phage were exposed to SKBR3 cells

(oestrogen receptor negative breast cancer cell line) which had reached 50% confluency. The library was allowed contact for two hours, after which surface bound phage were removed. Cell membrane integrity was compromised using acetone, thus allowing the recovery of the internalised phage particles, which were subsequently detected using biotinylated anti-M13 immunoglobulins. The authors demonstrated for the first time that phage displaying an anti-receptor antibody can be specifically endocytosed by receptor expressing cells and can be recovered from the cytosol in infectious form.

Another example has been illustrated more recently (Casey et al., 2004). In this case, the authors constructed a linear peptide display library of 20 amino acid residues fused to the N-terminus of pIII of the M13 phage, which was exposed to the monoclonal antibody (MAb) for the apical membrane antigen-1 (AMA-1) – one of the leading malaria vaccine candidates (Bueno et al., 2009, Epstein et al., 2007). Of the strongest binding peptides, none were found to have any sequences similar to the primary sequence of AMA-1; yet, binding of the peptide to the anti-AMA-1 antibody was disrupted by the addition of AMA-1 whilst none would bind to the isotype control MAb. Immunogenic studies in rabbits then showed that inoculation with the phage-derived peptides resulted in high titres of peptide-specific antibodies that were shown to be cross-reactive with recombinant AMA-1, indicating that the peptides behave as immunogenic mimics of the natural antigen.

Another, perhaps more innovative, use of phage display has been demonstrated in a study which sought to bind one of the components of the toxin of the Thai cobra *(Naja kaouthia)*. The toxin is a combination of agents: neurotoxin (paralytic) which acts upon nicotinic acetylcholine receptors, and cardiotoxic (cytolytic) acting upon cell membranes. The neurotoxic agents have been separated into four component parts (α, β, γ, and δ) (Cooper and Reich, 1972). Of these, α-cobratoxin constitutes the major component present in the venom. In this study (Byeon and Weisblum, 2004), the authors immobilised the α-cobratoxin to a micro-titre plate and carried out three rounds of panning against this target. The peptides of interest were chemically synthesised and used to create an "affinity resin" by their inclusion in an agarose gel, which was shown to then effectively deplete α-cobratoxin from crude venom.

1.2.5.3 Medicine

Phage display libraries have also been implicated for applications in modern healthcare. Two recent reviews (Nilsson et al., 2000, Ruoslahti, 2000) have discussed the use of phage display technology in the determination of peptides that target tumours and tumour vasculature. The vascular endothelium varies throughout the body with respect to the levels of various markers that are expressed (Pusztaszeri et al., 2006). Tumour microvasculature represents an excellent target for site-specific drug delivery as current anti-cancer treatments rely on

toxicity to the rapidly proliferating tumour cells, although the high doses over long periods which are often required can be very debilitating as there is also significant toxicity to proliferating non-malignant cells. The concept of the "magic bullet" illustrates the desire to target the tumour itself, sparing healthy tissue from the damaging effects of the cytotoxic agent. To this end, many efforts have been made to specifically target the tumour vasculature, more recently using phage display as the technology of choice; an example of this being the selection of "antibodies to novel cancer-induced antigens expressed by tumours and by the tumour vasculature" (Mutuberria et al., 1999). As each type of blood vessel in the body displays endothelial markers that vary according to the type of tissue in which the vessel is found, a "magic bullet" could, in theory, be aimed specifically at any tissue.

Another imaginative application of phage display comes in the form of a potential vaccine to Human Immunodeficiency Virus (HIV). In a study (Zwick et al., 2003) involving antibody phage display, the point was made that one of the major frustrations in HIV vaccine development is the inability to form antibodies to the virus – due to the very nature of the disease. In this study, the authors identified a novel antibody found to bind to a complex epitope on HIV-1 involving several of the key structures unique to HIV.

1.2.5.4 Low Molecular Weight Compounds

1.2.5.4.1 Drugs

Few studies have attempted to obtain binding peptides to targets of the scale of low-molecular weight drugs. Studies published to date include phage display against dexamethasone (Yu et al., 2007) in which binding sequences were identified that matched albumin and a subunit of cytochrome c oxidase; methotrexate (Takakusagi et al., 2008) in which a binding sequence was identified that matched the drug's target in the body (dihydrofolate reductase); and paracetamol (Smith et al., 2007) in which a peptide was isolated that bound preferentially to paracetamol over its structural isomers and was shown to reduce cellular toxicity in a hepatic cell culture model.

1.2.5.4.2 Texas Red

Several binding peptides were isolated from an M13 pIII expressed phage display library that were found to modulate the spectral properties of target fluorophores (Rozinov and Nolan, 1998). Their work examined the interaction of the library, and subsequently the peptides, with Texas Red, Rhodamine Red, Oregon Green 514, and fluorescein.

After four rounds of biopanning with Ph.D-12 phage display peptide library a total of six clones were sequenced. Five of the clones shared a common sequence, designated TR401: KHVQYWTQMFYS. Initial binding studies used His_6-tagged peptides bound to cobalt-containing

beads producing beads which bound Texas Red very strongly, demonstrating a K_D value of 1.6μM, although the binding affinity of the whole phage with the dye was very different, quoted as 0.27nM. On the whole, the peptide alone immobilised to beads is likely to provide the more accurate estimation of K_D as the binding system itself does not alter during attempts to separate bound dye from unbound. This is in contrast to the whole phage system in which equilibrium is reached, and then polyethylene glycol (PEG) is added to precipitate the phage. This process was repeated for two further precipitations when dry phage pellets were then assessed for their Texas Red content. This modification of a system would disrupt the equilibrium as PEG changes the properties of the solution e.g. osmolarity, ligand concentration and solubility, thereby rendering subsequent K_D determinations potentially inaccurate.

The remainder of this original paper and indeed the follow-up work (Marks et al., 2004) focuses upon the evolution of the peptides into progressively stronger binders. In fact, one of the "descendants" of TR401, designated TRS311, was quoted as having a K_D of 0.09nM, although this was estimated using the phage precipitation method.

1.3 Functional Plastibodies – Aims and Objectives

Whilst the molecularly imprinted polymer is potentially of great value in any area where recognition or sequestration of a specific compound would be necessary, in reality, the binding specificity and affinity of the currently available MIPs would, in general, not meet the requirements for accurate and reliable sensing in critical areas of clinical or environmental science.

It is hypothesised that incorporation of a specific peptide, able to bind a specific ligand, into the imprinting process would allow for greater affinity and specificity in the interactions of ligand with the MIP, i.e. binding interactions with the MIP would involve ligand-imprinted peptide interactions.

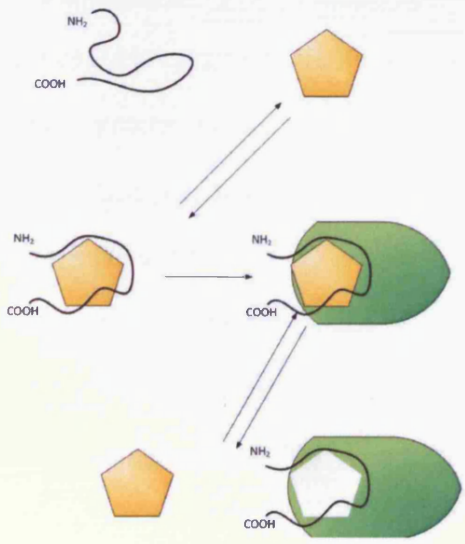

Figure 10: Representation of the "Plastibody". In this situation, a peptide which has been found to bind with high affinity and specificity to a template molecule is imprinted in its binding conformation, producing a robust, highly specialised binding site.

The principle aim of this project is to create such a peptide-conjugated molecularly imprinted polymer. The resulting material, whilst able to bind to its target with high affinity and specificity, should also be robust enough to withstand chemical or physical insult which would normally render a peptide or antibody system useless. Potentially, due to a restriction in the number of conformations the peptide is able to adopt, there may be a reduction in the energy required for the peptide to form a binding conformation making binding more favourable.

Specific objectives:

- To obtain a peptide capable of binding a low molecular weight compound with high affinity and specificity. Initial attempts were made to isolate such a peptide from a phage display library with propranolol as the biopanning target; although, when this proved unsuccessful, a peptide derived from phage display is described in the literature capable of binding the fluorophore Texas Red.
- Devise an assay protocol capable of thoroughly testing binding, both for the peptide *in situ* on the phage unit, and also immobilised to a solid support.
- Develop a polymerisation protocol that allows the undamaged peptide to retain a binding conformation such that it may rebind this target whilst retaining specificity and (possibly improving) affinity.

Chapter 2

Phage Display against Propranolol

"Success consists of going from failure to failure without loss of enthusiasm."

Sir Winston Churchill

2.1 Introduction

While phage display has met many applications in recent years, the majority focus on binding of the phage with large molecular structures, e.g. antibodies, proteins, or even cell surfaces. Comparatively few studies have been performed where the biopanning target is a small molecule, e.g. low molecular weight drug.

In this current work propranolol has been selected as the target of choice principally due to its wide use in imprinted polymer science (Kantarovich et al., 2009, Jantarat et al., 2008, Suedee et al., 2008, Reimhult et al., 2008), and particularly in the laboratory in which these studies were conducted (Castell et al., 2006). Propranolol is well characterised, comparatively safe, and somewhat inexpensive. Further, there are a number of other structurally similar molecules readily available to test the selectivity of ligand interactions. For these reasons,

propranolol served as an ideal target.

The phage library used for these experiments was the Ph.D-C7C library available from New England Biolabs (MA, USA), which displayed on the N-terminus of the minor coat protein pIII a random 7-mer peptide sequence flanked by cysteine residues, which spontaneously form a disulfide bridge, thus conferring some degree of secondary structure to the peptide sequence Figure 11.

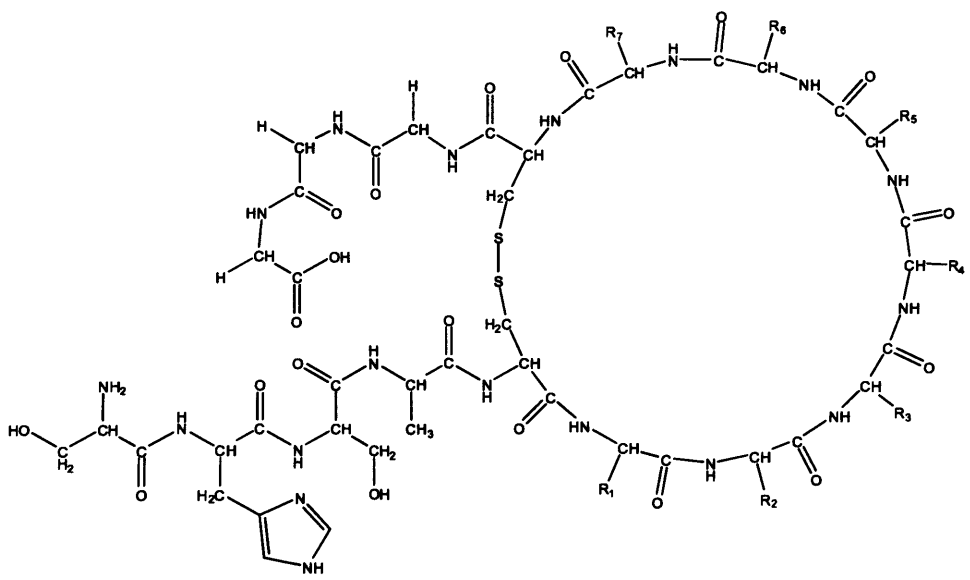

Figure 11: Template phage displayed peptide structure from Ph.D-C7C Library.

Several biopanning strategies were employed which should result in a number of peptides with high affinity and specificity for propranolol (Figure 12), which can then be taken forward into the polymer conjugation and imprinting stage of the project.

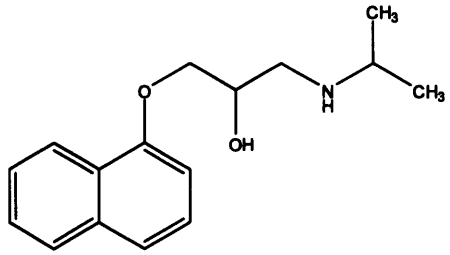

Figure 12: Propranolol falls into the therapeutic category of antihypertensive. Its mechanism of action is through the blockade of beta-adrenergic receptors (beta blocker), thereby reducing sympathetic stimulation.

In order to force the selection of highly specific phage displayed peptides, it was considered necessary to include related compounds in the panning protocols. A "pre-screening" step was introduced in addition to the standard in-house phage display protocols making use of nabumetone (Figure 13), a compound which, whilst having a different pharmacological action to propranolol, shares certain structural aspects: the naphthyl group leading into the ether moiety resembles that of propranolol; also the ketone group on the aliphatic side-chain is approximately the same distance from the aromatic region as the hydroxyl group in propranolol. As nabumetone is only slightly soluble in water, pre-screening took place against the surface of precipitate.

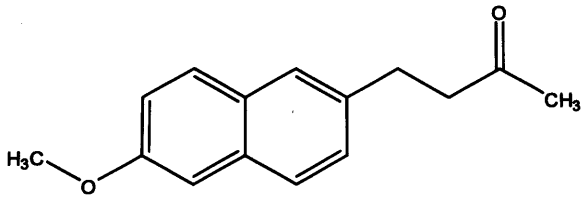

Figure 13: Nabumetone is a non-selective non-steroidal anti-inflammatory drug (NSAID).

During exposure of propranolol to the phage library, compounds with far

greater water-solubility bearing the same aminopropanol-based side-chain were introduced, with the intention that any peptides with affinity only for this region of the molecule should be discarded with the initial washing steps. Only phage bearing peptides with affinity for the propranolol molecule as a whole should remain.

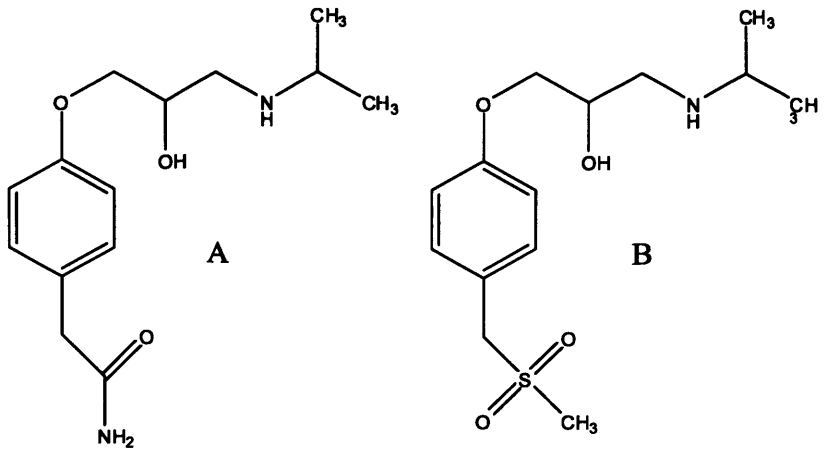

Figure 14: Atenolol [A] and sotalol [B]. Both compounds fall into the therapeutic category of "beta-blocker".

One "Round" of panning consisted of pre-screening against nabumetone, followed by four "sub-rounds" of exposure to propranolol in the presence of the competing compounds.

Once clones bearing peptides of interest were isolated from the phage library, it was necessary to measure the strength of the binding event.

A variety of approaches (Franz diffusion cell, filter centrifugation, a diffusion study in which the membrane was replaced with a biological layer (Madin-Derby canine kidney (MDCK-1) cells), and a

microcentrifuge tube equilibrium dialysis system) were employed to determine the relative affinity of selected clones.

Specific objectives of this chapter were to isolate from the phage library a peptide with high binding affinity and specificity to the target molecule propranolol, and to develop methodology capable of assessing this binding.

2.2 Materials and Methods

2.2.1 Media and Solutions

(Adapted from Pharmaceutical Cell Biology, Welsh School of Pharmacy, Cardiff University Phage Display Protocol)

Unless otherwise stated, all reagents were obtained from Sigma-Aldrich, Gillingham, UK.

Agarose top: 20g/L of LB broth (Sigma L3022-1KG) in ddH20 +0.5mM $CaCl_2$ +1g $MgCl_2.6H_2O$ +7g agarose. Autoclaved and stored solid at room temperature.

Blocking Buffer: 0.1M $NaHCO_3$ (pH 8.6), 5mg/ml BSA, 0.02% NaN_3. Filter sterilized and stored at 4°C.

TBS: 50mM Tris-HCl (pH 7.5), 150mM NaCl. Autoclaved and stored at room temperature.

PEG/NaCl: 20% (w/v) polyethylene glycol-8000, 2.5M NaCl. Autoclaved and stored at room temperature.

Iodide Buffer: 10mM Tris-HCl (pH 8.0), 1mM EDTA, 4M NaI. Stored at room temperature in the dark.

SM Buffer: 5.8g NaCl, 2.0g $MgSO_4.7H_20$, 50ml 1M Tris-HCl (pH 7.5), 5ml of 2% gelatin solution, H_2O to 1L. Autoclaved and stored at room temperature.

Competing solution comprised 50µg atenolol (Sigma – A7655-1G, BN# 095K1644), 50µg sotalol (as hydrochloride, Sigma – S-0278, BN# 054K4074) per 1ml TBST. Competing solution was then stored in the dark in the fridge.

LB Medium: 20g/L of LB broth (Sigma – L3022-1KG) in ddH_2O with 0.5mM $CaCl_2$. (LB Broth is 10g Bacto-Tryptone, 5g yeast extract, 5g NaCl per litre.) Autoclaved and stored at room temperature.

LB/IPTG/Xgal Plates: 35g/L LB agar (Sigma – L2897-1KG) in ddH_2O with 0.5mM $CaCl_2$. (LB agar comprises 10g Bacto-Tryptone, 5g yeast extract.) Plates were stored in the dark at 4°C.

Propranolol was covalently attached to glass beads in-house by Dr. Jimmy Hedin-Dahlström using a method adapted from (Venter et al., 1972).

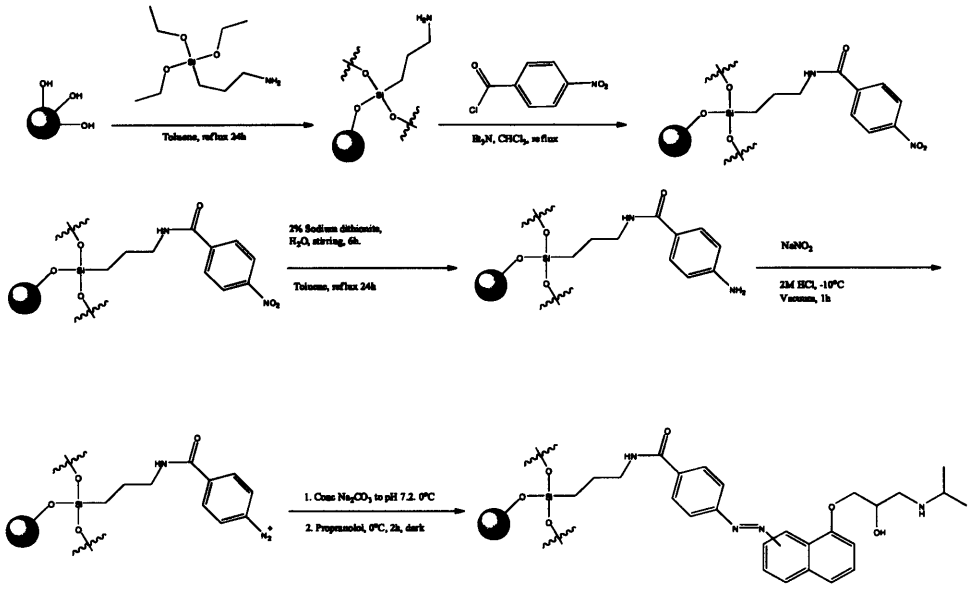

Figure 15: Reaction scheme for the coupling of propranolol to glass beads. Ref: J. Hedin-Dahlström (MRRU, WSP, Cardiff University) – personal communication.

Propranolol free base: *R/S*-Propranolol hydrochloride (500mg, Acros Organics – 207320050, BN#A0201432) was dissolved in distilled water (500ml). Sodium Hydroxide solution (1M) was added dropwise and a white precipitate was formed. The resulting mixture was vacuum-filtered using a 0.45µm-pore Whatman cellulose acetate filter. The filtrate was washed with distilled water and freeze-dried for 24 hours. The free base was stored in the dark with desiccation at 4°C.

2.2.2 Phage Amplification Procedure

An overnight culture of *E. coli* was centrifuged at 10,400G at 4°C for 10 minutes, the supernatant discarded and the pellet re-suspended in 20ml LB broth. A 3ml aliquot was placed into a sterile flask and diluted with

LB broth (17ml), therefore producing culture in an early log phase. The phage eluate was then added to this allowing overnight contact time at 37°C with vigorous shaking.

2.2.2.1 First Centrifugation Step

The culture was transferred to a centrifuge tube and spun at 10,400G at 4°C for 10 minutes. The supernatant was transferred to a fresh centrifuge tube and re-spun. This should result in near complete removal of *E. coli* from the system. The upper 90% of the supernatant was transferred into a fresh tube with 1/6 volume of PEG/NaCl, allowing phage precipitation at 4°C for at least 60 minutes.

2.2.2.2 Second Centrifugation Step

This mixture was then centrifuged at 10,400G at 4°C for 15 minutes, the supernatant discarded, re-spun for 30 seconds and the residual supernatant removed with a micro-pipette. The phage pellet was re-suspended in TBS (1ml), transferred to a micro-centrifuge tube and spun for 5 minutes at 4°C to pellet any residual bacterial cells. The supernatant was transferred to a fresh micro-centrifuge tube and re-precipitated with 1/6 volume PEG/NaCl, incubating on ice for at least 15 minutes.

This mixture was micro-centrifuged for 10 minutes at 4°C, the

supernatant discarded, re-spun for 30 seconds and residual supernatant removed with a micro-pipette. The phage pellet was re-suspended in 200µl TBS with 0.02% NaN_3. This was micro-centrifuged for one minute at 4°C to pellet any remaining insoluble matter and the supernatant transferred to a fresh tube and labelled as the amplified eluate.

2.2.3 Gene Sequencing of Identified Phage Clones

(Adapted from Pharmaceutical Cell Biology Welsh School of Pharmacy, Cardiff University Phage Display Protocol)

Individual phage plaques were removed from an agar plate and transferred into LB broth (3ml) where they were maintained for two hours at room temperature to allow diffusion of phage particles from the agar. *E. coli* culture (30µl) was then added and the tubes were incubated at 37°C with shaking for four to five hours. Samples of the cultures (1.5ml) were then placed into microcentrifuge tubes for sequencing. The remaining culture was retained and diluted with an even volume of glycerol and stored at -80°C.

The samples for sequencing were precipitated using PEG/NaCl (200µl) at room temperature for 10 minutes, centrifuged at 14,500G for 10 minutes and the supernatant discarded. The pellet was suspended in 4M iodide buffer (100µl) then absolute ethanol (250µl) was added. The

resultant mixture was incubated at room temperature for 10 minutes to precipitate single-stranded DNA.

The samples were then centrifuged at 14,500G for 10 minutes and the supernatant discarded. The pellets were washed gently in 70% ethanol and dried briefly under vacuum. Molecular biology grade water (30µl) was added to each pellet and incubated at 65°C for 15 minutes before being transferred to 96 well plates for storage at -20°C.

The plated samples were processed at the Psychological Medicine department at the University Hospital of Wales, Heath Park on a Beckman Coulter Agencourt machine using the AMPure kit (Beckman Coulter Genomics, Buckinghamshire, UK).

2.2.4 Panning Against Propranolol

2.2.4.1 Panning Against Propranolol Free-Base as Suspension

Four centrifuge tubes were incubated with blocking buffer (50ml) for at least one hour at 4°C. Blocking buffer was then discarded and the tubes washed six times rapidly in TBST (TBS with 0.1% v/v Tween-20). The final wash of TBST was discarded and replaced with fresh TBST (2ml) and nabumetone (50mg, Sigma – N6142-5G, BN#104K0801). Phage inoculate equivalent to $1x10^{11}$ plaque forming units (PFUs) was

then added, allowing contact time of one hour with orbital shaking at 150rpm.

This mixture was centrifuged at 10,400G at 4°C for 20 minutes. The supernatant was placed in the next centrifuge tube with competing solution (1ml) and propranolol (50mg as free base), allowing contact time of one hour with orbital shaking at 150rpm. This mixture was centrifuged at 10,400G at 4°C for 30 minutes and the supernatant discarded. The propranolol sediment was washed three times with TBST, centrifuging each time for 30 minutes as above.

After removal of the final TBST wash, glycine buffer at pH2.2 (6ml) was used to dissolve the propranolol and to disrupt the peptide binding of the phage. After five minutes contact time, PEG/NaCl (1ml) was added, allowing at least one hour contact time at 4°C. This mixture was centrifuged at 10,400G at 4°C for 20 minutes and the supernatant discarded, re-spun briefly and residual supernatant removed with a micro-pipette. The phage pellet was then re-suspended in TBST (500µl) and placed in the next centrifuge tube with TBST (1.5ml), competing solution (1ml) and propranolol (50mg as free base) to commence next sub-round as above.

After the third sub-round, the phage pellet was suspended in TBS (200µl) ready for amplification in *E. coli.*

2.2.4.2 Panning Against Propranolol Covalently Bound to Glass Beads

2.2.4.2.1 Standard Protocol

TBST (2ml) and glass beads functionalised with arylamines as shown in Figure 15 (10mg) were added to a pre-blocked centrifuge tube and phage inoculate added (2.2.4.1). After incubation for one hour at room temperature, this mixture was centrifuged at 10,400G at 4°C for 2 minutes. The supernatant was placed in the next pre-blocked centrifuge tube with competing solution (1ml) and propranolol beads (10mg), allowing contact time of one hour with orbital shaking at 150rpm. This mixture was centrifuged at 10,400G at 4°C for 2 minutes and the supernatant discarded. The glass beads were washed six times with TBST. After the final wash with TBST was removed, the beads were washed with glycine buffer at pH 2.2 (1ml). After five minutes contact time, the supernatant was removed and neutralised with neutralising buffer at pH 9.1 (200µl). This step was repeated for a further two washes. PEG/NaCl (1ml) was added to each glycine wash, allowing at least one hour contact time at 4°C. This mixture was centrifuged at 10,400G at 4°C for 20 minutes and the supernatant discarded, re-spun briefly and residual supernatant removed with a micro-pipette. The phage pellets were each re-suspended in TBS (200µl), and the third glycine wash was amplified in *E. coli* for the next round of panning.

An alternative experimental treatment was also devised in which phage were exposed to propranolol free base as insoluble complex, using the amplified eluate from the end of biopanning round one as input to an additional glass experiment, as summarised in Figure 16.

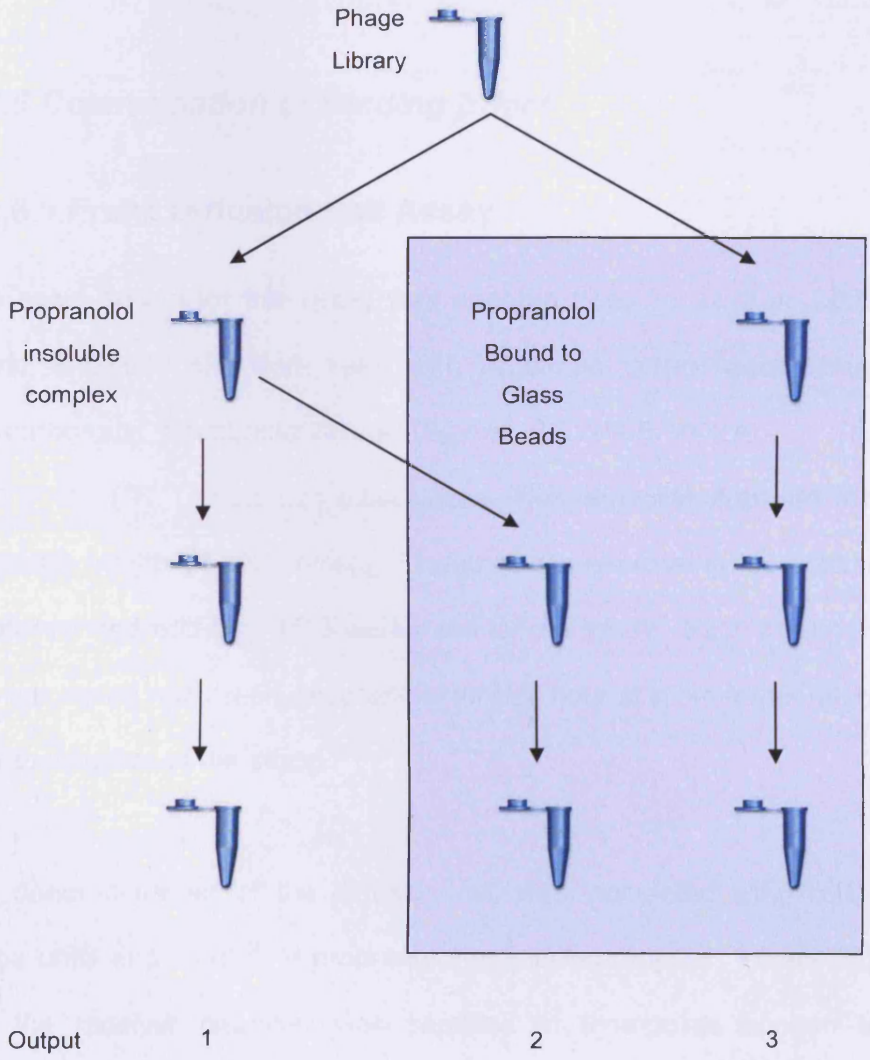

Figure 16: The passage of phage from library to output through various biopanning strategies.

2.2.4.2.2 Additional Protocol

When the protocols outlined in 2.2.4.2.1 did not appear to provide consensus binding clones, one additional biopanning protocol was developed in which the target remained propranolol covalently attached to glass beads, although biopanning was extended to five rounds, with the fourth and fifth rounds being treated with five glycine washes. All other details are as described in 2.2.4.2.1.

2.2.5 Determination of Binding Effect

2.2.5.1 Franz Diffusion Cell Assay

The basic design for this assay was adapted from Smith et al. 2007. Franz diffusion cells were used with Whatman 0.1μm track-etched polycarbonate membrane filters (Sigma, Z612405-100EA). DL-propranolol (^{3}H) (Amersham Biosciences, TRK495)) was supplied with a specific activity of 29Ci/mmole. Phage clones expressing the peptide of interest and wild-type M13 were used for this study. Each treatment was incubated with ^{3}H-DL-propranolol for one hour at room temperature prior to initiation of the study.

The donor chamber of the diffusion cell was inoculated with $1x10^{11}$ phage units and $1x10^{12}$ ^{3}H-propranolol molecules (approx. 1.6pmoles), and the receiver chamber was sampled at time-points chosen to represent the initial rate of flux and the subsequent level of equilibrium

(n=4).

This experiment was revisited several months later, with the same basic experimental setup but the replacement of the polycarbonate membrane with a Viskin dialysis membrane with molecular weight cut-off of 12,000-14,000 Da.

2.2.5.2 Side-by-Side Franz Cell Study

Two base units from the Franz cells were attached to each other such that both sides of the membrane could be stirred with magnetic stirrers (Figure 17).

One side of the system (the donor chamber) was loaded with 1.6nM ^{3}H-propranolol solution prepared as described previously (2.6ml) and the other side (receiver) was loaded with phage suspension (2.6ml) containing $1x10^{12}$ PFU/ml. The donor chamber was sampled at various time-points to observe depletion of the ^{3}H-propranolol. Sample volumes were replaced with TBS. The membrane employed was Viskin dialysis membrane with molecular weight cut-off of 12,000-14,000 Da.

Figure 17: "Side-by-side" Franz cell setup.

2.2.5.3 MDCK-1 Transport Study

Madin-Derby canine kidney (MDCK) cells were cultured to 70-80% confluence in DMEM-F12 containing 10% heat inactivated foetal bovine serum. Cells were seeded at a density of 4 x 10^5 cells.cm^{-2} onto Transwell® Clear culture inserts (6.5mm diameter, 0.4µm pore polyester membrane, Corning, Sigma Aldrich, Gillingham, UK) allowing five days in vitro time (IVT) for the formation of a confluent monolayer with well developed tight junctions. Transepithelial electrical resistance (TER) was measured using an endohm (World Precision Instruments, Florida, USA) daily from 48 hours IVT to ensure adequate barrier function of the monolayer.

In addition to ^{3}H-propranolol as the substance under test (which diffuses transcellularly), ^{14}C-mannitol (Sigma, 53mCi/mmol), a paracellular marker, was also employed thus monitoring the continued quality of the

intercellular tight-junctions.

Phage inoculation ($1x10^{11}$ PFUs, either biopanning-enriched clone or wild-type M13) was allowed one hour to equilibrate with ^{3}H-propranolol and ^{14}C-mannitol in TBS. This mixture (200µl) was placed in the apical chamber of the Transwell© insert, with serum-free media (Dulbecco's Modified Eagle's Medium (DMEM), Invitrogen, 42430-025.) in the basolateral chamber. Samples of 200µl were taken from the basolateral chamber at each time-point (0, 5, 10, 15, 20, 30, 40, 50, 60, 75, and 90 minutes) and the volume replaced with fresh DMEM. Each sample was placed in a scintillation tube to which was added Optiphase-Hisafe 3 (3ml, PerkingElmer, MA, USA), the radioactivity was then measured using dual-channel counting on a Tri-Carb 2900TR Liquid Scintillation Analyzer (Wolf Laboratories Ltd., Pocklington, UK).

2.2.5.4 Filter Centrifugation

A phage suspension was prepared in TBS to give $1x10^{11}$PFUs per ml. Phage suspension was allowed one hour to equilibrate with a 1:1 molar solution of ^{3}H-propranolol. The equilibrated mixture (500µl) was loaded into a Microcon centrifuge filter and spun at 500G for 30 minutes. The filtrate was then counted using Liquid Scintillation.

2.2.5.5 Propranolol Affinity for Experimental Materials

Experimental stock ^{3}H-propranolol was diluted to 0.4nM (1ml) and

placed in glass sample tubes. The materials were each added to the tubes and allowed to equilibrate for 24 hours at 37°C. Samples (200µl) were then taken from the solution to ascertain depletion of ^{3}H-propranolol. The samples were measured using Liquid Scintillation.

2.2.5.6 Microcentrifuge Tube Equilibrium Dialysis

The basic design for this study comes from (Reinard and Jacobsen, 1989). Briefly, the lid was cut from a microcentrifuge tube, inverted and filled with a pre-equilibrated 1:1 stoichiometric ratio of ^{3}H-propranolol and phage clones of interest or control (260µl mixture). Basic setup is illustrated in Figure 18: Basic microcentrifuge dialysis setup.

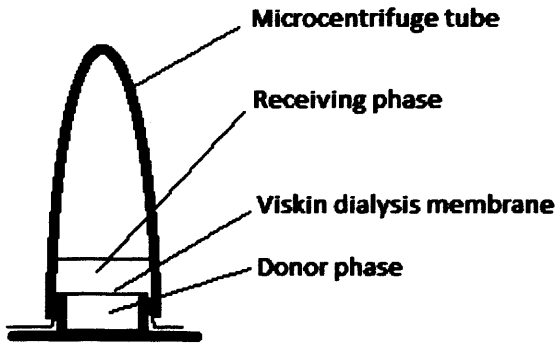

Figure 18: Basic microcentrifuge dialysis setup.

A section of Viskin dialysis membrane (MWCO: 12-14,000 Da) was placed over the lid and the body of the microcentrifuge tube was then replaced. Using a hypodermic needle, a small hole was made in the body of the tube through which was injected 260µl TBS. This dialysis

unit was then wrapped in parafilm and incubated at 37°C with orbital shaking at 100rpm for 24 hours. Experiments were performed in quadruplicate and the assay was verified by the inclusion of a positive control consisting of ^{3}H-propranolol and slices of polycarbonate membrane in the donor chamber.

2.3 Results and Discussion

2.3.1 Panning Against Propranolol

The phage populations at each stage in the panning were as should be expected, bearing in mind that the weakest binders and non-binders are removed before the glycine elutions in the washes with TBST. Each elution with glycine buffer then removes phage with progressively stronger binding affinities from the target. By the third glycine wash, only those with the greatest affinity should remain. However, in standard phage display protocol, the target would normally be washed six times with TBST. Whilst this was possible with the experiment that involved panning against propranolol covalently bound to glass beads, it was impractical to do this when panning against propranolol free-base as an insoluble complex. The reason for this is that each wash with TBST required centrifugation to re-sediment the base to allow removal of the supernatant, and even this was not always as efficient as would be expected as the propranolol had a tendency to readily resuspend at the slightest agitation.

Typical results are shown in Figure 19 demonstrating the relative numbers of phage recovered at each stage in the panning process.

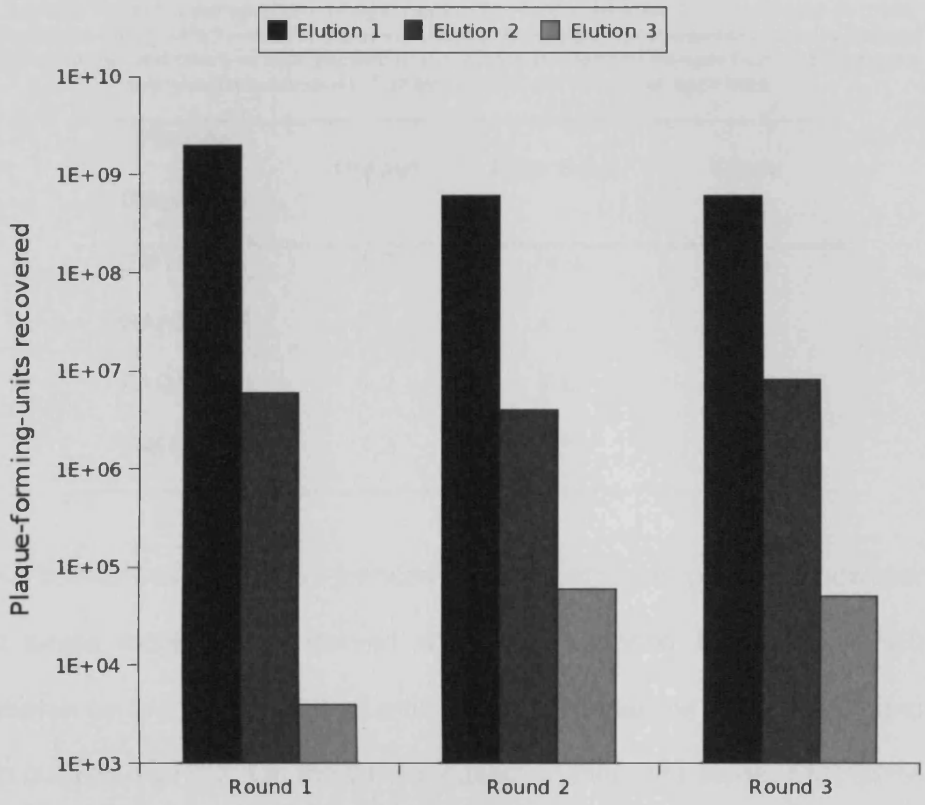

Figure 19: Number of plaque forming units recovered from each elution with glycine buffer pH 2.2 over three rounds of panning against propranolol free base as precipitate.

At the end of round one, only the third glycine elution was amplified for inclusion in the second round. This accounts for the decrease in numbers of phage present in the first glycine elution of round 2 and the increase observed in the third elution of round 2, which contained the enriched highest affinity binders.

Table 1: Peptides derived from phage display against propranolol. Table shows peptide sequence along with in which output number(s) the peptide was present (outputs defined in Figure 16) and the % of that peptide in the whole sequenced sample from the free base and glass experiments. Full structures are shown in Appendix 1.

Peptide Sequence	Output	Free Base	Glass
EMTSTRA	1,2	14.4	8.0
NANNRLY	1	4.1	Nil
PAQDPRY	1,2	1.0	4.0
QIKHRHM	1,2	4.1	4.0

No consensus binding sequences were observed in output 3, however a single clone was observed with the sequence EPRATST, which shares certain structural similarities with the sequence EMTSTRA found in outputs 1 and 2. On the whole, based on this data alone, EMTSTRA would seem to be the most promising peptide to take forward into the binding assessments, as it was present in the phage panning procedures against propranolol free base, and was enriched when free base-exposed phage were then exposed to propranolol-functionalised glass beads. EMTSTRA was present in the highest proportion in both free-base and glass experiments.

2.3.2 Demonstration of Binding

2.3.2.1 Franz Diffusion Cell Assay

During these experiments, a peptide-phage clone was incubated with the ligand, propranolol, in the apical chamber. If an interaction occurred

between peptide and propranolol the expectation was that a reduced amount of propranolol would be free for diffusion from the apical chamber across the semi-permeable membrane to the basal chamber. Sampling the receiving chamber in the diffusion cell system affords calculation of a rate of accumulation of propranolol. This rate of accumulation should be lower as the phage present in the donor chamber bind to the propranolol.

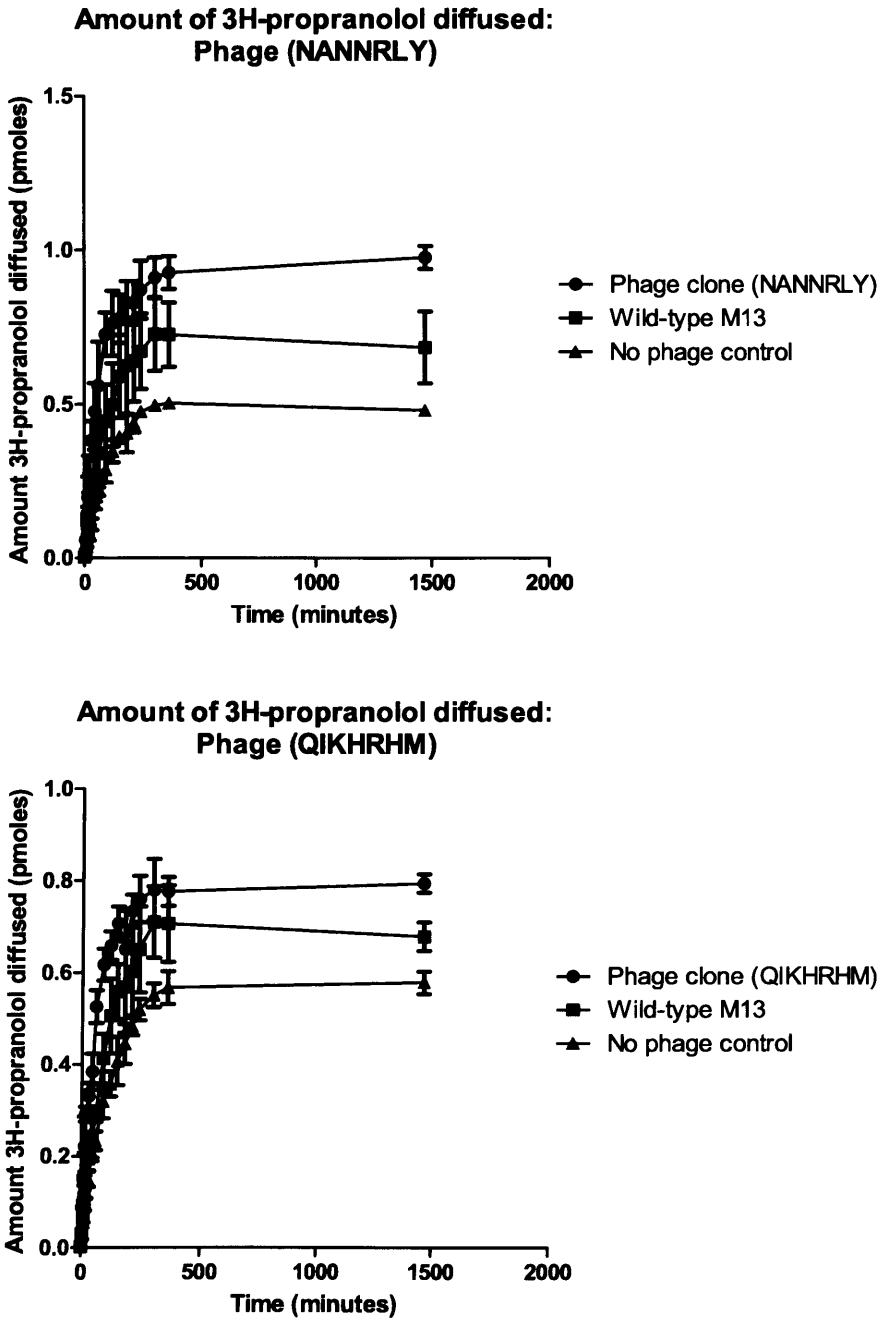

Figure 20: Franz cell diffusion pattern of 3H-propranolol through polycarbonate membrane (n=4±SD).

Figure 20 shows the diffusion of propranolol across polycarbonate membrane. In each case, a significant difference ($p<0.05$) was found

between the phage clone and the non-phage control. However, the difference is contrary to hypothesis, suggesting that the presence of the phage is somehow facilitating the diffusion of propranolol across the membrane. At the time, no logical reason could be proposed for this effect; therefore different binding assessment methodologies were employed.

When the Franz cell system was revisited several months later with a more thorough understanding of the materials involved, the polycarbonate membrane was replaced with Viskin dialysis membrane, thus greatly reducing the amount of propranolol lost in non-specific binding to experimental materials.

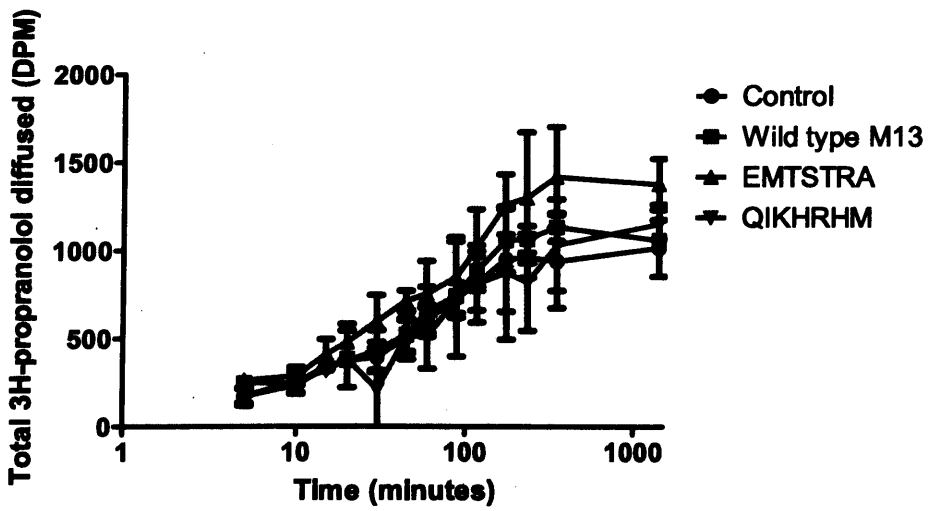

Figure 21: Franz cell diffusion pattern of 3H-propranolol through viskin dialysis membrane (n=4±SD).

Figure 21 shows the diffusion of propranolol across viskin dialysis membrane. Whilst there is the unusual effect of all phage treatments visually appearing to have enhanced propranolol transmission

compared to control, no statistically significant difference is found when comparing any of the treatments to control using one-way ANOVA and Dunnett's multiple comparison test.

This unusual diffusion pattern may have been, in part, related to the fact that only the receiving chamber was stirred in the conventional Franz cell setup. This could allow a layer of phage particles to build up on the donor side of the membrane, which may, in turn, affect propranolol diffusion. Therefore, the new "side-by-side" method was devised in which two Franz cell bases (with sampling arms) were clamped together to allow stirring of the phases on each side of the partition membrane (Section 2.1).

2.3.2.2 Side-by-Side Franz Cell Study

In this study, ^{3}H-propranolol was placed on one side of the membrane and phage inoculum was placed on the other. Therefore, the observation is of depletion of propranolol from the donor chamber over time.

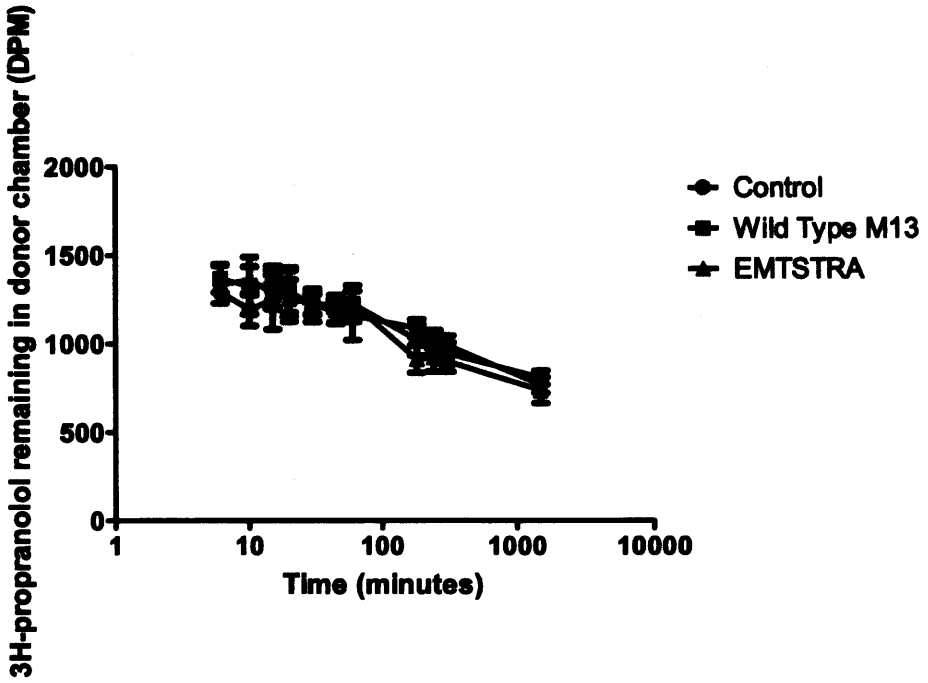

Figure 22: Diffusion of ^{3}H-propranolol from the donor chamber of a side-by-side Franz cell setup (n=4 ±SD).

This experiment still showed no significant difference ($p>0.05$) in the amount of propranolol diffused whether the receiving chamber contained phage clone, insert-less wild type M13, or control (blank TBS).

An interesting observation was made during the course of this experiment: the level of the liquid in the sampling arms either side of the membrane were equalised before the experiment began, yet, by the end of the experiment the level was consistently higher in the sampling arms that contained phage – whether library clone or wild type. This would suggest that the phage exert another force upon the system, possibly through an osmotic effect. The level of this osmotic effect would probably be irrelevant at higher concentrations of propranolol but

where the concentrations were in the nanomolar range it may have been sufficient to give rise to the observed phenomenon.

2.3.2.3 MDCK-1 Transport Study

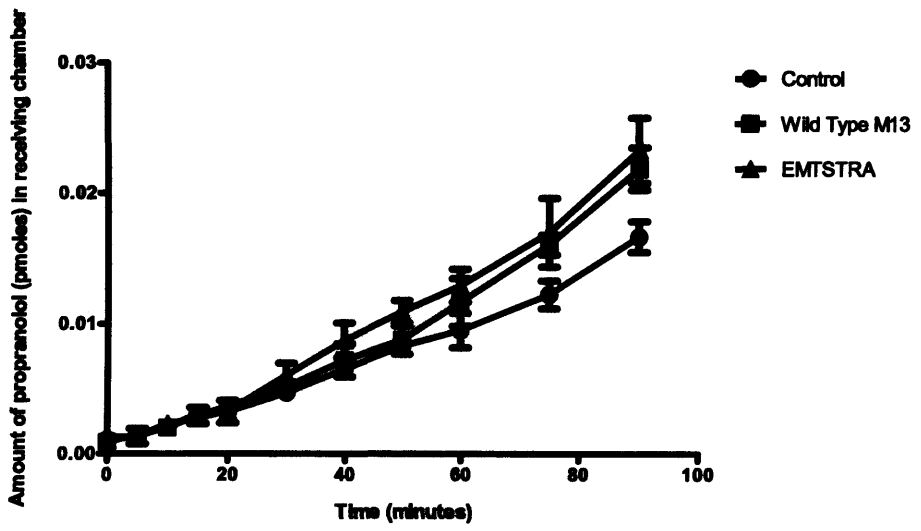

Figure 23: Total amount of 3H-propranolol diffused into receiving chamber when exposed to phage expressing the sequence EMTSTRA (n=4±SD).

As apparent from Figure 23, equilibrium was not reached over the course of the 90 minutes of sampling. The unusual artefact observed in the Franz cell experiment is also observed here, in that the greatest levels of flux appear to be associated with treatments containing phage.

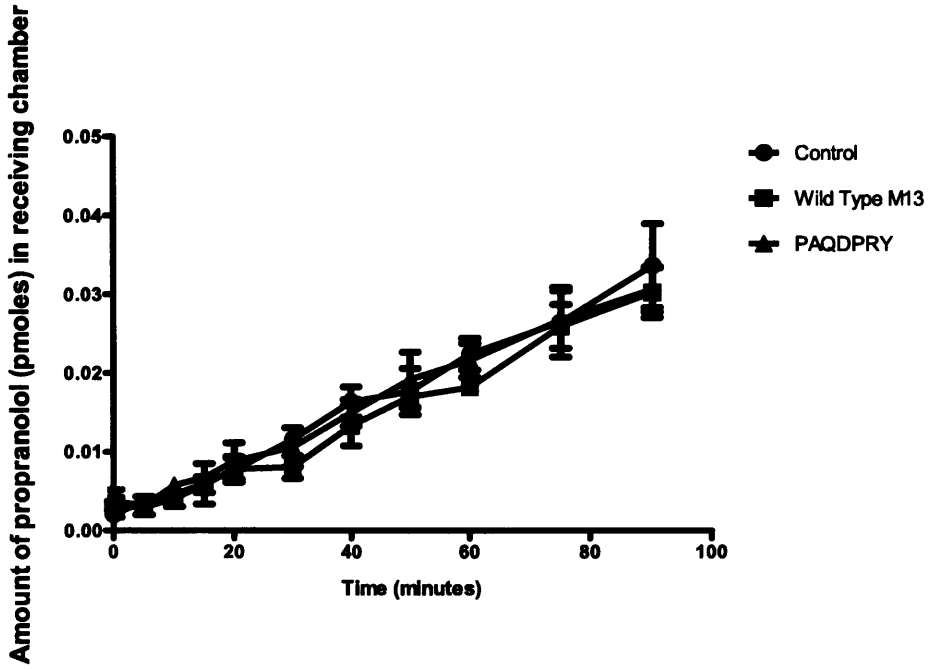

Figure 25: Total amount of 3H-propranolol diffused into receiving chamber when exposed to phage expressing the sequence PAQDPRY (n=4±SD).

Figure 24 shows only the first four time points from Figure 23.

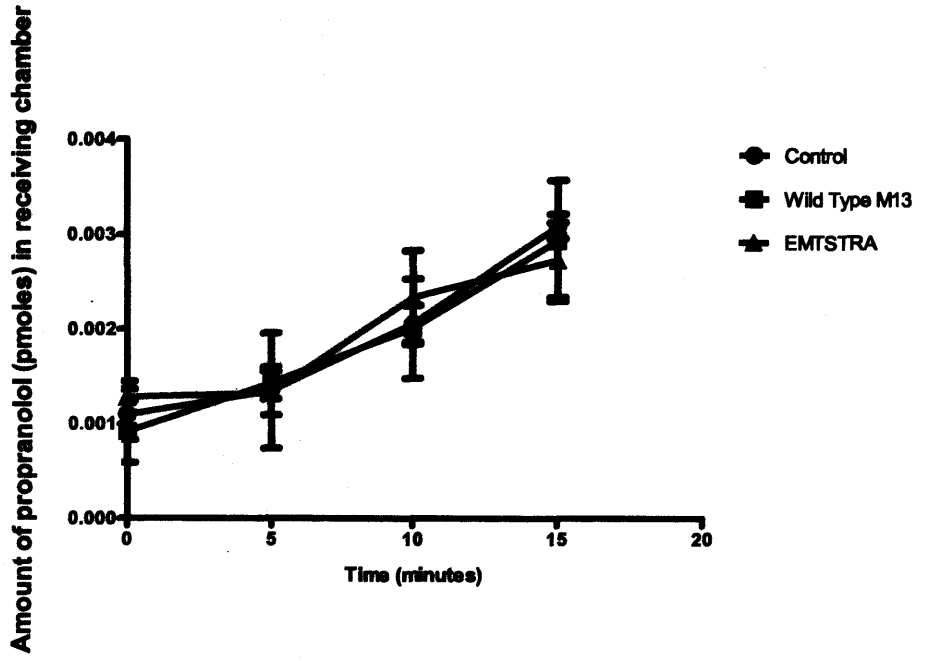

Figure 24: Total amount of 3H-propranolol diffused into receiving chamber when exposed to phage expressing the sequence EMTSTRA (n=4±SD). First four points only.

These data suggest that in the initial phase of propranolol transport through the MDCK-1 cells, there is no significant difference between wild-type phage, phage clone or control.

Figure 25 and Figure 26 show a repeat of the MDCK cell transport studies using a phage clone with a different peptide insert (PAQDPRY).

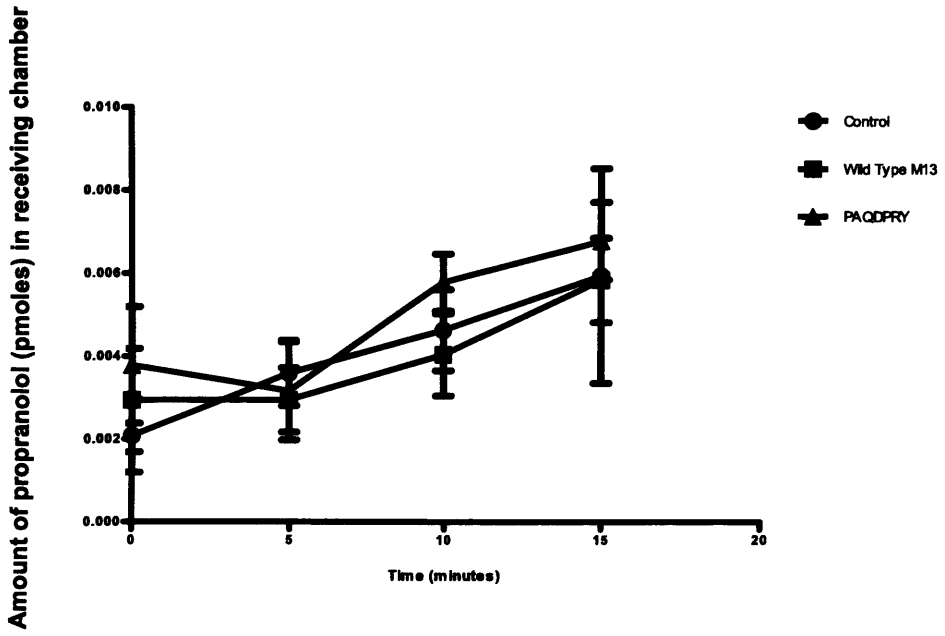

Figure 26: Total amount of 3H-propranolol diffused into receiving chamber when exposed to phage expressing the sequence PAQDPRY (n=4±SD). First four points only.

As in the previous experiment, there is no significant difference ($p>0.05$) between treatments in the transport of propranolol.

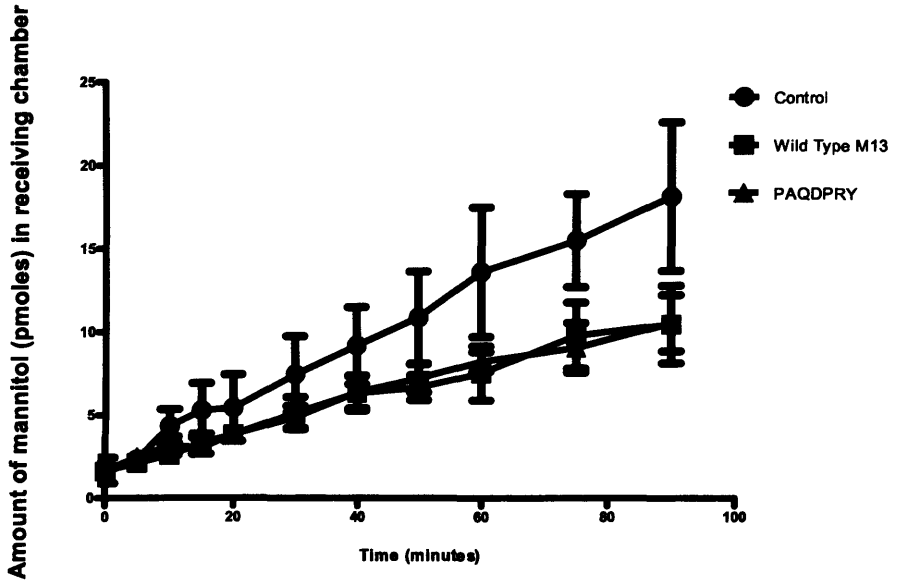

Figure 27: Total amount of 13C-mannitol diffused into receiving chamber when exposed to phage expressing the sequence PAQDPRY; mean and standard deviation shown (n=4±SD).

Whilst the permeability of the monolayer to mannitol appeared greater in the control group, which suggests that the presence of phage has affected the transmission of mannitol from the apical to the basolateral chamber, the difference is in fact not considered to be statistically significant ($p>0.05$).

Two further controls were carried out, but this time without the MDCK-1 cell layer. Thus, ^{3}H-propranolol was passed across the Transwell© insert alone (Figure 28).

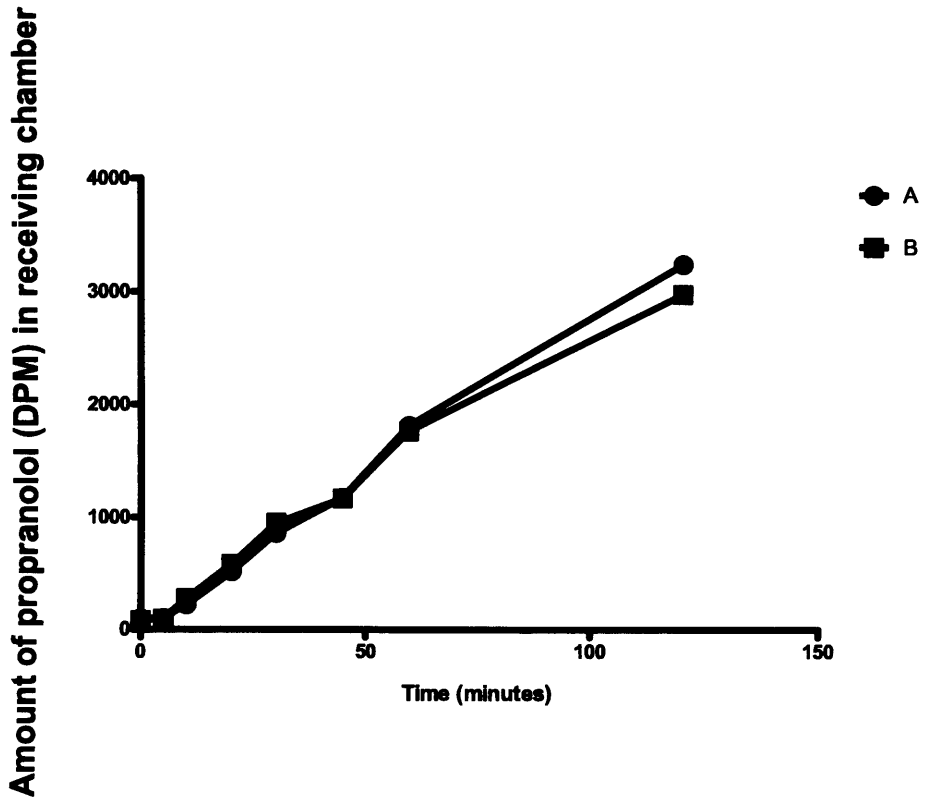

Figure 28: Amount of 3H-propranolol diffused across the Transwell© polycarbonate insert without the presence of MDCK cells.

With no cells to provide a barrier function, it was assumed that

equilibrium would be reached within a few minutes, although, as is evident from Figure 28, equilibrium had not yet been reached after two hours incubation. An important observation at this stage relates to the materials test shown later in Figure 31. The inserts in the Transwell© system are manufactured from polycarbonate, which was shown to bind a significant amount of propranolol (Section 2.3.2.5). The rate at which equilibrium is reached may be affected by this extra binding event.

2.3.2.4 Filter Centrifugation

In the first experiment, a 1:1 ratio of phage to ^{3}H-propranolol molecules was allowed to equilibrate, and then dosed into a Microcon microcentrifuge filter. Figure 29 shows the amount of propranolol that passed through the filter under each treatment.

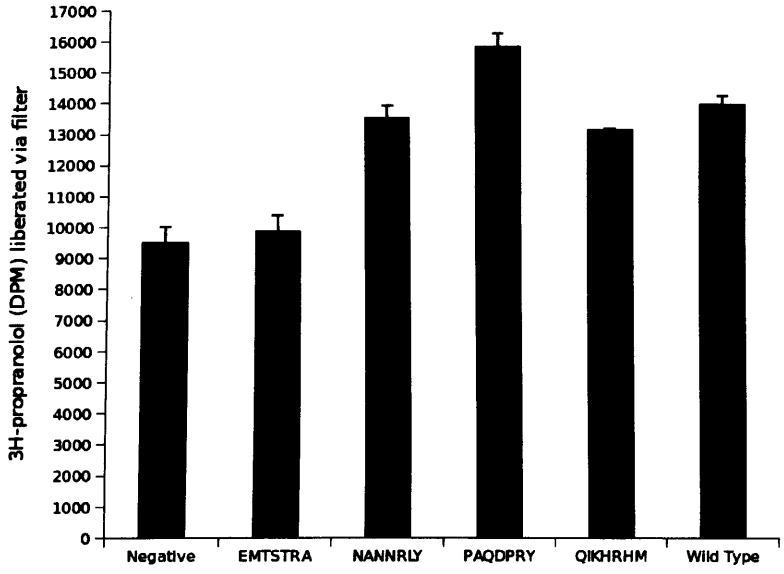

Figure 29: Propranolol (DPM) liberated by filter under each treatment (n=4±SD).

Much of the propranolol has been lost during this experiment; the initial

dose for each compartment was 26,000 DPM, although it is clear that the presence of the phage is causing an increase in the amount of propranolol passing through the filter under centrifugation. This is irrespective of whether the phage carries a peptide insert or is wild-type M13.

The experiment was repeated with one clone, increasing the ratio of phage to propranolol to 4:1. Figure 30 shows the results with the EMTSTRA clone clearly affording increased filtration of propranolol against control.

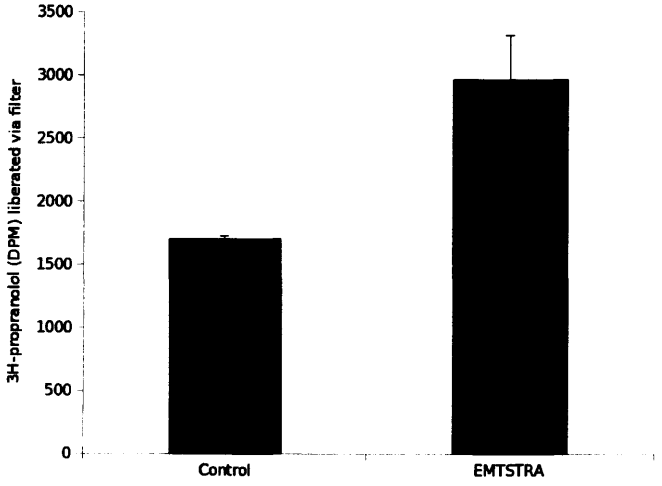

Figure 30: 3H-propranolol liberated via centrifuge filter. Four-fold excess of propranolol to phage was used (n=4±SD).

The filters in the microcentrifuge tubes used for the "filter centrifugation" experiments are regenerated cellulose with 100kDa molecular weight exclusion. The insert containing the filter is made of polycarbonate. Propranolol was shown (Figure 31) to bind extensively to polycarbonate

remove varying amounts of propranolol from solution: Diaflow removes only 0.40% of propranolol, Cellulose Nitrate removes 87.3%, Polycarbonate removes 40.98%, MSI removes 52.06%, Polypropylene removes 6.33%, Whatman filter paper #1 removes 34.58%, and Whatman filter paper #54 removes 41.22%.

After carrying out the above experiment, a further material was considered: Viskin dialysis membrane, shown in Figure 32.

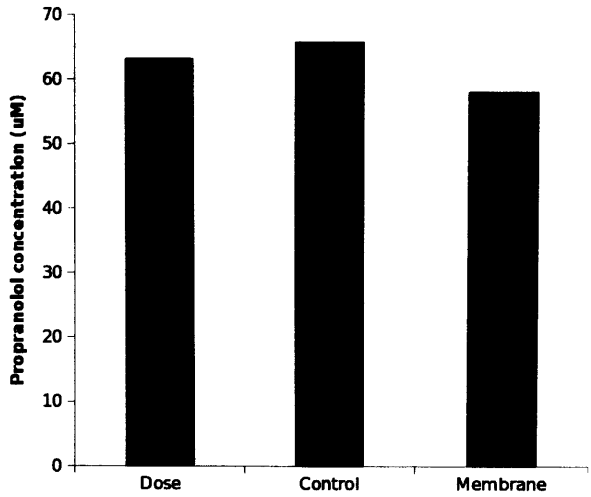

Figure 32: Depletion of 3H-propranolol from solution after 60 minutes incubation with Viskin dialysis membrane.

Although this experiment was carried out at a far higher concentration of propranolol than is used in the binding assays, it provided enough encouragement to continue with this membrane, as 88.1% of the propranolol remained free. This membrane was then used to perform the revisited Franz cell studies described in sections 2.2.5.1 and 2.3.2.1.

at low concentrations. It is apparent from the combined data that the phage compromise the filters in the microcentrifuge tubes, thus allowing a greater permeation of propranolol.

In short, most of the propranolol is removed from the system by non-specific binding with experimental components (membranes, membrane inserts), while the presence of phage in the system appears to increase the amount of propranolol passing through the filter. There is no evidence of selectivity, as the wild-type M13 provided the same effect as the biopanning-enriched clones.

2.3.2.5 Propranolol Affinity for Experimental Materials

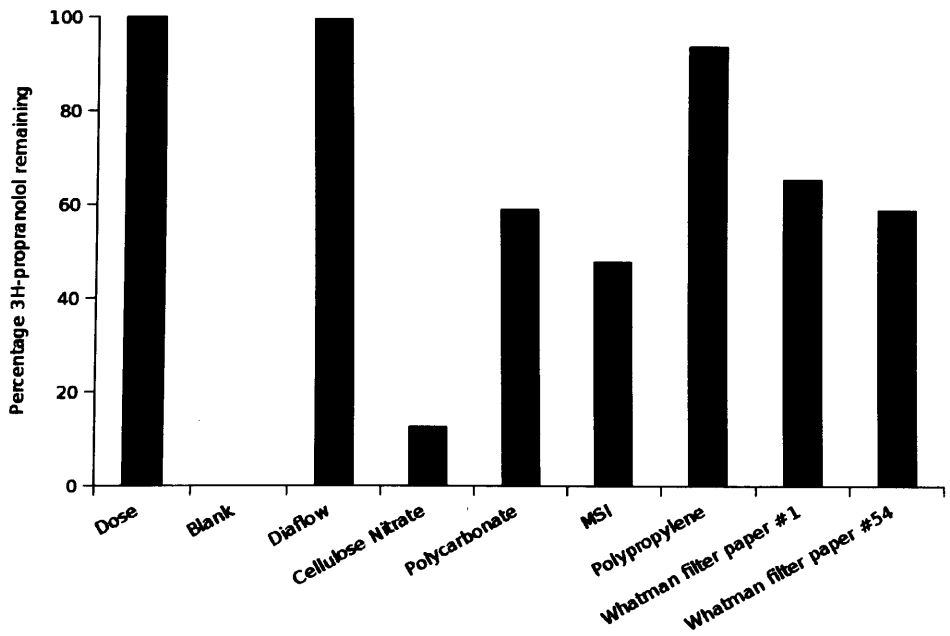

Figure 31: Percentage of the original 3H-propranolol dose recovered from solution after 60 minutes incubation with various materials.

After incubation with propranolol, the various materials were seen to

2.3.2.6 Microcentrifuge Tube Equilibrium Dialysis

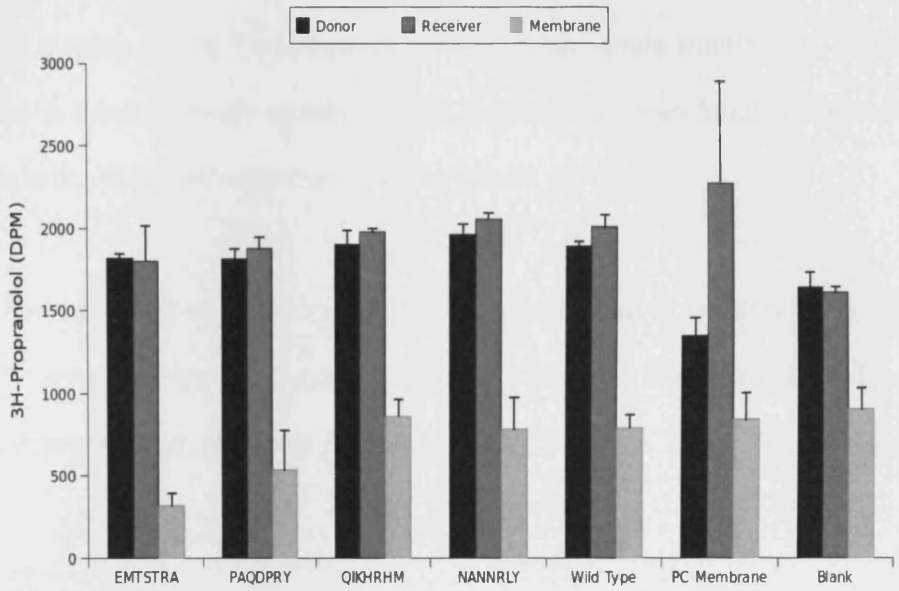

Figure 33: Diffusion of 3H-propranolol molecules in the presence of 1:1 ratio of phage particles, n=4±SD.

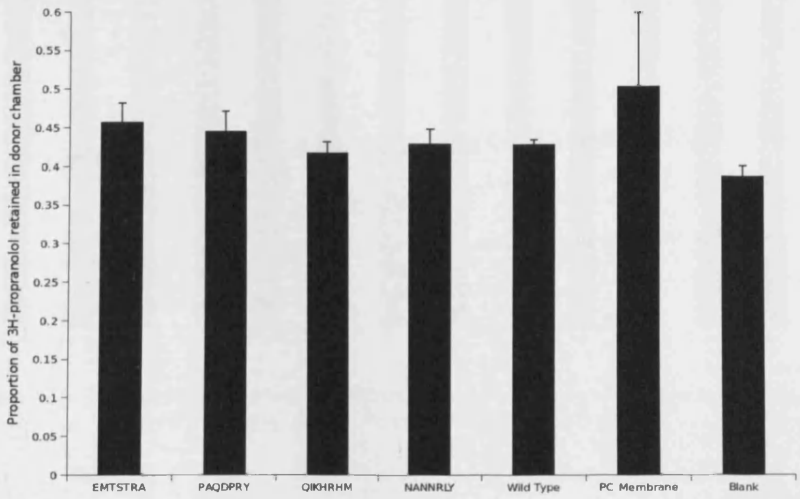

Figure 34: Proportion of 3H-propranolol found in the phage-containing chamber after 24 hours (1:1 ratio of phage particles to propranolol molecules). Polycarbonate membrane is included to demonstrate the effect of binding propranolol, n=4±SD.

These data clearly show no difference in the proportion of propranolol

free to diffuse to the receiving chamber between any of the phage treatments, which suggests that none of the four phage clones exhibit any binding effect. The treatment with polycarbonate membrane, which has previously been shown to bind propranolol, was found to have a statistically significant difference from blank ($p<0.05$).

After the modified biopanning procedure described in Section 2.2.4.2.2, 12 further clones were examined using the same microcentrifuge tube dialysis method, shown in Figure 35.

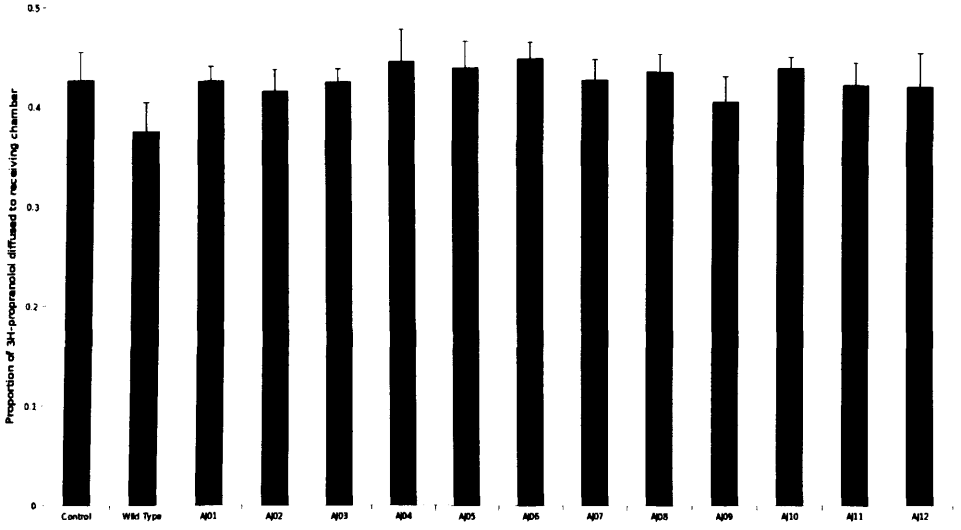

Figure 35: Twelve further clones examined using the microcentrifuge tube dialysis method using viskin dialysis membrane, (n=4±SD).

None of these clones have shown any significant difference in the diffusion pattern of ^{3}H-propranolol in any of the methods attempted, suggesting that the specific binding of phage clones to propranolol was

very limited. An important observation was that propranolol was shown to bind non-specifically to a range of materials. Therefore it is possible that further non-specific interactions, between propranolol and other phage components, may have been responsible for the absence of target selectivity.

2.4 Further Discussion

The construction of the experiment should have provided binding peptides with high affinity (due to the use of three to five glycine washes), and high specificity (due to the use of a pre-screening step with nabumetone and the presence of competing structurally related compounds).

As propranolol is only slightly soluble in water, the vast majority of the base will remain as an insoluble complex. However, as with most systems, equilibrium will exist in which some portion of the propranolol, however small, is always in solution. A limitation of panning against propranolol as an insoluble complex is the possibility that the peptides derived from this method bind more strongly to the surface presented by the insoluble propranolol complex as compared to individual propranolol molecules in solution. It is possible that some phage that displayed peptides that bound to propranolol in solution may have been excluded from further rounds of panning during the washes with TBST.

Fundamentally, the concept of phage display against low-molecular-weight compounds is sound, when due consideration is given for the properties of that compound. However, in hindsight, propranolol was a poor choice for target molecule due to the large hydrophobic region which partly is responsible for the high levels of non-specific binding observed in the materials test (section 2.3.2.5).

The principle aim of this chapter was to isolate from the PhD-C7C Phage Display Library a novel peptide capable of binding propranolol with high affinity and specificity. Several biopanning protocols were employed, and whilst some peptide-phage clones were enriched, no binding effect was observed despite use of multiple binding assay methodologies.

An important consideration is the choice of biopanning target. In this instance, a racaemic mixture of R/S-propranolol was used, which, when combined with the low molecular weight and few functional groups, may have contributed to the inability to isolate binding clones.

With the understanding that a target molecule is chosen diligently, phage display is a powerful tool for the isolation of high quality binding peptides. A good target molecule should have several functional groups, providing a unique "fingerprint" when exposed to the phage peptide. It

should also exhibit only a low level of non-specific binding to, for example, the plasma protein albumin. When considering drug molecules, warfarin (which is ~99% albumin-bound in the blood (Chan et al., 1994)) would be a poor choice, whereas sotalol (which is not albumin-bound (Carr et al., 1992)) would be far less likely to bind non-specifically to phage components or experimental materials.

2.5 Conclusions

In conclusion, whilst phage display has shown some success in the search for binding ligands to some low molecular weight drugs, namely paracetamol, dexamethasone, and more recently methotrexate, such a process may not be suitable for all small molecules. Work in subsequent chapters focuses on a peptide identified previously, aiming to tackle the challenges encountered upon the incorporation of the binding peptide into the polymer scaffold whilst retaining a conformation that favours binding.

Chapter 3

Texas Red and the binding peptide: TR401

"A wise man will make more opportunities than he finds."

Francis Bacon

3.1 Introduction

Sulforhodamine 101 acid chloride (Texas Red, Mw: 625), is widely used as a fluorescent agent to stain cell specimens and in other applications including fluorescent-activated cell sorting, immunohistochemistry, and fluorescence microscopy (Titus et al., 1982, Park et al., 2010, Lanier and Loken, 1984, Richardson et al., 2008). The acid chloride group on Texas Red provides the reactivity required to link the probe to amines or alcohols. As the free acid has essentially the same physicochemical properties as the acid chloride, and conjugation was not required, it was used throughout in these studies.

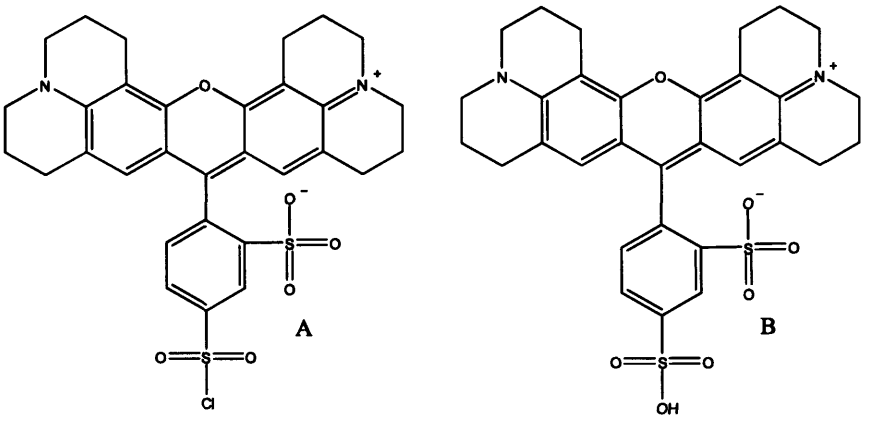

Figure 36: Sulforhodamine 101 acid chloride (Texas Red) (A), and sulforhodamine 101 (B).

The first stage in this assessment was to carefully establish the excitation and emission maxima for sulforhodamine 101 (SR) and determine whether the available filters for the BMG Labtech FLUOstar OPTIMA plate-reader used in earlier experiments were appropriate; then to construct calibration curves to assure linearity of the fluorescent response. A thorough investigation of the fluorescent properties of SR is presented in Appendix 2.

For the purposes of this study the peptide identified by Rozinov and Nolan (described in Chapter 1, section 1.2.5.4.2) (Rozinov and Nolan, 1998) TR401, was used with a minor modification (although, for ease of description, this modified peptide is still referred to as TR401): the C-terminus of the original peptide now hosts a glycine-glycine-glycine spacer followed by a terminal cysteine residue (Figure 37).

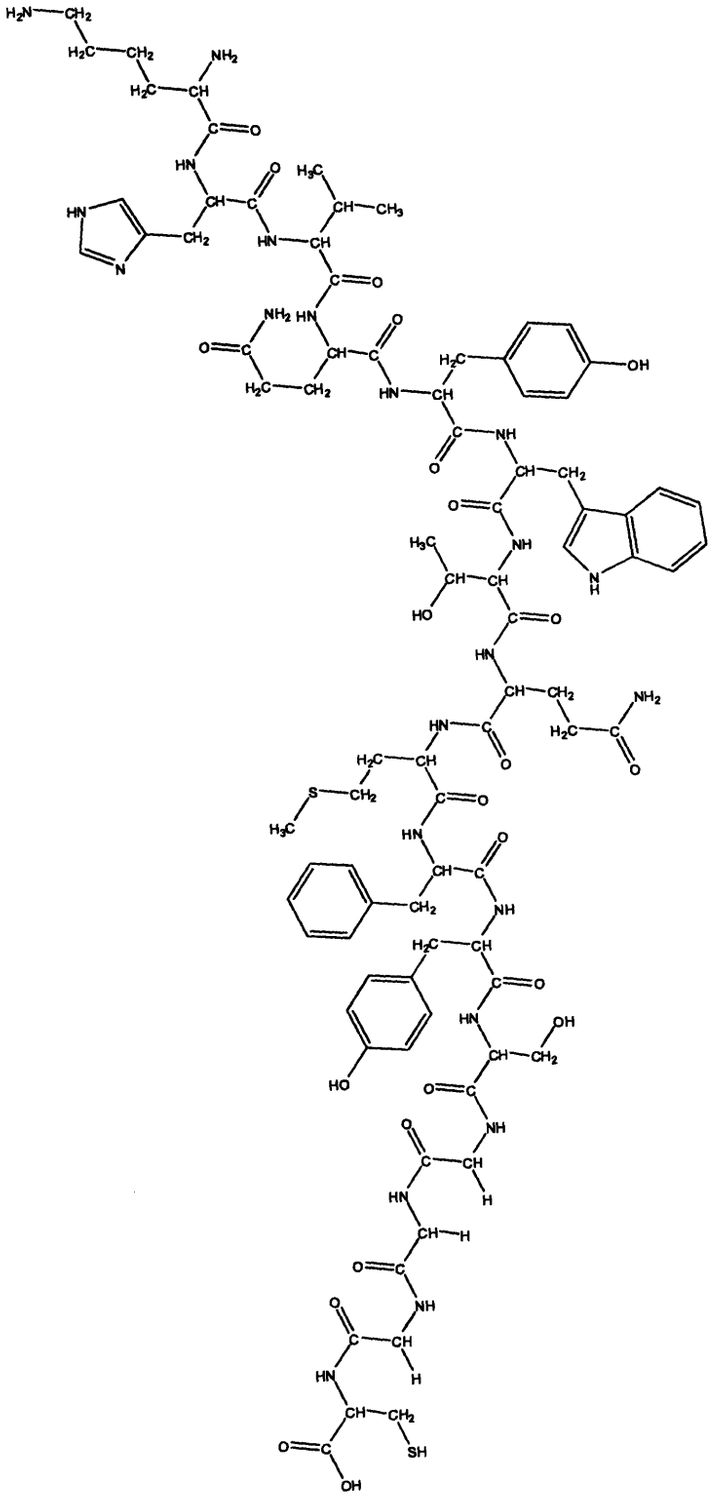

Figure 37: Structure of TR401 (KHVQYWTQMFYS) with the addition of three glycine and one cysteine residues to the C-terminus.

This provided specific functionality through which the peptide could be conjugated to solid supports. The N-terminus hosts the only two primary amines in the peptide while the C-terminal cysteine residue provided a unique sulfhydryl group.

After several failed attempts to demonstrate binding when TR401 was covalently attached to glass surfaces (Appendix 3), Merrifield Resin was chosen as a solid support for the attachment of the peptide via the C-terminal sulfhydryl group.

Merrifield Resin is a chloromethylated copolymer of styrene and divinylbenzene. Robert Bruce Merrifield developed the material (Merrifield, 1963) which he first described as an alternative approach to peptide synthesis.

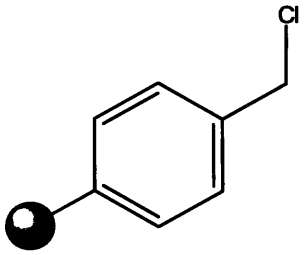

Figure 38: Merrifield Resin.

The methylchloride may be modified in several ways to add functionality to the resin to which a peptide may be attached, and subsequently, polymerisation may be established.

Sulfosuccinimidyl 4-[*N*-maleimidomethyl]cyclohexane-1-carboxylate

(Sulfo-SMCC, Figure 39) has been used extensively as a linking group in projects such as synthesis of dendrimer-antibody conjugates (Thomas et al., 2004) and peptide modification of surfaces for guided cell adhesion (Yu and Shoichet, 2005).

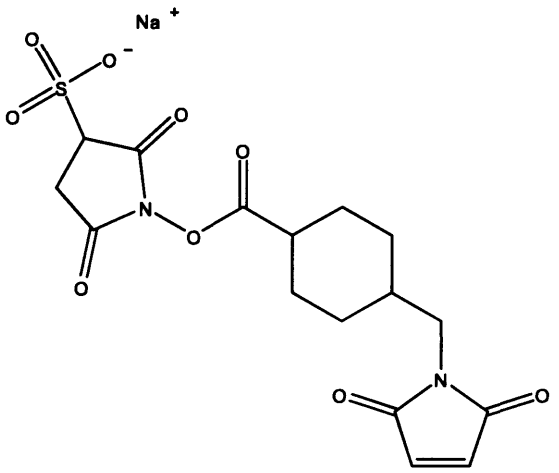

Figure 39: Sulfosuccinimidyl-4-[N]maleimidomethyl] cyclohexane-1-carboxylate (Sulfo-SMCC).

N-Hydroxysuccinimide (NHS) esters react with primary amines at pH 7-9 to form stable amide bonds. Maleimides react with sulfhydryl groups at pH 6.5-7.5 to form stable thioether bonds.

Before it was possible to proceed with the molecular imprinting aspect of the project, it was necessary to obtain a thorough understanding of the binding properties of the peptide, and also its limitations. With this in mind, the experiments in this section assessed Bmax and K_D for the SR-TR401 interaction in a range of solvents, and also the specificity of TR401 for SR.

The naphthyl group of naphthyl ethylenediamine (NED) Figure 40 exhibits a fluorescence spectrum that may shift if the primary amine reacts to form a stable amide bond (Sturgeon and Schulman, 1975).

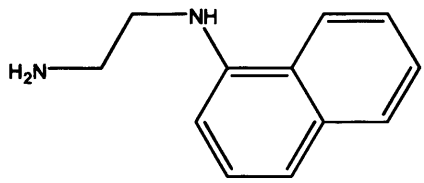

Figure 40: Naphthyl ethylenediamine (NED).

The first assay in this set assessed the binding of SR to TR401 in distilled water. In the second assay, water was replaced with TBS (pH 7.5) in order to assess the effect of pH or buffering capacity on binding. The third assay was intended to explore TR401 affinity for SR in ethanol, anticipating the use of ethanol in subsequent imprinting strategies. The fourth, fifth and sixth assays in this section looked at the specificity of TR401 for SR by challenging the peptide with the potential cross-reactants fluorescein, rhodamine 123, and rhodamine 6G (Figure 41).

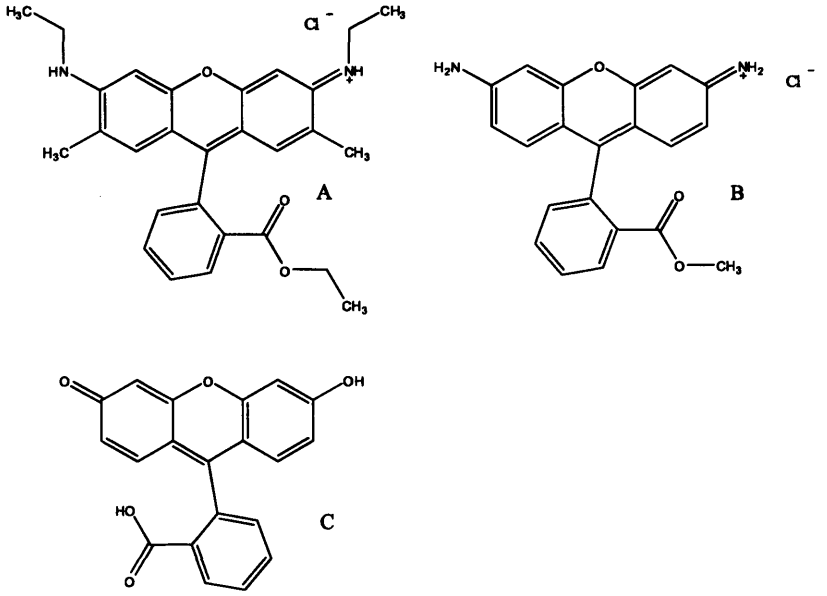

Figure 41: Rhodamine 6G (A), rhodamine 123 (B), and fluorescein (C).

The principle aim of this section of work was to develop a reliable and robust assay that would give consistent values for K_D and fully test the binding properties of TR401.

3.2 Materials and Methods

3.2.1 Linking chemistry

3.2.1.1 Solution Chemistry – 1

Solutions of (3-aminopropyl)triethoxysilane (APTES) or (3-mercaptopropyl)triethoxysilane (MPTES) (both Sigma-Aldrich, Gillingham, UK, catalogue numbers A3648-100ML and 63797-25ML-F, respectively) (1%) in ddH_2O were incubated with Sulfo-SMCC (Sigma, M6035, Schnelldorf, Germany) in saline buffered to pH 7 at room temperature for one hour with vigorous stirring.

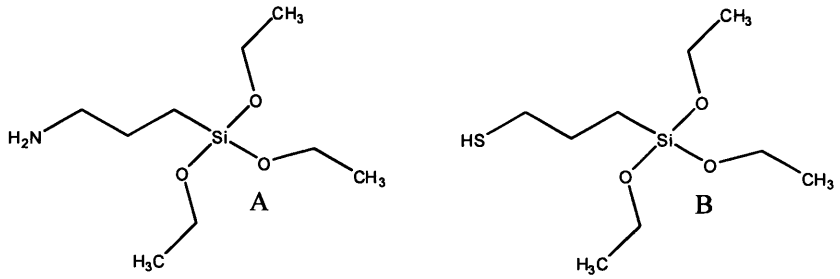

Figure 42: APTES (A) and MPTES (B).

The solutions were then treated with ninhydrin (Figure 43) (1% in acetone) or Ellman's reagent (Figure 44) (2mM in 50mM sodium acetate aqueous solution), respectively, and colour changes observed.

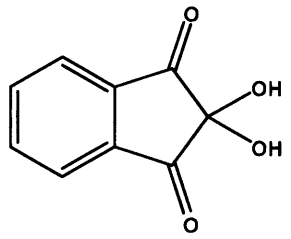

Figure 43: Ninhydrin (2,2-Dihydroxyindane-1,3-dione).

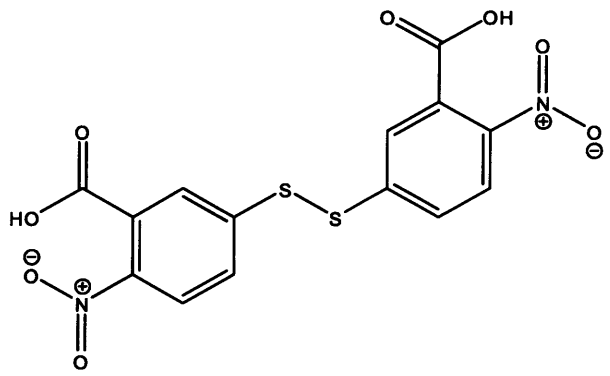

Figure 44: Ellman's reagent, (5,5'-dithiobis-(2-nitrobenzoic acid))

3.2.1.2 Solution Chemistry – 2

Naphthyl ethylenediamine (NED) was conjugated in solution to Sulfo-SMCC to confirm the effect demonstrated using the ninhydrin reaction described in 3.2.1.1.

A 1:1 molar ratio of NED and Sulfo-SMCC was dissolved in water (1μM) and incubated at room temperature for two hours with stirring. Excitation and emission fluorescence scans were performed prior to addition of the Sulfo-SMCC and at completion of the reaction.

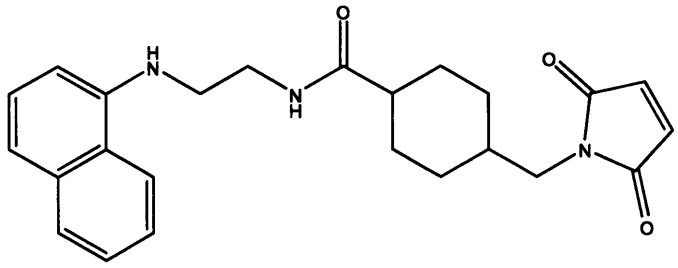

Figure 45: Conjugated product of NED with Sulfo-SMCC.

This experiment relied upon the fluorescence spectrum of the product (Figure 45) shifting from that of untreated NED by a sufficient margin to be detectable.

3.2.1.3 Peptide attachment to Merrifield Resin

Merrifield Resin (MR) (200-400 mesh, 1% cross-linked with DVB, 1.8-2.0 mmol Cl/g, Acros Organics – 349160500, BN#A0249177) was functionalised to express primary amines via azide reduction (performed in-house by J. Bowen). Briefly, MR was reacted with sodium azide in DMF at 70°C for 24 hours, followed by treatment with triflic acid in dichloromethane at 0°C for one hour. The amine-functionalised MR was suspended in distilled water at 10mg/ml, of which 0.5ml was added dropwise to a solution of Sulfo-SMCC (2ml of 1mg/ml). This was maintained at room temperature with stirring for one hour. The resin was then centrifuged at 10,400G for 5 minutes and the supernatant removed. The resin was then washed twice in distilled water (2ml) to remove any unreacted Sulfo-SMCC.

The resin was re-suspended in 0.5ml distilled water, of which 100µl was

added slowly to 2ml TR401 solution in distilled water (0.5mg/ml). This was maintained at room temperature with stirring for one hour, washed twice with 2ml of distilled water, and then re-suspended in 1ml distilled water. Functionalised resins were stored at 4°C and used within 48 hours.

A solution of TR401 was prepared in distilled water for which a UV absorption scan was acquired. This solution was then used in the linking reaction with functionalised Merrifield Resin, and the reaction mixture scanned again. It was assumed that the difference between the two readings illustrates a loss of peptide from solution to the resin.

3.2.2 Development of Binding Assay Protocol

3.2.2.1 Calibration using polypropylene plates

Standard solutions of SR in distilled water were prepared ranging from 100nM to 4000nM. Aliquots (200µl) were then placed into a black polypropylene 96-well plate (Nunc, Thermo Scientific) and read using a FLUOstar OPTIMA (BMG Labtech, Offenburg, Germany) (Ex 544nm; Em 590nm). Two replicates of each concentration were examined.

3.2.2.2 Excitation and emission scans of sulforhodamine 101

A solution of SR (150nM) was prepared in distilled water and scanned using an Aminco-Bowman Luminescence Spectrometer (Thermo

Spectronic, Madison, WI). An excitation scan from 450nm to 590nm was performed, measuring the intensity of fluorescence emitted at 603nm. An emission scan from 560nm to 700nm was performed using an excitation wavelength of 544nm (gain=750V).

3.2.2.3 Fluorescence Titration

Solutions were prepared of SR (0.2mM) and TR401 (0.2mM). The SR solution was mixed with distilled water in equal parts and this was used as the starting solution (now 0.1mM). The TR401 solution was mixed with the initial SR solution in equal parts and this was used as the titration solution (now 0.1mM SR and 0.1mM TR401).

Amounts and concentrations of each compound are shown in Table 2 including monomer-to-template (M/T) ratio, which allows an indication of the number of peptide molecules present for each molecule of SR.

Emission intensities at each addition were observed using the Luminescence Spectrometer using excitation and emission wavelengths of 585nm and 603nm, respectively (gain=1020V).

Table 2: Volumes added and resultant monomer: template ratio of titration experiment with SR and TR401.

	Addition (µl)	Total vol (µl)	[SR] µM	[TR401] µM	M/T ratio
1	0	500	0.1	0	0
2	0.5	500.5	0.1	0.100	1.00
3	0.5	501	0.1	0.200	2.00
4	0.5	501.5	0.1	0.299	2.99
5	0.5	502	0.1	0.398	3.98
6	1	503	0.1	0.596	5.96
7	1	504	0.1	0.794	7.94
8	1	505	0.1	0.990	9.90
9	2	507	0.1	1.381	13.81
10	2	509	0.1	1.768	17.68
11	3	512	0.1	2.344	23.44
12	5	517	0.1	3.288	32.88
13	10	527	0.1	5.123	51.23
14	20	547	0.1	8.592	85.92
15	30	577	0.1	13.345	133.45
16	40	617	0.1	18.963	189.63
17	50	667	0.1	25.037	250.37

3.2.2.4 Merrifield Resin Titration

A solution of SR in water (10nM) was placed in a microcentrifuge tube, to which resin was added gradually in small increments. The resin was

present in a suspension of 1µg/µl in water. Cumulative amounts added were 0, 1, 3, 5, 10, 15, 20, and 25µg. Treatments used were "No Resin", "Untreated Resin", "Amine-functionalised Resin", "Sulfo-SMCC-functionalised Resin", and "TR401-functionalised Resin"; n=4. Tubes were spun at 10,400G for five minutes, and then the supernatant was scanned at excitation and emission wavelengths of 585nm and 603nm, respectively. The supernatants were then returned to the tubes for the next addition of resin.

3.2.2.5 Effect of Incubation Time on Binding

Solution of SR in water (10nM - 1ml) was placed in a microcentrifuge tube, to which 25µg resin was added. The samples were spun at 14,000rpm for five minutes, and then the supernatant was examined using an Aminco-Bowman Luminescence Spectrophotometer using excitation and emission wavelengths of 585nm and 603nm, respectively. The supernatants were then returned to the tubes and vortexed thoroughly. The process was repeated over a period of two hours to assess the consistency of the binding event over time. Treatments used were "No Resin", "Untreated Resin", "Amine-functionalised Resin", "Sulfo-SMCC-functionalised Resin", and "TR401-functionalised Resin".

3.2.3 Final Titration Protocol and Binding Assays

Resin suspension (25µl of 1mg/ml) was placed in microcentrifuge tube

and made up to 125µl with distilled water. A solution of SR (330nM) was then added by small increments (volumes ranging from 10µl to 100µl, summarised in Table 3), thus gradually increasing the amount of SR available to the resin. Treatments used were "No Resin", "Untreated Resin", "Amine-functionalised Resin", "Sulfo-SMCC-functionalised Resin", and "TR401-functionalised Resin"; n=4. Tubes were spun at 10,400G for five minutes, and then the supernatant was examined using an Aminco-Bowman Luminescence Spectrophotometer using excitation and emission wavelengths of 585nm and 603nm, respectively. The supernatants were then returned to the tubes, which were vortexed thoroughly for the next addition of SR solution.

Table 3: Example of SR additions during a binding assay; starting volume is 125µl resin suspension to which 330nM SR solution is added.

Volume added (µl)	Cumulative addition (µl)	Total volume (µl)	Cumulative SR addition (moles)	Concentration (nM)
0	0	125	0	0
10	10	135	3.3 E-12	24.44
10	20	145	6.6 E-12	45.52
10	30	155	9.9 E-12	63.87
20	50	175	1.65 E-11	94.29
20	70	195	2.31 E-11	118.46
50	120	245	3.96 E-11	161.63
50	170	295	5.61 E-11	190.17
50	220	345	7.26 E-11	210.43
100	320	445	1.056 E-10	237.30

3.3 Results and Discussion

3.3.1 Linking Chemistry

3.3.1.1 Solution Chemistry – 1

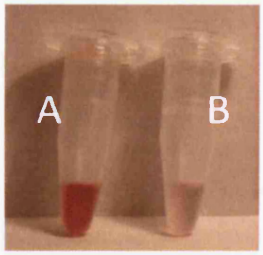

Figure 46: APTES reaction with ninhydrin (A) compared with APTES-Sulfo-SMCC product reacted with ninhydrin (B).

In Figure 46, tube A contains free APTES reacted with ninhydrin. Tube B contains APTES that was reacted with Sulfo-SMCC for one hour at room temperature, and then treated with ninhydrin. The reaction of amines with the cross-linker shows no colour change with ninhydrin treatment, illustrating that the primary amine group has been reacted successfully with the NHS-ester of Sulfo-SMCC.

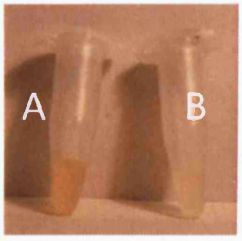

Figure 47: MPTES reaction with Ellman's (A) compared with MPTES-Sulfo-SMCC product reacted with Ellman's (B).

In Figure 47, tube A shows free MPTES treated with Ellman's reagent. Tube B contains MPTES that was reacted with Sulfo-SMCC for one

hour at room temperature, and then treated with Ellman's reagent. Prior reaction of sulfhydryls shows no colour change with Ellman's treatment, illustrating the successful conjugation of MPTES to Sulfo-SMCC through reaction with the maleimide group.

3.3.1.2 Solution Chemistry – 2

Figure 48 shows the shift in excitation and emission spectra of NED after reaction with Sulfo-SMCC, the former shifting from 372nm to 369nm, with the latter shifting from 427nm to 433nm.

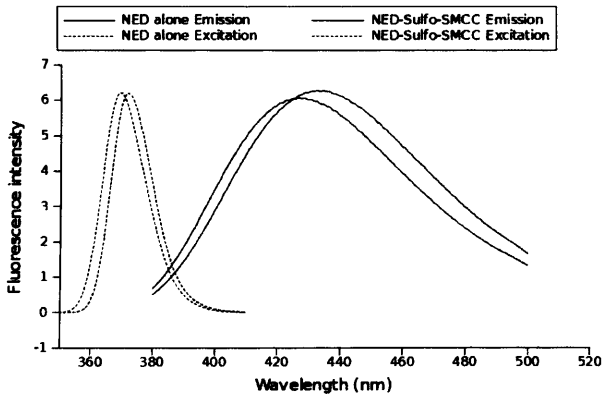

Figure 48: Spectral shifts observed when comparing untreated NED with NED-Sulfo-SMCC conjugate.

The linking chemistry performed in solution illustrated that Sulfo-SMCC was capable of reacting with both sulfhydryl groups and amines as hypothesised, in which free amines present on APTES were rendered non-reactive with ninhydrin after their exposure to Sulfo-SMCC, likewise, MPTES with Ellman's reagent. Also, the excitation and emission spectra of NED were altered following conjugation to Sulfo-SMCC. This provided the confidence to take Sulfo-SMCC forward into peptide-conjugation steps.

3.3.1.3 Peptide attachment to Merrifield Resin

Initially, TR401 (2mg) was dissolved in distilled water (2ml). UV absorbance was measured both before and after incubation with the surface-activated resin, which indicated that ~0.5mg TR401 was loaded to the surface of 2mg resin.

3.3.2 Development of Binding Assay Protocol

3.3.2.1 Calibration using polypropylene plates

The relationship between the fluorescence emission intensity and concentration of SR was shown to be non-linear (Figure 49). Since this was not expected, a number of experiments were carried out in order to eliminate systematic error, e.g. pipetting errors. Previous studies have not made reference to this non-linear response (Miyaki et al., 2005, Kumemura et al., 2005), although other studies have raised dispute over the quality of calibration standards (Kurebayashi et al., 1993, Westerblad and Allen, 1994). So this raises the question as to whether it is correct to fit a straight line to the calibration standards, or to use a polynomial expression.

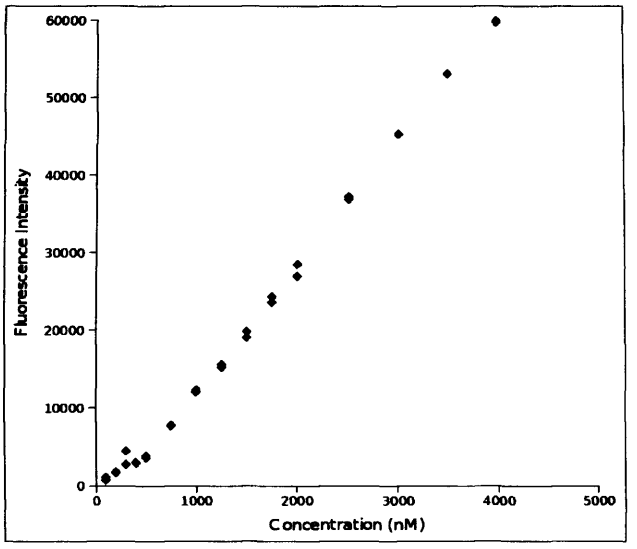

Figure 49: The fluorescence associated with solutions of sulforhodamine 101 in water. Filters used were Excitation at 544nm and Emission at 590nm. Each point is an individual sample.

Although fluorescence quenching at high concentrations is well documented (Williams and Bridges, 1964) this low concentration biphasic effect is less common although it has been observed with some other fluorophores (Krezel and Maret, 2007).

There are a number of possible explanations, including the potential that complexes of SR are formed which fluoresce differently from the individual molecules. These complexes may only form once a critical concentration is reached, resulting in the curve at low concentrations, then the linear region thereafter.

3.3.2.2 Excitation and emission scans of sulforhodamine 101

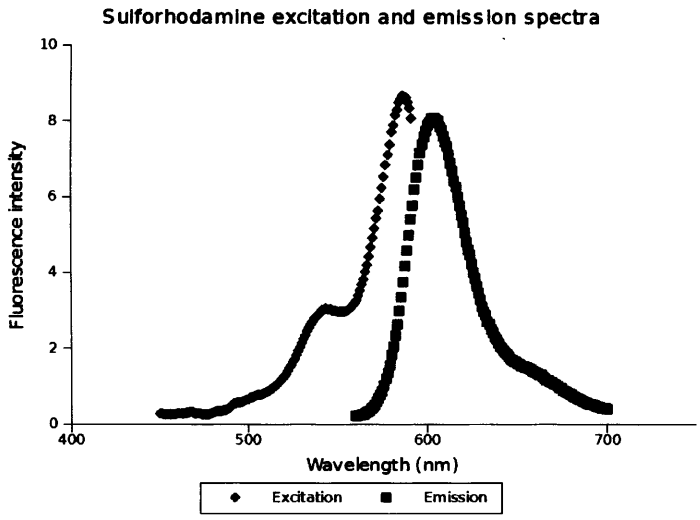

Figure 50: Excitation and emission spectra of sulforhodamine 101 in water.

Excitation and emission maxima were determined as 585nm and 603nm, respectively. The filters available for the FLUOstar OPTIMA were therefore not appropriate for accurate quantification of low levels of SR. In subsequent studies fluorescence was measured using the Aminco-Bowman Luminescence Spectrophotometer as the required wavelengths could be set manually.

3.3.2.3 Fluorescence Titration

Over the course of the experiment it is obvious from Figure 51 that there is some element of quenching as fluorescent intensity drops. There is also a shift in the emission peak from the initial 602nm to 607nm. Such a shift in peak emission wavelength indicates an interaction occurring between the fluorophore and another compound (Hunt and Ansell, 2006).

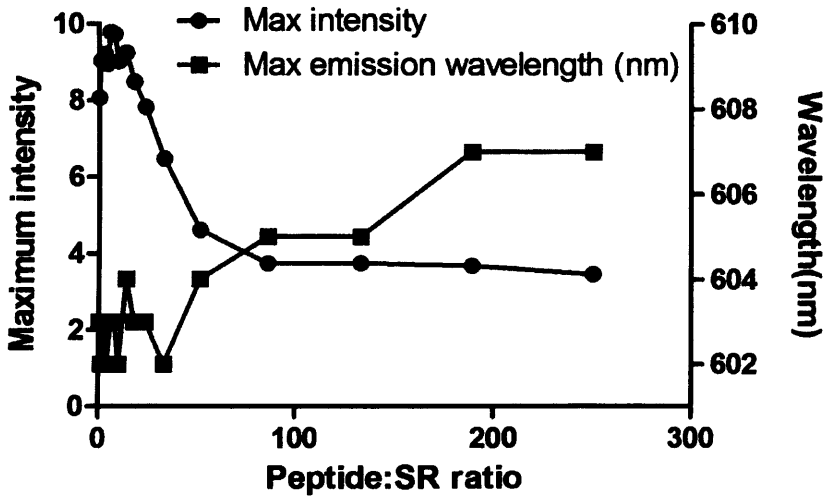

Figure 51: Fluorescence intensity and maximum emission wavelength change as peptide to SR ratio increases.

After an initial increase, the emission intensity tails off rapidly. This quenching effect is also likely to be the result of a direct interaction of SR with TR401. Close proximity of the two moieties results in hindrance of the passage of light to/from the fluorophore. It is therefore reasonable to suppose that there is some form of molecular interaction occurring between the two compounds in solution.

3.3.2.4 Merrifield Resin Titration

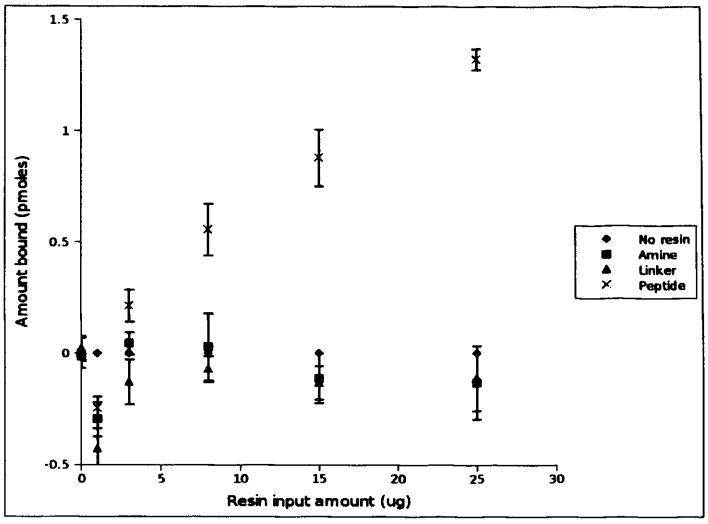

Figure 52: Amount of sulforhodamine 101 bound from aqueous solution upon exposure to increasing amounts of Merrifield Resin.

From Figure 52, the TR401-functionalised resin caused a significant depletion in SR from solution, whereas there was no apparent change in the amount of SR bound to control resins. This clearly demonstrates a concentration-dependant binding event between SR and TR401, whilst there is no difference between any of the controls. Four replicates of each treatment were performed, resulting in a total use of 100µg resin at the end of the assay. As the functionalised resin was a precious commodity, it was decided not to continue past this quantity, as a treatment of 25µg was sufficient for a large difference to be observed.

3.3.2.5 Effect of Incubation Time on Binding

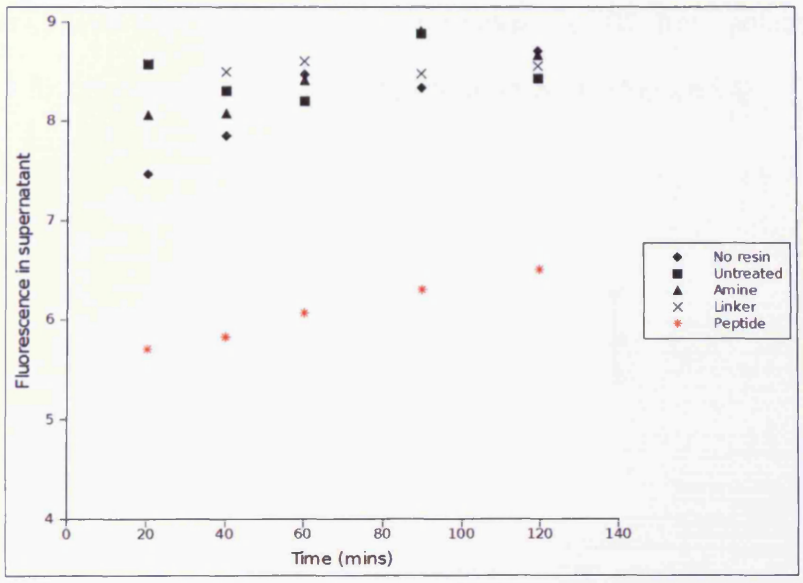

Figure 53: Fluorescence associated with sulforhodamine 101 free in solution after contact with functionalised Merrifield resin over time; n=1.

The level of SR binding to TR401-functionalised resin reduced over time (Figure 53). This could be due to a time-dependant hydrolysis of the peptide, resulting in lower availability of binding sites. Therefore, in further work, binding was assessed as soon as practicable: less than 10 minutes. No binding was observed to control resin.

3.3.3 Binding Assays

An assay was performed to determine binding of SR from solution by TR401-functionalised MR from suspension in water (Figure 54).

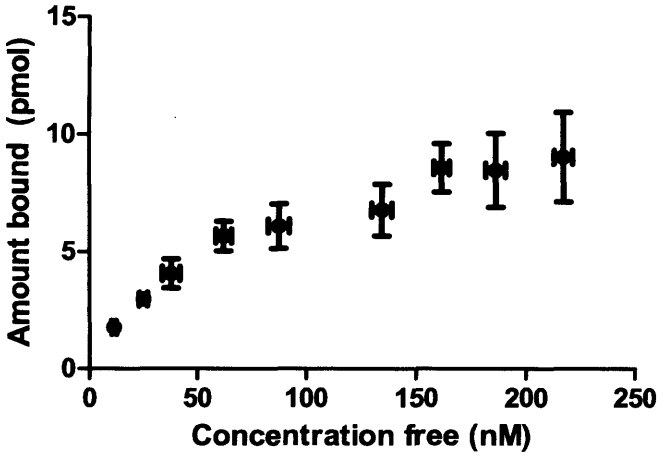

Figure 54: Amount of sulforhodamine 101 bound from aqueous solution by 25μg of TR401-functonalised Merrifield Resin (n=4±SD).

Non-linear regression analysis using GraphPad Prism version 5.00 yielded values for K_D and Bmax of 74.87nM and 11.87pmoles, respectively, where the model used was:

$$Bound = \frac{Bmax \times C}{K_D + C}$$

A further assay sought to assess the binding when water was replaced with TBS (Figure 55).

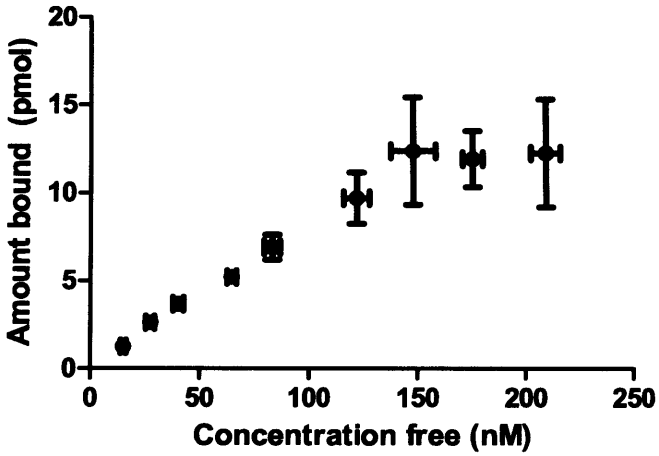

Figure 55: Amount of sulforhodamine 101 bound from TBS by 25μg of TR401-functonalised Merrifield Resin (n=4±SD).

Non-linear regression analysis yielded values for K_D and Bmax of 275.8nM and 30.73pmoles, respectively.

This shows a large reduction in binding affinity, but an increase in the number of available binding sites when the resin is suspended in TBS rather than distilled water. Reasons for this are unclear but may be due to the adoption of a different peptide conformation in TBS, albeit a conformation which only binds more slowly. TR401 contains a tryptophan residue, which can sometimes affect the secondary structure of short peptides (Dr. A. Smithson, Peptide Chemist, Severn Biotech, Personal Communication – Appendix 4) and the proportions of each conformer can vary depending upon solvent (Appendix 4).

Simply, in this case, the difference observed is, in fact, rather small. Bmax is calculated to be 11.87pmoles and 30.73 pmoles for the water-

based and TBS-based experiments, respectively. In each case, 25μg of resin was used, so the 2.5-fold difference in the number of binding sites available may be due to the buffering of the system at pH7.5: an important factor to consider in future work.

No differences were observed from controls when the dye was replaced with fluorescein, rhodamine 123, or rhodamine 6G.

There was no detectable SR binding when the resin was suspended in 25%, 50%, or indeed absolute ethanol. This is somewhat disappointing, yet unsurprising as the peptide is likely to refold in alcoholic media, redistributing charged and uncharged groups in search of the lowest energy conformation (Karle et al., 1993). Considering this refolding, it is entirely possible that any "binding pocket" present on the peptide has been folded away. An interesting step to build in on any subsequent experiments in this area would be to dry the resin, return it to water and assess any residual binding affinity to determine whether the peptide is destroyed or just temporarily hindered. This question is addressed in Chapter 4.

3.4 Further Discussion

Although the error bars shown on Figure 54 and Figure 55 appear somewhat large, it is necessary to have an appreciation of the error/consistency of the original data.

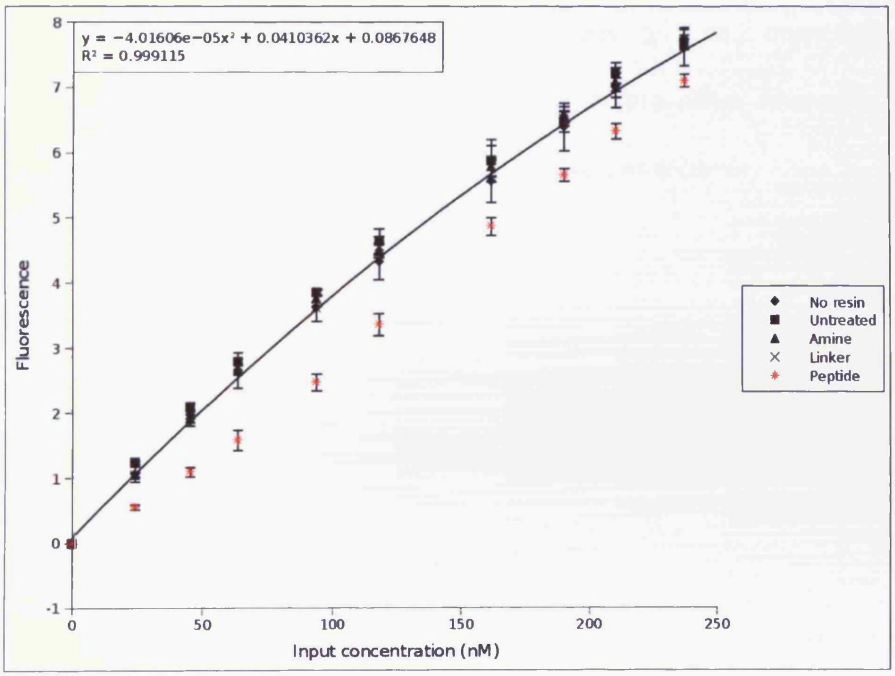

Figure 56: Raw data of fluorescence associated with sulforhodamine 101 remaining free in aqueous solution upon exposure to 25µg of resin at various concentrations.

Figure 56 shows the raw data, and therefore the intrinsic error, relating to the experiment illustrated in Figure 54. Whilst the difference observed here is clear when raw data is examined, the error bars appear to expand when the data is presented on narrower axes.

3.5 Conclusions

In conclusion, linking chemistry was developed to functionalise Merrifield resin with the glycine-cysteine-modified TR401 and a reliable and robust assay was developed which allowed quantification of SR binding to the TR401-functionalised resin. A high degree of specific binding has been demonstrated between SR and the immobilised peptide, as illustrated by the fact that none of the other fluorophores exhibited any binding. Binding was not observed in ethanol.

Chapter 4

Peptide-Conjugated Molecularly Imprinted Polymers: The Plastibody

"Do not go where the path may lead,
go instead where there is no path and
leave a trail."

Ralph Waldo Emerson.

4.1 Introduction

The work presented in this chapter sought to combine the high affinity and specificity of the peptide derived from phage display with the robust and protective properties of a molecularly imprinted polymer.

Polymerisation was controlled using dithiocarboxysarcosine (DTCS, Figure 57), a water-soluble photo-iniferter.

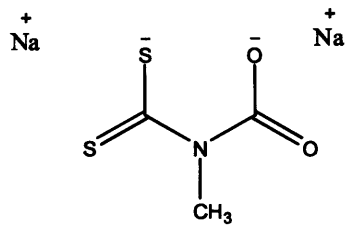

Figure 57: Dithiocarboxysarcosine (DTCS).

Methylene bisacrylamide (MBA, Figure 58) was selected as functional monomer as it is known to provide cross-linking functionality (Stevens, 1999) and should therefore form a cross-linked network in the resultant polymer.

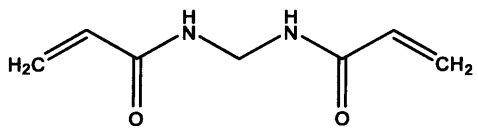

Figure 58: Methylene bisacrylamine (MBA).

The solid support employed in these experiments was MR with some surface-modification to express 50% primary amines, with the remainder of the surface being the native methyl chloride. This allowed attachment of TR401 using methods described in Section 3.2.1.3 to the amine functionality, whilst allowing attachment of the iniferter through an ion-replacement reaction with the chloride group (Qin et al., 2009) (Figure 59).

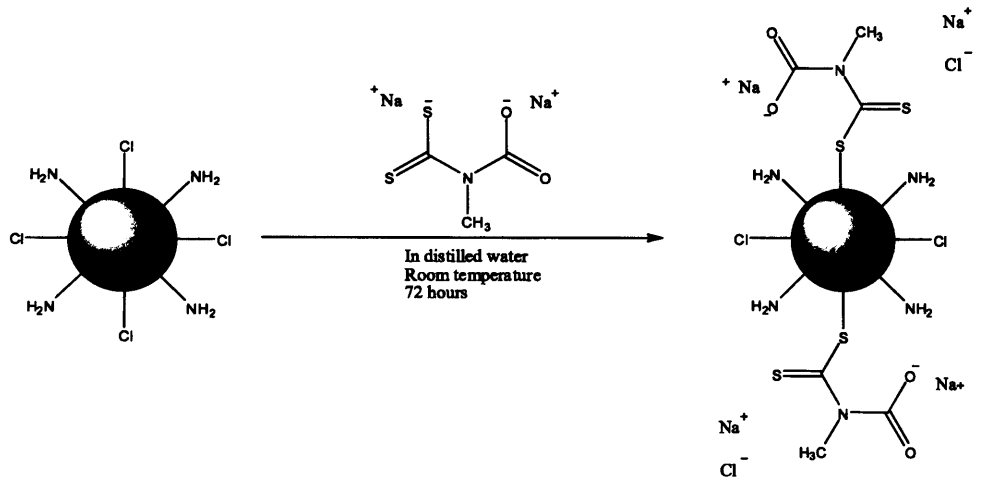

Figure 59: Reaction of bifunctionalised MR with DTCS to produce iniferter-functionalised resin.

Having demonstrated in Chapter 3 (Section 3.3.3) that TR401 cannot bind SR in ethanol, two issues were presented: firstly that the polymerisation environment must be aqueous to allow interaction between SR and TR401, and if SR did not bind to TR401 in ethanol, it makes a suitable eluent with which to wash SR from the polymer.

The principle aims of this set of experiments were to optimise polymerisation conditions and then assess the binding properties of the resulting polymers. Specifically, MR was bifunctionalised to express DTCS and TR401 together, peptide stability was assessed upon exposure to functional monomers, and MR and TR401 were each exposed to ethanol to determine its suitability as an eluent. Polymerisation experiments were performed with TR401-DTCS bifunctionalised resin in the presence and absence of the template SR, treatments being referred to as P-MIP and P-NIP, respectively.

4.2 Methods

4.2.1 Functionalisation of Resin

4.2.1.1 Attachment of Iniferter

Merrifield Resin (200-400 mesh, 1% cross-linked with DVB, 1.8-2.0 mmol Cl/g, Acros Organics – 349160500, BN#A0249177) was bifunctionalised to express on the surface equal portions of both chloride and amine groups via Staudinger reaction (performed in-house by J. Bowen). The resulting bifunctionalised resin (10mg) was suspended in distilled water (3ml) and kept stirring while a solution of DTCS (manufactured in-house by M. Kelly) (2ml of 25mg/1ml) was added dropwise. The reaction mixture was shielded from light and maintained at room temperature for 72 hours. The mixture was then transferred to microcentrifuge tubes and spun at 10,400G for 4 minutes to sediment the resin. The supernatant was discarded, and replaced with distilled water. This process of centrifugation was repeated a further three times to wash off any unreacted DTCS.

DTCS-functionalised resin was stored in the dark at room temperature and used within 48 hours.

4.2.1.2 Attachment of Peptide, TR401

The basic method is as described in Chapter 3 (Section 3.2.1.3) using

DTCS-functionalised MR with shielding from light. The UV absorbance of TR401 solutions pre- and post-reaction were again obtained to determine hypothetical peptide-loading to resin. The resulting TR401-DTCS bifunctionalised MR construct was then subjected to binding assessment as described in Section 3.2.3.

4.2.2 Peptide Exposure to Monomers

A sample of peptide-functionalised MR (500µg) was incubated with a solution of MBA (Sigma Aldrich Cat. No.: 146072, Gillingham, UK) (1mg/ml) in distilled water (1ml) in the dark for one hour, washed with distilled water either once, or three times, then subjected to a binding assay using standard protocol.

4.2.3 Ethanol as Eluent

4.2.3.1 Effect of Ethanol on MR

4.2.3.1.1 Microscopy

A small hole was drilled in a Petri dish and a coverslip glued to cover the underside of the hole. A small amount of resin was then placed into the resulting depression and observed under a light microscope. The edges of the

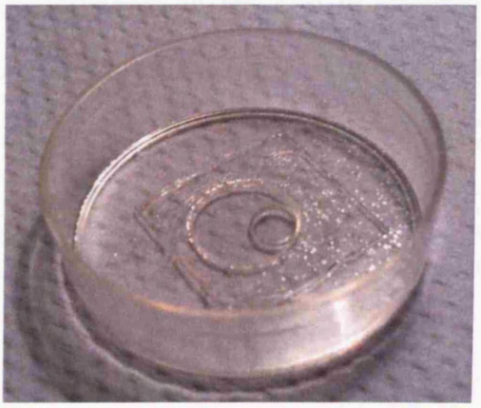

Figure 60: Petri dish with drilled hole with coverslips above and below creating a space for an ethanolic suspension of resin.

depression were then coated thinly with vacuum grease and another coverslip was slid across to partially obscure the depression. Ethanol (100µl) was then added to the resin and covered rapidly by sliding the coverslip across the remaining aperture. Images were captured under a light microscope over a period of 10 minutes. Treatments were untreated Merrifield resin, polymerised Merrifield resin, iniferter-functionalised Merrifield resin, and polymerised iniferter-functionalised Merrifield resin.

4.2.3.1.2 Particle-Size Analysis

Suspensions of untreated Merrifield resin were prepared in water and in ethanol and incubated at room temperature for 48 hours before being read on a Malvern Instruments Mastersizer 2000 (Malvern, Worcestershire, UK).

4.2.3.2 Effect of Ethanol on Peptide

A sample of TR401 (0.5mg) was dissolved in either ethanol or distilled water (10ml) and incubated at room temperature for one hour. The solvent was then evaporated under vacuum for 30 minutes at 25°C. The dry peptide residue was then dissolved in water and subjected to chemical linkage to bifunctionalised Merrifield resin as described in Section 4.2.1. A binding assay using the standard protocol was performed.

Further studies were performed making use of arginine buffer and

sonication in the search for an efficient elution protocol, summarised in Appendix 4.

4.2.4 Polymerisation

Polymerisation mixtures were prepared in HPLC vials containing 100µg of the appropriate resin and 1mg methylene bisacrylamide. These mixtures then had either 100µl SR solution (6µM) or 100µl water added.

Polymerisation was carried out under UV (λ=325nm, 100mW/cm^2, at a distance of 15cm with the light entering through the glass walls of the HPLC vial) and samples were removed at time-points: 0,1,2,5,10,15,20,30,60,90, and 120 minutes. Each sample was washed in ethanol to remove the template and any unreacted monomer. Samples were re-suspended in distilled water and SR binding assays were carried out as described in Section 3.2.3.

4.3 Results and Discussion

4.3.1 Functionalisation of Resin

4.3.1.1 Attachment of Iniferter

Attachment of the DTCS was assessed very simply through a change in the physical properties of the resin. Bifunctionalised Merrifield resin is somewhat hydrophobic (due to the continued presence of methyl chloride groups) and therefore does not disperse easily in water; whereas once the water-soluble iniferter coats the surface (replacing the chloride) the resin forms a very fine suspension easily as hydrophobicity decreases. Dry samples were also ground to a fine powder and assessed through Fourier-Transform Infrared Spectroscopy (FTIR) using a Varian 3100 Excalibur FTIR running the Varian Resolutions Pro software.

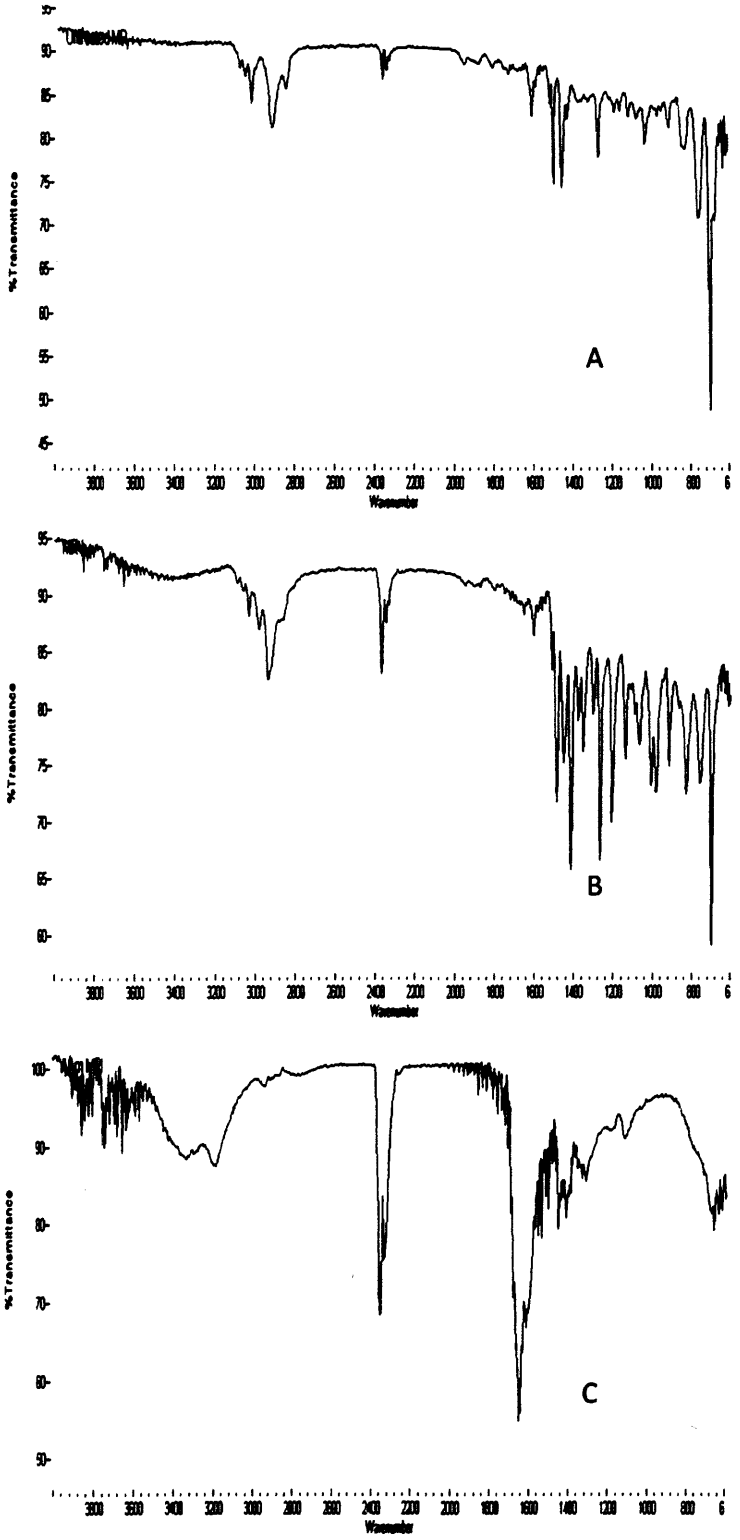

Figure 61: FTIR spectra of untreated MR (A), DTCS-coupled MR (B), and DTCS-coupled MR exposed to acrylamide under UV for 24 hours (C). FTIR experiments were performed by J. Bowen and M. Kelly.

Spectrum (A) in Figure 61 shows untreated MR. Spectrum (B) shows DTCS-functionalised MR. The stretches at 1030-1275 indicate the C=S bond of DTCS, illustrating that the conjugation has been successful. Spectrum (C) shows DTCS-functionalised MR that has been exposed to acrylamide under polymerisation conditions. The peak at 1600 is indicative of the carbonyl group of acrylamide. This demonstrates that DTCS has retained functionality in that polymer growth was achieved.

4.3.1.2 Attachment of Peptide, TR401

Analysis of UV spectra of peptide solutions before and after reaction with functionalised Merrifield resin indicates the loss of approximately 0.232mg TR401 from solution to the resin. Figure 62 shows the result of binding assay performed with bifunctionalised Merrifield resin, after peptide attachment:

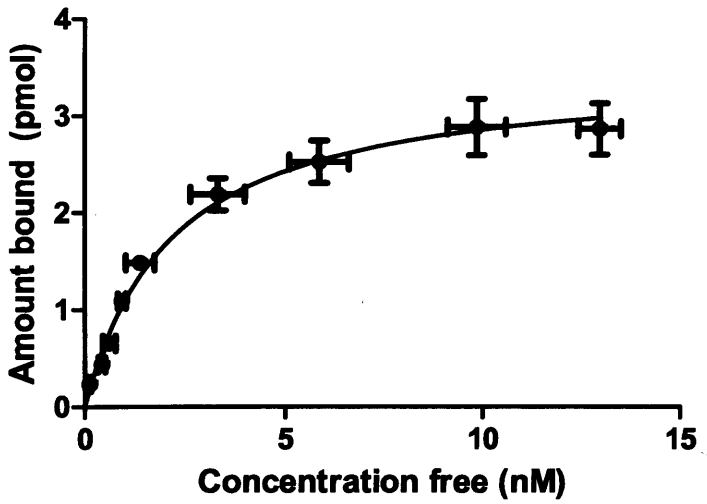

Figure 62: Sulforhodamine binding assay performed with Bifunctionalised Merrifield resin to which TR401 has been linked alongside iniferter. K_D = 2.14nM, Bmax = 3.47pmoles (n=4±SD)

Loss of 0.232mg TR401 to 1mg resin should result in 3.05nmoles per 25μg resin, however, Bmax is 1000-fold below this at only 3.47pmoles. This may be as a result of degradation upon storage, although in some respects, it is expected that fewer binding sites would be available, as only approximately half the surface of the resin has been functionalised to receive the peptide. Bmax and K_D for these systems are based upon the assumption that the binding properties of each peptide unit on the surface of the resin are identical. However, stability data for TR401 (Appendix 5) suggests that fragmentation of the peptide could have occurred even before it was conjugated to the surface. Many of the surface amine groups may have been occupied by various C-terminal fragments of TR401 and not the entire structure.

HPLC analysis of TR401 shows some peak splitting which is likely to be the result of the bulky tryptophan residue which can bring about multiple folding conformations of the peptide (also Appendix 5). TR401 may therefore exist in multiple conformers with different binding properties in an aqueous environment.

4.3.2 Peptide Exposure to Monomers

A comparison is drawn between peptide-functionalised MR that had been washed once or three times in water, with peptide-functionalised MR incubated in the dark with a monomer solution prior to washing.

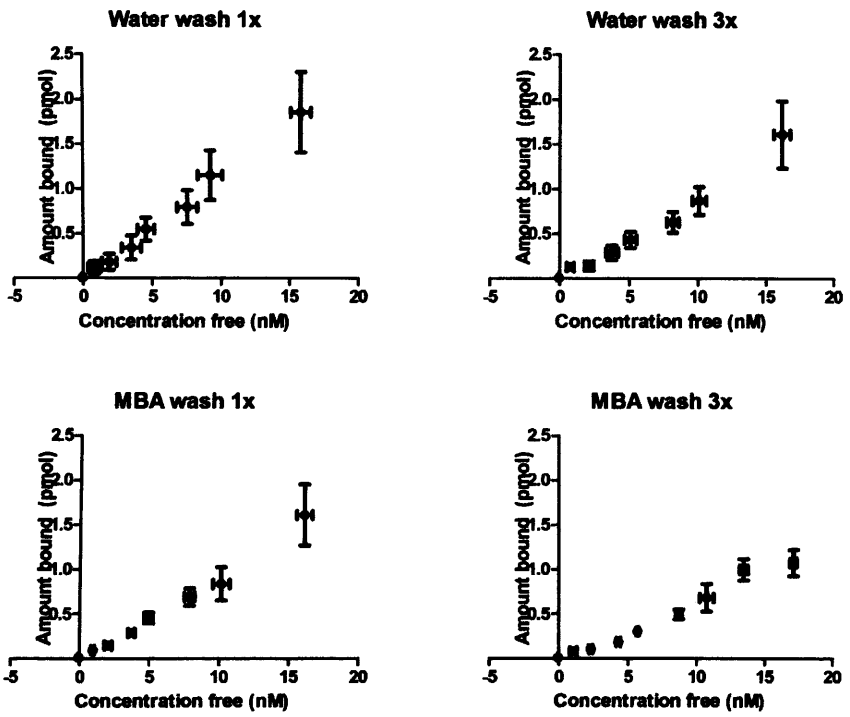

Figure 63: Sulforhodamine binding assays performed with peptide-functionalised resin which has either been incubated with MBA solution or with water, then washed either once or three times (n=4±SD).

It is apparent from Figure 63 that there is a drop in the availability of binding sites once the peptide has been exposed to the monomer solution. Clearly, in this instance, it is unwise to attempt estimation of K_D and Bmax as saturation is not reached. However, it is apparent that washing the resin three times in distilled water produced a marked reduction in binding potential in comparison to a single wash. This is

likely to be on account of loss of small amounts of resin during the washing steps. Incubation with MBA reduced binding further, probably through some level of binding to the peptide, which is encouraging for further work as the imprinting process should encapsulate the peptide-ligand complex.

4.3.3 Ethanol as Eluent

4.3.3.1 Effect of Ethanol on MR

4.3.3.1.1 Microscopy

This study initially sought to visualise the swelling effect of ethanol on Merrifield resin with light microscopy.

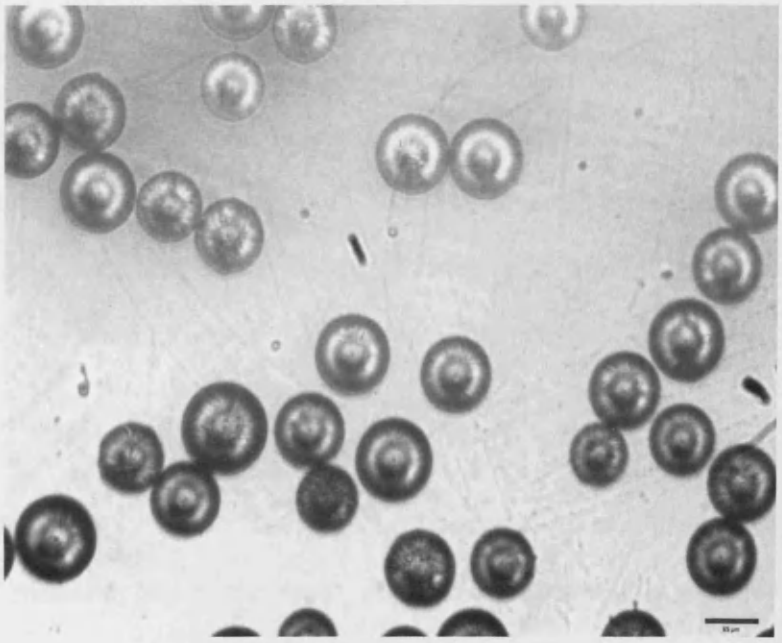

Figure 64: Example image from the sequence of Merrifield resin exposure to ethanol. No size changes were visible of the duration of the experiment (10 minutes). (Scale bar = 65μm)

Over the course of the experiment (10 minutes) no swelling effect was visible for any of the treatments under light microscopy.

4.3.3.1.2 Particle-Size Analysis

MR was suspended in either water or ethanol then analysed using Malvern Mastersizer.

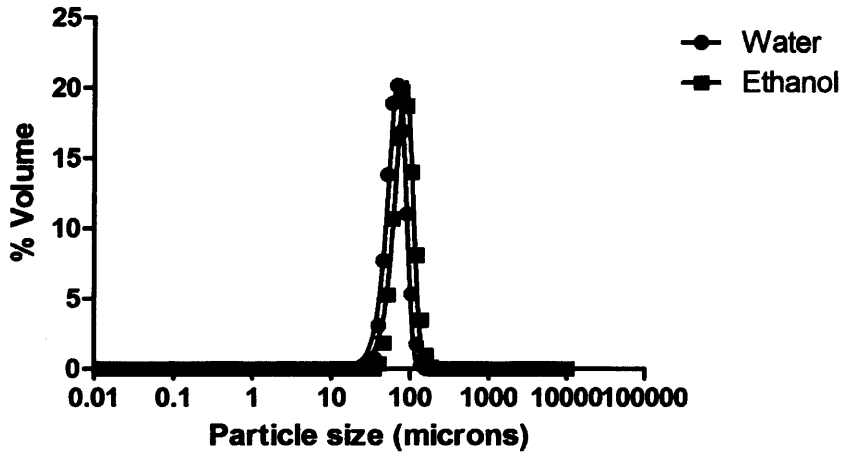

Figure 65: Malvern Mastersizer data comparing particle sizes of Merrifield resin after incubation in water or ethanol.

The Merrifield resin particles were seen to swell only marginally, from a mean diameter of 70.72μm to 75.94μm upon exposure to ethanol. This equates to spherical volumes of 5235μm^3 and 6036μm^3, respectively. The volume has increased by approximately 15%.

4.3.3.2 Effect of Ethanol on Peptide

Untreated peptide was dissolved in ethanol, dried, and then attached to bifunctionalised Merrifield resin. Figure 66 shows the results of the subsequent binding assay.

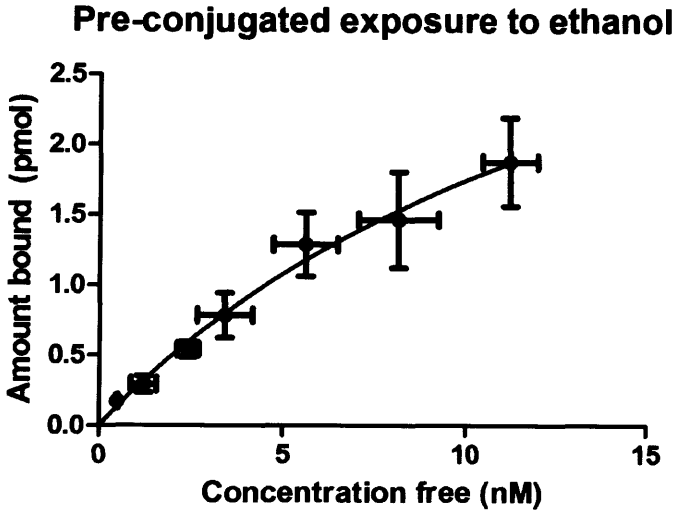

Figure 66: Binding assay performed using resin functionalised with peptide which had been dissolved in ethanol prior to its immobilisation (n=4±SD).

Non-linear regression (Figure 66) yielded Bmax and K_D of 4.5pmol and 15.9nM, respectively, comparative to the values of 3.5pmol and 2.1nM, respectively, that were obtained from the aqueous control. While Bmax in the low-pmole region is directly comparable, the increase in K_D from 2.1nM to 15.9nM indicates some slight loss of binding affinity. Although peptides are generally stable in ethanol (Guo and Karplus, 1994), there may have been some minor damage to the peptide in its recovery from the solvent. Whilst an aqueous control was performed in the same conditions, the boiling point and relative density of ethanol are both lower than water, therefore the conditions when subjected to rotary evaporation will no doubt have varied slightly. Whether this subtle variation was enough to allow oxidation of side-chains or hydrolysis of the peptide is difficult to say.

4.3.4 Polymerisation

Polymerisation mixtures were prepared and exposed to UV light for the times indicated in Table 4. Treatments were Merrifield resin with iniferter modification, with or without peptide functionalisation, in the presence or absence of SR as a molecular template (P-MIP, P-NIP, MIP, or NIP).

Full binding isotherms are shown in Appendix 6. Summary data shown:

Table 4: Summary of K_D and Bmax values for sulforhodamine binding assays carried out at varying P-NIP polymerisation times.

Polymerisation Time (minutes)	K_D (nM)	Bmax (pmoles)
0	94.24	36.26
1	212.1	62.55
2	240.1	55.12
5	177.0	46.69
10	150.6	50.79
15	193.5	53.93
20	100.5	35.33
30	13.75	3.46
60	51.10	12.39
90	35.63	10.23
120	94.49	29.44

Table 5: Summary of K_D and Bmax values for sulforhodamine binding assays carried out at varying P-MIP polymerisation times.

Polymerisation Time (minutes)	K_D (nM)	Bmax (pmoles)
0	420.6	13.00
1	6436	114.4
2	317.1	31.27
5	2111	132.8
10	135.2	28.75
15	~	~
20	~	~
30	50.51	11.75
60	~	~
90	~	~
120	190.1	41.29

Whilst binding assays were performed for all polymerisation treatments, some polymers either showed no binding affinity at all, or the data would not fit standard non-linear regression models; this accounts for the missing values in Table 5. Data is presented in full in Appendix 6.

4.3.4.1 Key Observations

Figure 67 shows the binding isotherm plotted from the bifunctionalised resin 20-minute polymerisation treatment in the absence of SR as template.

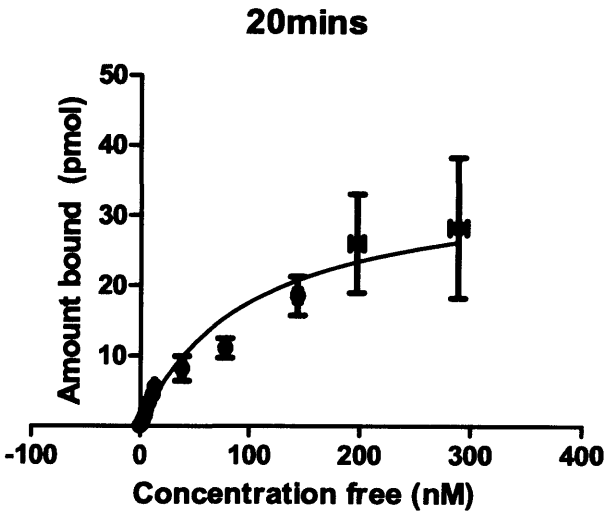

Figure 67: Sulforhodamine binding assay at optimal polymerisation time for P-NIP (n=4±SD).

K_D and Bmax were determined as 100.5nM and 35.33pmoles, respectively.

Figure 68 shows the binding isotherm plotted from the 120-minute polymerisation treatment with the inclusion of SR as template. K_D and Bmax were determined as 190.1nM and 41.29pmoles, respectively. These figures represent the optimum conditions for producing TR401-polymer constructs with the greatest overall binding potential (low K_D and high Bmax).

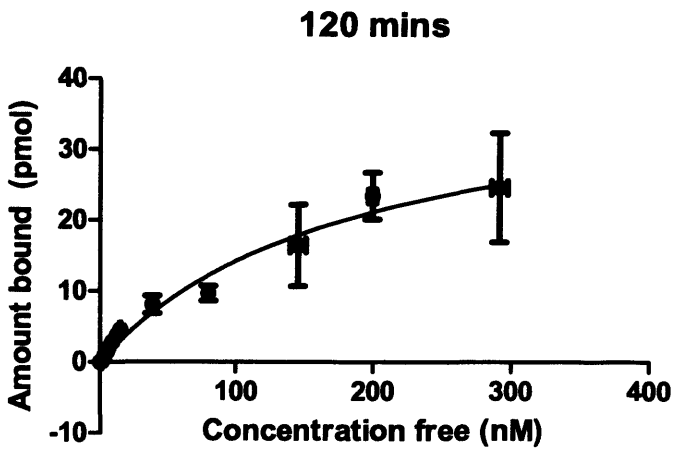

Figure 68: Sulforhodamine binding assay at optimal polymerisation time for P-MIP (n=4±SD).

Interestingly, the P-MIP exhibits higher values for both K_D and Bmax when compared to P-NIP. This is contrary to the hypothesis that an imprinted system would show higher binding affinity and greater availability of binding sites when compared to a non-imprinted control. Therefore, it is likely that some template remains trapped in the imprinted matrix and an improved washing protocol must be developed for more thorough elution.

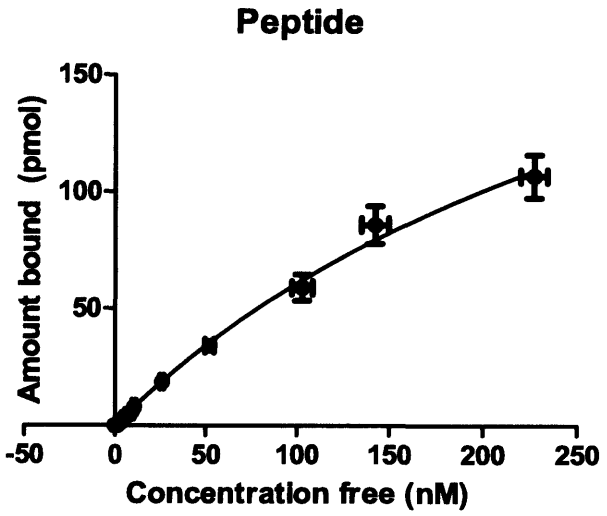

Figure 69: Sulforhodamine binding to Peptide-functionalised, iniferter-derivatised Merrifield resin. K_D 370.0nM, Bmax 286.4pmoles (n=4±SD).

Figure 69 shows the result of a binding assay using TR401-DTCS bifunctionalised resin, without polymerisation. K_D and Bmax are both far higher than TR401-resin alone: K_D 370.0nM compared to 2.141nM, and Bmax 286.4pmoles compared to 3.47pmoles. The far higher Bmax indicates greater coverage of the MR surface with functional TR401; although the increase in K_D (binding affinity falling) is less easily explained. K_D, of course, is a parameter describing a combination of effects: the rate at which binding complexes are formed, and the rate at which they dissociate again. If the rate of formation of these complexes (K_{on}) remains constant, but the rate of dissociation (K_{off}) increases, K_D rises. Likewise, if K_{off} remains constant but K_{on} decreases, this will cause a drop in K_D. Any interaction of DTCS with TR401 or with SR is likely to influence either, or both, of these rates.

No binding was evident to the non-peptide, non-imprinted polymer treatments at any time-point, whereas, at later points the non-peptide molecularly imprinted polymer treatment began to show some level of binding, albeit very low comparative to the peptide treatments (data shown in Appendix 6).

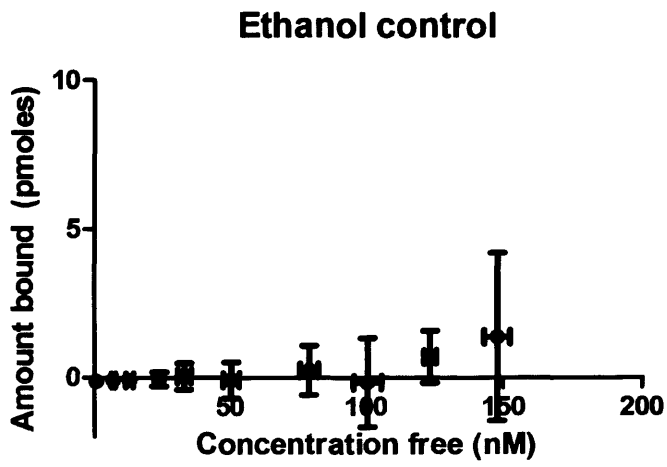

Figure 70: Peptide-functionalised, iniferter-derivatised Merrifield resin washed in ethanol (n=4±SD).

When TR401-DTCS bifunctionalised resin was washed in ethanol (Figure 70), the binding capability of the peptide appeared to be almost completely removed, whereas, some degree of polymerisation as demonstrated in the P-MIP and P-NIP treatments retained binding to a high degree.

Table 6: Summary of K_D and Bmax for the peptide-polymerisation treatments under optimum conditions.

	K_D (nM)	Bmax (pmoles)
TR401-DTCS resin	370	286.4
Ethanol washed peptide-resin	N/A	N/A
P-MIP	190.1	41.29
P-NIP	100.5	35.33

Both P-NIP and P-MIP appear to bind with greater affinity than peptide-functionalised resin (K_D 370nM). However, the total number of binding sites available appears to drop once polymerisation is initiated. The TR401-functionalised MR demonstrates a Bmax of 286.4pmol, whereas P-NIP and P-MIP have values of 35.3pmol and 41.3pmol, respectively.

This would suggest that although the peptide that remains after the polymerisation process appears to bind with higher affinity than before polymerisation, a great deal of damage is done to the peptides and only a small proportion of peptide molecules survive the process.

4.4 Further Discussion

A wash in ethanol of the TR401-functionalised resin renders the attached peptide non-binding, but the resin-swelling effect caused by ethanol is low, and ethanol does not damage the peptide alone. As

binding was evident to P-NIP and P-MIP it is surmised that the polymerisation process is in some way conferring protection to the peptide, as the surfaces were not damaged by the ethanol wash. Perhaps there is a conformation the immobilised peptide favours in ethanol which cannot be recovered upon its return to water. The presence of the supportive polymer shell may hinder these conformational changes of the peptide. As described in Section 3.4, HPLC analysis of TR401 (presented in Appendix 4) indicates that choice of solvent may affect the conformation of peptides with bulky residues such as tryptophan.

The value for Bmax obtained from the assays in which TR401 was conjugated to bi-functionalised MR was 3.47pmoles. However, if the bi-functionalised resin had first been treated to express DTCS, Bmax was far higher at 286.4pmoles. The amount of resin in each assay was, of course, the same (25µg), so the question is raised as to what could be causing such an increase in Bmax. In the case of bi-functionalised resin, primary amines were conjugated to TR401 (reaction scheme illustrated in Figure 71). The remainder of the surface is methyl chloride. However, in the case of the TR401-DTCS-functionalised resin, the chloride groups that had been present on the surface have been replaced with hydrophilic iniferter species. Indeed, the very presence of DTCS on the surface of the resin may have resulted in greater access of TR401 to the surface during the conjugation step, as the surface was

more hydrophilic.

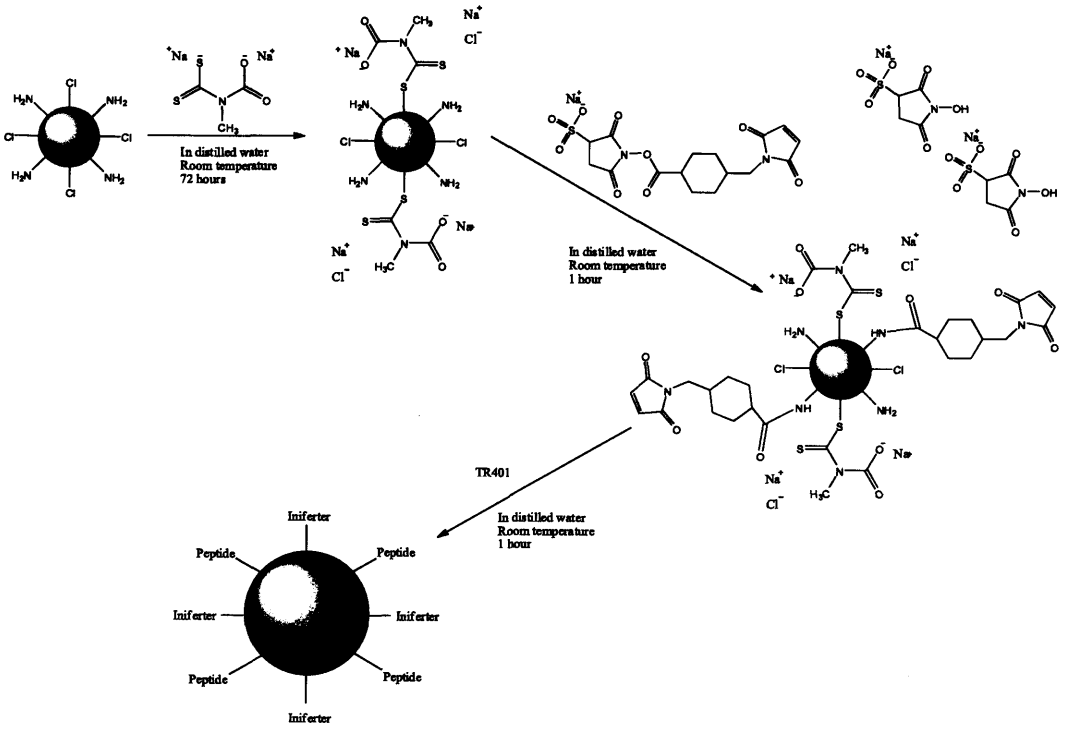

Figure 71: Reaction scheme showing the production of TR401-DTCS bi-functionalised Merrifield Resin.

4.5 Conclusions

The binding affinity of TR401 to SR appeared greater in the polymerised systems than the non-polymerised system, although the extent of that binding (Bmax) has been greatly reduced. It is likely that, in general, damage is occurring to the surface-immobilised peptides, although those peptide units which escape this damage bind with higher affinity than peptide alone. Basic proof-of-principle is demonstrated in that a peptide derived from phage display was incorporated into a molecular-

imprinting system and retained binding affinity for its target. Moreover, the binding affinity (K_D) was slightly improved for the polymerisation. However, this does, of course, require much optimisation with regard to polymerisation conditions and components. Additionally, an improved washing regime must be devised, as the results shown in Section 4.3.4.1 suggest that the binding sites of P-MIP may still be occupied with template SR included in the polymerisation stage.

Chapter 5

General Discussion

"Nothing shocks me. I'm a scientist."
Harrison Ford, as Indiana Jones

The principle aim of this project was to produce a peptide-MIP conjugate which showed higher affinity and specificity to a given target than is currently possible with imprinted polymer technology alone, whilst being more robust than simple peptide-binding systems or indeed antibody-based systems.

5.1 Phage Display

The intention had been to begin with a phage display library and take the technology through from start to finish. However, the panning against propranolol failed to yield binding consensus sequences. The underlying strategy of screening the phage library against low molecular weight molecules and using structurally-related compounds to optimise selection for the target is not unknown (Smith et al., 2007), and logic would suggest that the use of competing compounds in solution whilst panning against a sedimentary surface should have yielded peptides with high specificity. One possibility for the failure of the panning is that

this level of stringency from the outset was too high. Comparative to the scale of the library (10^9 unique units), the inoculation of phage at each round was 10^{11} particles, around 100 copies of each displayed peptide. If round one was too stringent, any strongly binding peptides with lower specificity will have been excluded, whilst peptides with moderate binding affinity (which would still have been useful in later studies) were discarded with the competing compounds in solution, *das Kind mit dem Bade ausschütten* (German Proverb, c.1512). Another possible issue with panning against small molecules is that they present too few functional groups in the target to select for high affinity binding peptides.

Reports of phage display against small molecular targets include paracetamol (Smith et al., 2007), dexamethasone (Yu et al., 2007) and methotrexate (Takakusagi et al., 2008) (structures shown in Figure 72) with paracetamol having the simplest of structures and the least complex to serve as a target (see Table 7). Indeed, personal communication (M. Gumbleton and M.W. Smith (Smith et al., 2007)) indicated that the peptide-phage identified for paracetamol did not show a high degree of consensus in the peptide sequences and the affinities were not high. Propranolol also offers limited chemistry for peptide-phage panning compared to methotrexate and dexamethasone.

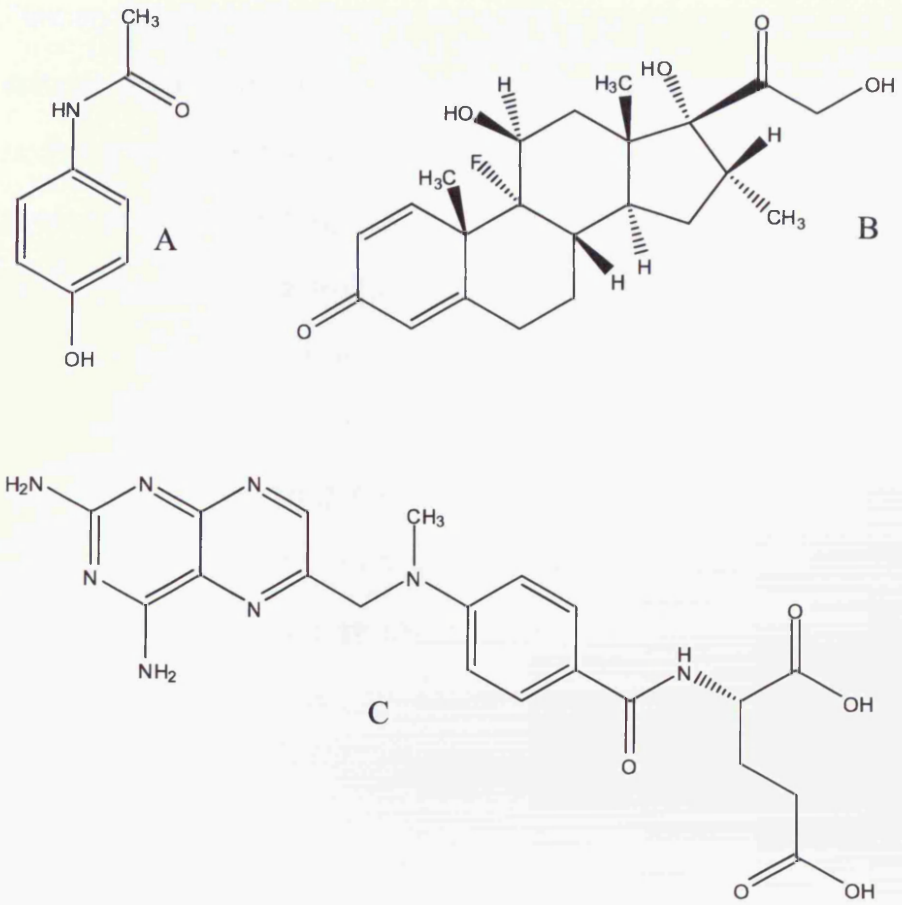

Figure 72: Paracetamol (A), dexamethasone (B), and methotrexate (C).

Table 7: Properties of the low molecular weight phage display biopanning targets.

Compound	Mw	LogP	H-bond Donors	H-bond Acceptors	Asymmetric Centres
Propranolol	259.3	3.35	2	3	1
Methotrexate	454.4	0.94	5	9	1
Dexamethasone	392.5	-0.21	3	5	8*
Paracetamol	151.2	0.28	2	3	0

*Whilst dexamethasone contains eight asymmetric centres, "dexamethasone" refers only to a single conformation.

Further, there is potentially a stereochemical issue in the choice of suitable targets for phage display. Whilst methotrexate has a chiral centre, it is located well away from the region of the molecule expected to bind to the isolated peptide, or indeed to the drug's target in the body (dihydrofolate reductase (Takakusagi et al., 2008)). The methotrexate study, in fact, made use of biotinylated methotrexate, although the authors do not specify through which functional group the biotin was attached. There is the possibility that the compound was immobilised such that the chiral centre would have little importance in the regions of the molecule exposed to the phage.

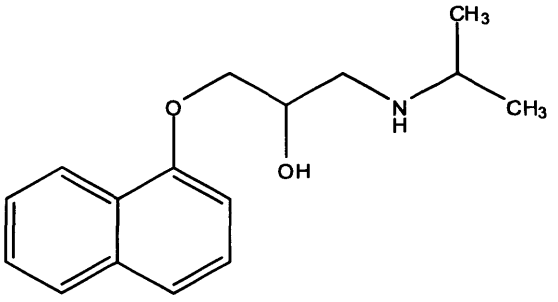

Figure 73: Propranolol.

Biopanning against propranolol (Figure 73), however, was either as free-base suspension, or immobilised through the naphthyl group to glass beads. This would result in exposure of the chiral centre to phage, which brings with it the possibility that there was simultaneous selection occurring for two targets: *R/S*-propranolol. An interesting observation at this stage is that one of the peptide-phage clones isolate from the suspension-panning experiment (Section 2.2.4.1) had the sequence EMTSTRA. This clone was retained when exposed to propranolol

covalently attached to glass beads (Section 2.2.4.2) (Outputs 1 & 2 from Figure 16). A single clone with the sequence EPRATST was recovered from the experiment in which propranolol was attached to glass beads. This presence of EMTSTRA and EPRATST sequences in separate biopanning experiments against a racaemic target may be indicative of peptides selective for individual enantiomers, although, unfortunately, no binding for these peptides was observed in any of the assay methods employed.

Several of the assay formats presented in Chapter 2 made use of materials which were subsequently found to bind propranolol. This highlights the importance of a thorough understanding of the substances and materials in use, and especially their limitations. The final binding assay protocol in Chapter 2 was the micro-centrifuge tube dialysis system. This was, by far, the most accurate system to determine propranolol concentrations at equilibrium, but even this was not perfect. There was still a low level of binding to the dialysis membrane which may have influenced experimental outcome.

Many phage display studies make use of technologies such as quartz crystal microbalance (QCM) (Wu et al., 2010, Hengerer et al., 1999) or surface plasmon resonance (SPR) (Swain Md Fau - Anderson et al., 2010, Weiger et al., 2010) both during biopanning and in subsequent peptide-phage binding assessments. These techniques are very

sensitive and can readily detect phage binding to an immobilised target; however, a functional group is lost in the immobilisation of the target. When assessing a molecule with as few functional groups as propranolol, any loss of functionality is undesirable.

A suitable target for biopanning with peptide-phage display would have a variety of functional groups, and would not display non-specific binding to experimental materials. If looking to medicinal drugs, plasma protein binding may give an indication as to whether this is likely.

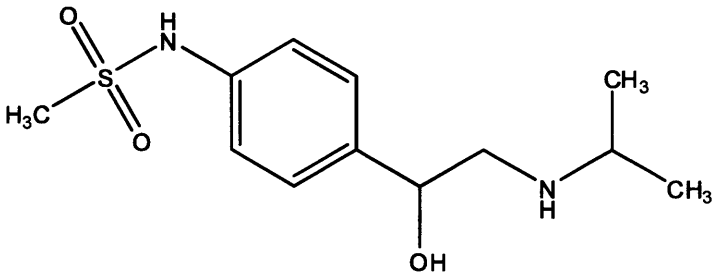

Figure 74: Sotalol.

A compound such as sotalol (LogP = -0.06) which is not bound in human plasma (Carr et al., 1992) would be much more appropriate, although sotalol (Figure 74) also contains a chiral centre, and therefore a single enantiomer should be considered.

5.2 TR401

When faced with the failure to produce a novel peptide, an example was chosen from the literature. TR401 is a peptide that binds Texas

Red and which was further characterised with respect to its binding capabilities in Chapter 3 of this thesis. TR401 was selected because the initial intention was to obtain a peptide from phage display with high affinity and specificity to a low molecular weight compound.

Although their original paper (Rozinov and Nolan, 1998) performed biopanning against Texas red, Rhodamine red, Oregon green 514, and fluorescein, TR401 was found to be the phage-derived peptide with highest affinity for its target (Texas Red). Rozinov and Nolan performed several experiments to determine K_D for the TR401-Texas Red interaction which they quoted as 0.27nM when peptide was *in situ* on the phage and 1.6μM for the synthetic peptide immobilised to magnetic beads via a histidine-tag. This illustrates clearly that K_D is a constant that is specific for a given system and therefore it was necessary to gain a thorough understanding of how TR401 behaved when attached to the Merrifield Resin support.

High levels of binding were seen when TR401-functionalised MR was exposed to sulforhodamine, both in distilled water and in TBS (K_D = 74.87nM, and 275.8nM, respectively), and this provided both a baseline to which comparison could be drawn for any binding observed once polymerisation was brought into the system, and confidence to proceed to the next stage of the project.

5.3 Peptide-Molecular Imprinted Polymers

Table 6 in Chapter 4 (Summary of K_D and Bmax for the peptide-polymerisation treatments under optimum conditions) shows an increase in binding affinity (reduction in K_D) in P-MIP and P-NIP treatments compared to non-polymerised peptide-functionalised resin, although the values attained for Bmax and K_D are similar for both P-NIP and P-MIP. This is not surprising as both treatments underwent TR401-conjugation in an identical manner, so should therefore have the same overall number of binding sites. The data suggest that the imprinting process is not, in fact, assisting with the formation of a binding site as would be expected when considering previous MIP literature (i.e. polymer interaction with the template). However, there is also a large drop in the number of available binding sites, so the overall binding potential of the system is compromised. This may be the result of the polymer growing across the peptide, causing the binding sites to be lost. Additionally, electron-rich amino acid residues are likely to be vulnerable to free-radical attack, which may damage the peptide irrecoverably. This may explain why some of the polymerisation treatments failed to demonstrate any binding whatsoever.

The structure of the polymer should have some degree of cross-linking due to the choice of methylene bisacrylamide as a cross-linking monomer, which was chosen for its ability to produce highly cross-linked structures. This would confer some degree of rigidity to the final

polymer and restrict any swelling effect when immersed in liquids (Nielsen, 1969). However, when growing a polymer from a surface-bound initiator, the degree of cross-linking may be reduced comparative to standard di-methacrylate cross-linking, and may require a tri-methacrylate (Deng et al., 2009).

Additionally, as the polymer was growing from a surface, rather than forming as pre-defined droplets in emulsion/suspension or as a bulk monolith, there is the possibility that it will reach a critical size and then collapse under its own weight. However, this is purely conjecture, and binding affinity was seen to be restored after further polymerisation. Clearly further investigation into the polymerisation protocol is called for.

As shown briefly in Figure 70, an ethanol wash of TR401-DTCS bifunctionalised resin appears to completely remove any ability of the surface-bound peptide to bind SR from solution. The resin was tested for swelling effects in ethanol, and TR401 was assessed for peptide stability; yet, the swelling effect of ethanol on MR was only marginal, and TR401 which had previously been dissolved in ethanol bound SR once conjugated to the MR surface. Therefore, the nature of the effect of ethanol on the TR401-functionalised MR system is currently unexplained. However, once polymerisation was initiated in the system, resistance to the ethanol wash seen. This implies direct interaction of the polymer with both the peptide and the resin support, conferring

stability and allowing some of the surface-immobilised TR401 to remain in a binding conformation.

5.4 Future Work

A starting point for future work would be the elucidation of the exact nature of the effect ethanol has on the peptide-functionalised resin by allowing a slower change in ethanol/water proportions to ascertain whether binding can be reinstated.

An effective washing regime must then be devised. This is evinced by the fact that the binding constants associated with P-NIP suggest greater binding ability than P-MIP, which is contrary to hypothesis. This is likely to be as a result of continued occupation of binding sites by template molecules which have resisted current washing efforts.

A large drop in Bmax is observed in the polymerised treatments when compared to non-polymerised control. This is likely to be the result of damage to the surface-bound peptide during the polymerisation and washing processes. The question must be addressed as to whether any resulting peptide damage has affected specificity. Further experiments should be performed to challenge P-NIP and P-MIP with related compounds (rhodamine-6G, rhodamine-123, and fluorescein) in an effort to determine any cross-sensitivity induced by the polymerisation.

Variation in polymer constitution should also be considered. There is a large range of compounds that are widely used in imprinting science (White and Byrne, 2010, Lasakova and Jandera, 2009, Holthoff and Bright, 2007) and further studies should consider the use of a wider variety of potential components, for example the use of a more complex functional monomer with a larger variety of functional groups, and the use of a trisacrylamide cross-linker to provide a more stable three-dimensional structure.

5.5 Conclusions

As the resulting polymers from many of the treatments exhibited binding, where the non-polymerised control did not, this goes some way towards supporting the original hypothesis, although further work is essential. Whilst the resultant peptide-polymer conjugates have shown a certain resistance to ethanol washing, further testing of their limitations is desirable, e.g. subjection to high temperatures, acidic/basic conditions, or enzymatic attack.

Although there are several studies in which peptides have been conjugated to polymers for various purposes (Veronese and Morpurgo, 1999, Jain and Jain, 2008, Magnusson et al., 2010), the concept of using a binding peptide in the imprinted cavity of a MIP system is entirely new.

The very nature of the technology of phage display can produce binding peptides with high specificity, given a suitable biopanning protocol, yet any effect that polymerisation has on that specificity should be considered.

Overall, the work presented here, the first of its kind, provides proof-of-principle towards the concept of the peptide-conjugated molecularly imprinted polymer: The Plastibody.

- A peptide can survive free-radical-based polymerisation.
- It can retain binding ability.
- The polymer shell confers some protection.

Further work in this area may lead to the development of a truly biomimetic artificial antibody for use in myriad applications wherever a high degree of binding affinity and specificity are called for, whether it's the detection of biological hazards, environmental threats, diagnostic testing, imaging, drug delivery, or therapeutic agents in their own right.

References

ALEXANDER, C., ANDERSSON, H. S., ANDERSSON, L. I., ANSELL, R. J., KIRSCH, N., NICHOLLS, I. A., O'MAHONY, J. & WHITCOMBE, M. J. (2006) Molecular imprinting science and technology: a survey of the literature for the years up to and including 2003. *J Mol Recognit,* 19, 106-80.

ANSELL, R. J. (2005) Molecularly imprinted polymers for the enantioseparation of chiral drugs. *Adv Drug Deliv Rev,* 57, 1809-35.

ANSELL, R. J. & KUAH, K. L. (2005) Imprinted polymers for chiral resolution of (+/-)-ephedrine: understanding the pre-polymerisation equilibrium and the action of different mobile phase modifiers. *Analyst,* 130, 179-87.

ARAKAWA, T., TSUMOTO, K., NAGASE, K. & EJIMA, D. (2007) The effects of arginine on protein binding and elution in hydrophobic interaction and ion-exchange chromatography. *Protein Expression and Purification,* 54, 110-116.

ARSHADY, R. & MOSBACH, K. (1981) Synthesis of substrate-selective polymers by host-guest polymerization. *Die Makromolekulare Chemie,* 182, 687-692.

ASCIONE, A., FLEGO, M., ZAMBONI, S., DE CINTI, E., DUPUIS, M. L. & CIANFRIGLIA, M. (2005) Application of a synthetic phage antibody library (ETH-2) for the isolation of single chain fragment variable (scFv) human antibodies to the pathogenic isoform of the hamster prion protein (HaPrPsc). *Hybridoma (Larchmt),* 24, 127-32.

ATHIKOMRATTANAKUL, U., KATTERLE, M., GAJOVIC-EICHELMANN, N. & SCHELLER, F. W. (2009) Development of molecularly imprinted polymers for the binding of nitrofurantoin. *Biosens Bioelectron,* 25, 82-7.

AZZAZY, H. M. & HIGHSMITH, W. E., JR. (2002) Phage display technology: clinical applications and recent innovations. *Clin Biochem,* 35, 425-45.

BAGGIANI, C., ANFOSSI, L. & GIOVANNOLI, C. (2007) Solid phase extraction of food contaminants using molecular imprinted polymers. *Anal Chim Acta,* 591, 29-39.

BAI, Y. & FENG, H. (2004) Selection of stably folded proteins by phage-display with proteolysis. *Eur J Biochem,* 271, 1609-14.

BECERRIL, B., POUL, M. A. & MARKS, J. D. (1999) Toward selection of internalizing antibodies from phage libraries. *Biochem Biophys Res Commun,* 255, 386-93.

BOLISAY, L. D., CULVER, J. N. & KOFINAS, P. (2007) Optimization of

virus imprinting methods to improve selectivity and reduce nonspecific binding. *Biomacromolecules,* 8, 3893-9.

BOYD, B., BJORK, H., BILLING, J., SHIMELIS, O., AXELSSON, S., LEONORA, M. & YILMAZ, E. (2007) Development of an improved method for trace analysis of chloramphenicol using molecularly imprinted polymers. *J Chromatogr A,* 1174, 63-71.

BUENO, L. L., MORAIS, C. G., DA SILVA SOARES, I., BOUILLET, L. E. M., BRUNA-ROMERO, O., FONTES, C. J., FUJIWARA, R. T. & BRAGA, É. M. (2009) Plasmodium vivax recombinant vaccine candidate AMA-1 plays an important role in adaptive immune response eliciting differentiation of dendritic cells. *Vaccine,* 27, 5581-5588.

BUSI, BASOSI, PONTICELLI & OLIVUCCI (2004) An innovative approach to the design of plastic antibodies:molecular imprinting via a non-polar transition state analogue. *Journal of Molecular Catalysis A: Chemical,* 217, 31-36.

BYEON, W. H. & WEISBLUM, B. (2004) Affinity adsorbent based on combinatorial phage display peptides that bind alpha-cobratoxin. *J Chromatogr B Analyt Technol Biomed Life Sci,* 805, 361-3.

CARLSON, C. A., LLOYD, J. A., DEAN, S. L., WALKER, N. R. & EDMISTON, P. L. (2006) Sensor for Fluorene Based on the Incorporation of an Environmentally Sensitive Fluorophore Proximal to a Molecularly Imprinted Binding Site. *Analytical Chemistry,* 78, 3537-3542.

CARO, E., MASQUE, N., MARCE, R. M., BORRULL, F., CORMACK, P. A. & SHERRINGTON, D. C. (2002) Non-covalent and semi-covalent molecularly imprinted polymers for selective on-line solid-phase extraction of 4-nitrophenol from water samples. *J Chromatogr A,* 963, 169-78.

CARR, R. A., FOSTER, R. T., LEWANCZUK, R. Z. & HAMILTON, P. G. (1992) Pharmacokinetics of sotalol enantiomers in humans. *J Clin Pharmacol,* 32, 1105-9.

CASEY, J. L., COLEY, A. M., ANDERS, R. F., MURPHY, V. J., HUMBERSTONE, K. S., THOMAS, A. W. & FOLEY, M. (2004) Antibodies to malaria peptide mimics inhibit Plasmodium falciparum invasion of erythrocytes. *Infect Immun,* 72, 1126-34.

CASTELL, O. K., ALLENDER, C. J. & BARROW, D. A. (2006) Novel biphasic separations utilising highly selective molecularly imprinted polymers as biorecognition solvent extraction agents. *Biosens Bioelectron,* 22, 526-33.

CERRUTI, M., JAWORSKI, J., RAORANE, D., ZUEGER, C., VARADARAJAN, J., CARRARO, C., LEE, S. W., MABOUDIAN, R. & MAJUMDAR, A. (2009) Polymer-oligopeptide composite coating for selective detection of explosives in water. *Anal Chem,* 81, 4192-9.

CHAN, E., MCLACHLAN, A. J., PEGG, M., MACKAY, A. D., COLE, R. B. & ROWLAND, M. (1994) Disposition of warfarin enantiomers and metabolites in patients during multiple dosing with rac-

warfarin. *Br J Clin Pharmacol,* 37, 563-9.
CHIANELLA, I., LOTIERZO, M., PILETSKY, S. A., TOTHILL, I. E., CHEN, B., KARIM, K. & TURNER, A. P. (2002) Rational design of a polymer specific for microcystin-LR using a computational approach. *Anal Chem,* 74, 1288-93.
COOPER, D. & REICH, E. (1972) Neurotoxin from venom of the cobra, Naja naja siamensis. Purification and radioactive labeling. *J Biol Chem,* 247, 3008-13.
CUNLIFFE, D., KIRBY, A. & ALEXANDER, C. (2005) Molecularly imprinted drug delivery systems. *Adv Drug Deliv Rev,* 57, 1836-53.
DAI, C. M., GEISSEN, S. U., ZHANG, Y. L., ZHANG, Y. J. & ZHOU, X. F. (2010) Performance evaluation and application of molecularly imprinted polymer for separation of carbamazepine in aqueous solution. *J Hazard Mater,* 2010, 17.
DAI, S. (2001) Hierarchically imprinted sorbents. *Chemistry,* 7, 763-8.
DE KIEVIT, T. R. & IGLEWSKI, B. H. (2000) Bacterial quorum sensing in pathogenic relationships. *Infect Immun,* 68, 4839-49.
DENG, J., WANG, L., LIU, L. & YANG, W. (2009) Developments and new applications of UV-induced surface graft polymerizations. *Progress in Polymer Science,* 34, 156-193.
DONG, C., LI, X., GUO, Z. & QI, J. (2009) Development of a model for the rational design of molecular imprinted polymer: computational approach for combined molecular dynamics/quantum mechanics calculations. *Anal Chim Acta,* 647, 117-24.
EJIMA, D., YUMIOKA, R., TSUMOTO, K. & ARAKAWA, T. (2005) Effective elution of antibodies by arginine and arginine derivatives in affinity column chromatography. *Analytical Biochemistry,* 345, 250-257.
EPSTEIN, J. E., GIERSING, B., MULLEN, G., MOORTHY, V. & RICHIE, T. L. (2007) Malaria vaccines: are we getting closer? *Curr Opin Mol Ther,* 9, 12-24.
FAIRHURST, R. E., CHASSAING, C., VENN, R. F. & MAYES, A. G. (2004) A direct comparison of the performance of ground, beaded and silica-grafted MIPs in HPLC and turbulent flow chromatography applications. *Biosens Bioelectron,* 20, 1098-105.
FEAS, X., SEIJAS, J. A., VAZQUEZ-TATO, M. P., REGAL, P., CEPEDA, A. & FENTE, C. (2009) Syntheses of molecularly imprinted polymers: Molecular recognition of cyproheptadine using original print molecules and azatadine as dummy templates. *Anal Chim Acta,* 631, 237-44.
GUO, H. & KARPLUS, M. (1994) Solvent Influence on the Stability of the Peptide Hydrogen Bond: A Supramolecular Cooperative Effect. *The Journal of Physical Chemistry,* 98, 7104-7105.
HAGINAKA, J., TABO, H. & KAGAWA, C. (2008) Uniformly sized molecularly imprinted polymers for d-chlorpheniramine: influence

of a porogen on their morphology and enantioselectivity. *J Pharm Biomed Anal,* 46, 877-81.
HANSEN, D. E. (2007) Recent developments in the molecular imprinting of proteins. *Biomaterials,* 28, 4178-91.
HART, B. R. & SHEA, K. J. (2001) Synthetic peptide receptors: molecularly imprinted polymers for the recognition of peptides using peptide-metal interactions. *J Am Chem Soc,* 123, 2072-3.
HAUPT, K. & MOSBACH, K. (1999) Molecularly imprinted polymers in chemical and biological sensing. *Biochem Soc Trans,* 27, 344-50.
HAUPT, K. & MOSBACH, K. (2000) Molecularly imprinted polymers and their use in biomimetic sensors. *Chem Rev,* 100, 2495-504.
HENGERER, A., KOSSLINGER, C., DECKER, J., HAUCK, S., QUEITSCH, I., WOLF, H. & DUBEL, S. (1999) Determination of phage antibody affinities to antigen by a microbalance sensor system. *Biotechniques,* 26, 956-60, 962, 964.
HILLBERG, A. L., BRAIN, K. R. & ALLENDER, C. J. (2005) Molecular imprinted polymer sensors: implications for therapeutics. *Adv Drug Deliv Rev,* 57, 1875-89.
HOLTHOFF, E. L. & BRIGHT, F. V. (2007) Molecularly templated materials in chemical sensing. *Anal Chim Acta,* 594, 147-61.
HOSHINO, Y., KOIDE, H., URAKAMI, T., KANAZAWA, H., KODAMA, T., OKU, N. & SHEA, K. J. (2010) Recognition, Neutralization, and Clearance of Target Peptides in the Bloodstream of Living Mice by Molecularly Imprinted Polymer Nanoparticles: A Plastic Antibody. *Journal of the American Chemical Society,* 132, 6644-6645.
HUFTON, S. E., MOERKERK, P. T., MEULEMANS, E. V., DE BRUINE, A., ARENDS, J. W. & HOOGENBOOM, H. R. (1999) Phage display of cDNA repertoires: the pVI display system and its applications for the selection of immunogenic ligands. *J Immunol Methods,* 231, 39-51.
HUNT, C. E. & ANSELL, R. J. (2006) Use of fluorescence shift and fluorescence anisotropy to evaluate the re-binding of template to (S)-propranolol imprinted polymers. *Analyst,* 131, 678-83.
HWANG, C. C. & LEE, W. C. (2002) Chromatographic characteristics of cholesterol-imprinted polymers prepared by covalent and non-covalent imprinting methods. *J Chromatogr A,* 962, 69-78.
JAIN, A. & JAIN, S. K. (2008) PEGylation: an approach for drug delivery. A review. *Crit Rev Ther Drug Carrier Syst,* 25, 403-47.
JANTARAT, C., TANGTHONG, N., SONGKRO, S., MARTIN, G. P. & SUEDEE, R. (2008) S-propranolol imprinted polymer nanoparticle-on-microsphere composite porous cellulose membrane for the enantioselectively controlled delivery of racemic propranolol. *Int J Pharm,* 349, 212-25.
KANTAROVICH, K., TSARFATI, I., GHEBER, L. A., HAUPT, K. & BAR, I. (2009) Writing droplets of molecularly imprinted polymers by nano fountain pen and detecting their molecular interactions by

surface-enhanced Raman scattering. *Anal Chem,* 81, 5686-90.
KARIM, K., BRETON, F., ROUILLON, R., PILETSKA, E. V., GUERREIRO, A., CHIANELLA, I. & PILETSKY, S. A. (2005) How to find effective functional monomers for effective molecularly imprinted polymers? *Adv Drug Deliv Rev,* 57, 1795-808.
KARLE, I. L., FLIPPEN-ANDERSON, J. L., UMA, K. & BALARAM, P. (1993) Unfolding of an α-helix in peptide crystals by solvation: Conformational fragility in a heptapeptide. *Biopolymers,* 33, 827-837.
KARLSSON, B. C., O'MAHONY, J., KARLSSON, J. G., BENGTSSON, H., ERIKSSON, L. A. & NICHOLLS, I. A. (2009) Structure and dynamics of monomer-template complexation: an explanation for molecularly imprinted polymer recognition site heterogeneity. *J Am Chem Soc,* 131, 13297-304.
KASMAN, L. M., KASMAN, A., WESTWATER, C., DOLAN, J., SCHMIDT, M. G. & NORRIS, J. S. (2002) Overcoming the phage replication threshold: a mathematical model with implications for phage therapy. *J Virol,* 76, 5557-64.
KATO, K., UCHIDA, E., KANG, E.-T., UYAMA, Y. & IKADA, Y. (2003) Polymer surface with graft chains. *Progress in Polymer Science,* 28, 209-259.
KEHOE, J. W. & KAY, B. K. (2005) Filamentous phage display in the new millennium. *Chem Rev,* 105, 4056-72.
KREZEL, A. & MARET, W. (2007) Different redox states of metallothionein/thionein in biological tissue. *Biochem J,* 402, 551-8.
KUMEMURA, M., ODAKE, T. & KORENAGA, T. (2005) Laser-induced fluorescence microscopic system using an optical parametric oscillator for tunable detection in microchip analysis. *Anal Bioanal Chem,* 382, 992-5.
KUNKEL, T. A. (1985) Rapid and efficient site-specific mutagenesis without phenotypic selection. *Proc Natl Acad Sci U S A,* 82, 488-92.
KUREBAYASHI, N., HARKINS, A. B. & BAYLOR, S. M. (1993) Use of fura red as an intracellular calcium indicator in frog skeletal muscle fibers. *Biophys J,* 64, 1934-60.
LANGE, U., ROZNYATOVSKAYA, N. V. & MIRSKY, V. M. (2008) Conducting polymers in chemical sensors and arrays. *Anal Chim Acta,* 614, 1-26.
LANIER, L. L. & LOKEN, M. R. (1984) Human lymphocyte subpopulations identified by using three-color immunofluorescence and flow cytometry analysis: correlation of Leu-2, Leu-3, Leu-7, Leu-8, and Leu-11 cell surface antigen expression. *J Immunol,* 132, 151-6.
LASAKOVA, M. & JANDERA, P. (2009) Molecularly imprinted polymers and their application in solid phase extraction. *J Sep Sci,* 32, 799-812.
LEONHARDT, A. & MOSBACH, K. (1987) Enzyme-mimicking polymers

exhibiting specific substrate binding and catalytic functions. *Reactive Polymers, Ion Exchangers, Sorbents,* 6, 285-290.

LIU, B., YU, W.-L., PEI, J., LIU, S.-Y., LAI, Y.-H. & HUANG, W. (2001) Design and Synthesis of Bipyridyl-Containing Conjugated Polymers: Effects of Polymer Rigidity on Metal Ion Sensing. *Macromolecules,* 34, 7932-7940.

LIU, J., DENG, Q., YANG, K., ZHANG, L., LIANG, Z. & ZHANG, Y. (2010) Macroporous molecularly imprinted monolithic polymer columns for protein recognition by liquid chromatography. *J Sep Sci,* 33, 2757-61.

LIU, Z. S., XU, Y. L., WANG, H., YAN, C. & GAO, R. Y. (2004) Chiral separation of binaphthol enantiomers on molecularly imprinted polymer monolith by capillary electrochromatography. *Anal Sci,* 20, 673-8.

LULINSKI, P. & MACIEJEWSKA, D. (2009) Examination of imprinting process with molsidomine as a template. *Molecules,* 14, 2212-25.

MAGNUSSON, J. P., BERSANI, S., SALMASO, S., ALEXANDER, C. & CALICETI, P. (2010) In situ growth of side-chain PEG polymers from functionalized human growth hormone-a new technique for preparation of enhanced protein-polymer conjugates. *Bioconjug Chem,* 21, 671-8.

MARKS, K. M., ROSINOV, M. & NOLAN, G. P. (2004) In vivo targeting of organic calcium sensors via genetically selected peptides. *Chem Biol,* 11, 347-56.

MAYES, A. G. & MOSBACH, K. (1996) Molecularly Imprinted Polymer Beads: Suspension Polymerization Using a Liquid Perfluorocarbon as the Dispersing Phase. *Analytical Chemistry,* 68, 3769-3774.

MERRIFIELD, R. B. (1963) Solid Phase Peptide Synthesis. I. The Synthesis of a Tetrapeptide. *Journal of the American Chemical Society,* 85, 2149-2154.

MIYAKI, K., GUO, Y., SHIMOSAKA, T., NAKAGAMA, T., NAKAJIMA, H. & UCHIYAMA, K. (2005) Fabrication of an integrated PDMS microchip incorporating an LED-induced fluorescence device. *Anal Bioanal Chem,* 382, 810-6.

MUTUBERRIA, R., HOOGENBOOM, H. R., VAN DER LINDEN, E., DE BRUINE, A. P. & ROOVERS, R. C. (1999) Model systems to study the parameters determining the success of phage antibody selections on complex antigens. *J Immunol Methods,* 231, 65-81.

NG, S. M. & NARAYANASWAMY, R. (2009) Molecularly imprinted [beta]-cyclodextrin polymer as potential optical receptor for the detection of organic compound. *Sensors and Actuators B: Chemical,* 139, 156-165.

NIELSEN, L. E. (1969) Cross-Linking Effect on Physical Properties of Polymers. *Polymer Reviews,* 3, 69-103.

NILSSON, F., TARLI, L., VITI, F. & NERI, D. (2000) The use of phage display for the development of tumour targeting agents. *Adv*

Drug Deliv Rev, 43, 165-96.
NISHINO, H., HUANG, C. S. & SHEA, K. J. (2006) Selective protein capture by epitope imprinting. *Angew Chem Int Ed Engl,* 45, 2392-6.
O'SHANNESSY, D. J., EKBERG, B. & MOSBACH, K. (1989) Molecular imprinting of amino acid derivatives at low temperature (0 degrees C) using photolytic homolysis of azobisnitriles. *Anal Biochem,* 177, 144-9.
OTSU, T., MATSUNAGA, T., KURIYAMA, A. & YOSHIOKA, M. (1989) Living radical polymerization through the use of iniferters: Controlled synthesis of polymers. *European Polymer Journal,* 25, 643-650.
ÖZCAN, L. & SAHIN, Y. (2007) Determination of paracetamol based on electropolymerized-molecularly imprinted polypyrrole modified pencil graphite electrode. *Sensors and Actuators B: Chemical,* 127, 362-369.
PAPAIOANNOU, E. H., LIAKOPOULOU-KYRIAKIDES, M., PAPI, R. M. & KYRIAKIDIS, D. A. (2008) Artificial receptor for peptide recognition in protic media: The role of metal ion coordination. *Materials Science and Engineering: B,* 152, 28-32.
PARK, B., YING, H., SHEN, X., PARK, J. S., QIU, Y., SHYAM, R. & YUE, B. Y. (2010) Impairment of protein trafficking upon overexpression and mutation of optineurin. *PLoS One,* 5, e11547.
PAYNE, R. J. & JANSEN, V. A. (2002) Evidence for a phage proliferation threshold? *J Virol,* 76, 13123; author reply 13123-4.
PEI, Q. & QIAN, R. (1991) Protonation and deprotonation of polypyrrole chain in aqueous solutions. *Synthetic Metals,* 45, 35-48.
PERCIVAL, C. J., STANLEY, S., BRAITHWAITE, A., NEWTON, M. I. & MCHALE, G. (2002) Molecular imprinted polymer coated QCM for the detection of nandrolone. *Analyst,* 127, 1024-6.
PEREIRA, L. A. & RATH, S. (2009) Molecularly imprinted solid-phase extraction for the determination of fenitrothion in tomatoes. *Anal Bioanal Chem,* 393, 1063-72.
PETCU, M., COONEY, J., COOK, C., LAUREN, D., SCHAARE, P. & HOLLAND, P. (2001) Molecular imprinting of a small substituted phenol of biological importance. *Analytica Chimica Acta,* 435, 49-55.
POLYAKOV (1931) Adsorption properties and structure of silica gel. *Zhur. Fiz. Khim.,* 2, 799–805.
PUSZTASZERI, M. P., SEELENTAG, W. & BOSMAN, F. T. (2006) Immunohistochemical expression of endothelial markers CD31, CD34, von Willebrand factor, and Fli-1 in normal human tissues. *J Histochem Cytochem,* 54, 385-95.
QI, P., WANG, J., WANG, L., LI, Y., JIN, J., SU, F., TIAN, Y. & CHEN, J. (2010) Molecularly imprinted polymers synthesized via semi-covalent imprinting with sacrificial spacer for imprinting phenols. *Polymer,* In Press, Accepted Manuscript.

QIN, L., HE, X. W., ZHANG, W., LI, W. Y. & ZHANG, Y. K. (2009) Surface-modified polystyrene beads as photografting imprinted polymer matrix for chromatographic separation of proteins. *J Chromatogr A,* 1216, 807-14.

RATHBONE, D. L. & BAINS, A. (2005) Tools for fluorescent molecularly imprinted polymers. *Biosens Bioelectron,* 20, 1438-42.

REIMHULT, K., YOSHIMATSU, K., RISVEDEN, K., CHEN, S., YE, L. & KROZER, A. (2008) Characterization of QCM sensor surfaces coated with molecularly imprinted nanoparticles. *Biosens Bioelectron,* 23, 1908-14.

REINARD, T. & JACOBSEN, H. J. (1989) An inexpensive small volume equilibrium dialysis system for protein-ligand binding assays. *Anal Biochem,* 176, 157-60.

RICHARDSON, S. C., WALLOM, K. L., FERGUSON, E. L., DEACON, S. P., DAVIES, M. W., POWELL, A. J., PIPER, R. C. & DUNCAN, R. (2008) The use of fluorescence microscopy to define polymer localisation to the late endocytic compartments in cells that are targets for drug delivery. *J Control Release,* 127, 1-11.

ROZINOV, M. N. & NOLAN, G. P. (1998) Evolution of peptides that modulate the spectral qualities of bound, small-molecule fluorophores. *Chem Biol,* 5, 713-28.

RUOSLAHTI, E. (2000) Targeting tumor vasculature with homing peptides from phage display. *Semin Cancer Biol,* 10, 435-42.

SCHLESINGER, M. (1932) Adsorption of phages to homologous bacteria. II.

Quantitative investigations of adsorption velocity and saturation. Estimation

of the particle size of the bacteriophage. *Z. Hyg. Immunitaetsforsch.,* 114, 149-160.

SELLERGREN, B. & ALLENDER, C. J. (2005) Molecularly imprinted polymers: a bridge to advanced drug delivery. *Adv Drug Deliv Rev,* 57, 1733-41.

SEONG, H., LEE, H. B. & PARK, K. (2002) Glucose binding to molecularly imprinted polymers. *J Biomater Sci Polym Ed,* 13, 637-49.

SHARMA, P. S., LAKSHMI, D. & PRASAD, B. B. (2007) Molecularly imprinted solid-phase extraction combined with molecularly imprinted polymer-sensor: a diagnostic tool applicable to creatine deficiency syndrome. *Biomed Chromatogr,* 21, 976-86.

SHOJI, E. & FREUND, M. S. (2002) Potentiometric Saccharide Detection Based on the pKa Changes of Poly(aniline boronic acid). *Journal of the American Chemical Society,* 124, 12486-12493.

SIDHU, S. S. (2001) Engineering M13 for phage display. *Biomol Eng,* 18, 57-63.

SMITH, G. P. (1985) Filamentous fusion phage: novel expression vectors that display cloned antigens on the virion surface. *Science,* 228, 1315-7.

SMITH, M. W., SMITH, J. W., HARRIS, C., BRANCALE, A., ALLENDER, C. J. & GUMBLETON, M. (2007) Phage display identification of functional binding peptides against 4-acetamidophenol (Paracetamol): an exemplified approach to target low molecular weight organic molecules. *Biochem Biophys Res Commun,* 358, 285-91.

SNOW, E. T., KUNKEL, T. A. & LOEB, L. A. (1987) Base substitution mutagenesis by terminal transferase: its role in somatic mutagenesis. *Mutat Res,* 180, 137-46.

STASSEN, A. P., FOLMER, R. H., HILBERS, C. W. & KONINGS, R. N. (1994) Single-stranded DNA binding protein encoded by the filamentous bacteriophage M13: structural and functional characteristics. *Mol biol rep,* 20, 109-127.

STEGEN, U. & HOFSCHNEIDER, P. H. (1970) Replication of the single-stranded DNA bacteriophage M13: Absence of intracellular phages. *Journal of Molecular Biology,* 48, 361-364.

STENT, G. S. (1963) *Molecular Biology of Bacterial Viruses,* San Francisco, Calif., W.H. Freeman and Company.

STEVENS, M. P. (1999) *Polymer Chemistry: An Introduction*, Oxford University Press: New York, NY.

STRIKOVSKY, A. G., KASPER, D., GRÃ¼N, M., GREEN, B. S., HRADIL, J. & WULFF, G. N. (2000) Catalytic Molecularly Imprinted Polymers Using Conventional Bulk Polymerization or Suspension Polymerization: Selective Hydrolysis of Diphenyl Carbonate and Diphenyl Carbamate. *Journal of the American Chemical Society,* 122, 6295-6296.

STURGEON, R. J. & SCHULMAN, S. G. (1975) Intramolecular Field effects on the adsorption and fluorescence spectra of N-(1-naphthyl)ethylenediamine. *Analytica Chimica Acta,* 74, 192-196.

SUEDEE, R., BODHIBUKKANA, C., TANGTHONG, N., AMNUAIKIT, C., KAEWNOPPARAT, S. & SRICHANA, T. (2008) Development of a reservoir-type transdermal enantioselective-controlled delivery system for racemic propranolol using a molecularly imprinted polymer composite membrane. *J Control Release,* 129, 170-8.

SULITZKY, C., RÃCKERT, B. R., HALL, A. J., LANZA, F., UNGER, K. & SELLERGREN, B. R. (2001) Grafting of Molecularly Imprinted Polymer Films on Silica Supports Containing Surface-Bound Free Radical Initiators. *Macromolecules,* 35, 79-91.

SVENSON, J., ANDERSSON, H. S., PILETSKY, S. A. & NICHOLLS, I. A. (1998) Spectroscopic studies of the molecular imprinting self-assembly process. *Journal of Molecular Recognition,* 11, 83-86.

SWAIN MD FAU - ANDERSON, G. P., ANDERSON GP FAU - ZABETAKIS, D., ZABETAKIS D FAU - BERNSTEIN, R. D., BERNSTEIN RD FAU - LIU, J. L., LIU JL FAU - SHERWOOD, L. J., SHERWOOD LJ FAU - HAYHURST, A., HAYHURST A FAU - GOLDMAN, E. R., GOLDMAN, E. R., WEIGER MC FAU - PARK, J. J., PARK JJ FAU - ROY, M. D., ROY MD FAU - STAFFORD, C. M., STAFFORD CM FAU - KARIM, A., KARIM A FAU -

BECKER, M. L. & BECKER, M. L. (2010) Llama-derived single-domain antibodies for the detection of botulinum A neurotoxin
Quantification of the binding affinity of a specific hydroxyapatite binding peptide.
TAKAKUSAGI, Y., KUROIWA, Y., SUGAWARA, F. & SAKAGUCHI, K. (2008) Identification of a methotrexate-binding peptide from a T7 phage display screen using a QCM device. *Bioorg Med Chem,* 16, 7410-4.
TAKEUCHI, T., DOBASHI, A. & KIMURA, K. (2000) Molecular imprinting of biotin derivatives and its application to competitive binding assay using nonisotopic labeled ligands. *Anal Chem,* 72, 2418-22.
TAKEUCHI, T., MURASE, N., MAKI, H., MUKAWA, T. & SHINMORI, H. (2006) Dopamine selective molecularly imprinted polymers via post-imprinting modification. *Org Biomol Chem,* 4, 565-8.
THOMAS, T. P., PATRI, A. K., MYC, A., MYAING, M. T., YE, J. Y., NORRIS, T. B. & BAKER, J. R., JR. (2004) In vitro targeting of synthesized antibody-conjugated dendrimer nanoparticles. *Biomacromolecules,* 5, 2269-74.
TITIRICI, M. M. & SELLERGREN, B. (2004) Peptide recognition via hierarchical imprinting. *Anal Bioanal Chem,* 378, 1913-21.
TITUS, J. A., HAUGLAND, R., SHARROW, S. O. & SEGAL, D. M. (1982) Texas Red, a hydrophilic, red-emitting fluorophore for use with fluorescein in dual parameter flow microfluorometric and fluorescence microscopic studies. *J Immunol Methods,* 50, 193-204.
TZAGOLOFF, H. & PRATT, D. (1964) The Initial Steps in Infection with Coliphage M13. *Virology,* 24, 372-80.
ULUDAG, Y., PILETSKY, S. A., TURNER, A. P. & COOPER, M. A. (2007) Piezoelectric sensors based on molecular imprinted polymers for detection of low molecular mass analytes. *FEBS J,* 274, 5471-80.
URRACA, J. L., CARBAJO, M. C., TORRALVO, M. J., GONZALEZ-VAZQUEZ, J., ORELLANA, G. & MORENO-BONDI, M. C. (2008) Effect of the template and functional monomer on the textural properties of molecularly imprinted polymers. *Biosens Bioelectron,* 24, 155-61.
VAIHINGER, D., LANDFESTER, K., KRÄUTER, I., BRUNNER, H. & TOVAR, G. E. M. (2002) Molecularly imprinted polymer nanospheres as synthetic affinity receptors obtained by miniemulsion polymerisation. *Macromolecular Chemistry and Physics,* 203, 1965-1973.
VAN WEZENBEEK, P. M. G. F., HULSEBOS, T. J. M. & SCHOENMAKERS, J. G. G. (1980) Nucleotide sequence of the filamentous bacteriophage M13 DNA genome: comparison with phage fd. *Gene,* 11, 129-148.
VENTER, J. C., DIXON, J. E., MAROKO, P. R. & KAPLAN, N. O. (1972) Biologically active catecholamines covalentyly bound to glass

beads. *Proc Natl Acad Sci U S A,* 69, 1141-5.
VERONESE, F. M. & MORPURGO, M. (1999) Bioconjugation in pharmaceutical chemistry. *Farmaco,* 54, 497-516.
VLATAKIS, G., ANDERSSON, L. I., MULLER, R. & MOSBACH, K. (1993) Drug assay using antibody mimics made by molecular imprinting. *Nature,* 361, 645-7.
WANG, J., CORMACK, P. A. G., SHERRINGTON, D. C. & KHOSHDEL, E. (2003) Monodisperse, Molecularly Imprinted Polymer Microspheres Prepared by Precipitation Polymerization for Affinity Separation Applications. *Angewandte Chemie International Edition,* 42, 5336-5338.
WEI, S. & MIZAIKOFF, B. (2007) Binding site characteristics of 17[beta]-estradiol imprinted polymers. *Biosensors and Bioelectronics,* 23, 201-209.
WEIGER, M. C., PARK, J. J., ROY, M. D., STAFFORD, C. M., KARIM, A. & BECKER, M. L. (2010) Quantification of the binding affinity of a specific hydroxyapatite binding peptide. *Biomaterials,* 31, 2955-63.
WESTERBLAD, H. & ALLEN, D. G. (1994) Methods for calibration of fluorescent calcium indicators in skeletal muscle fibers. *Biophys J,* 66, 926-8.
WHITCOMBE, M. J., RODRIGUEZ, M. E., VILLAR, P. & VULFSON, E. N. (1995) A New Method for the Introduction of Recognition Site Functionality into Polymers Prepared by Molecular Imprinting: Synthesis and Characterization of Polymeric Receptors for Cholesterol. *Journal of the American Chemical Society,* 117, 7105-7111.
WHITE, C. J. & BYRNE, M. E. (2010) Molecularly imprinted therapeutic contact lenses. *Expert Opin Drug Deliv,* 7, 765-80.
WIGGINS, B. A. & ALEXANDER, M. (1985) Minimum bacterial density for bacteriophage replication: implications for significance of bacteriophages in natural ecosystems. *Appl Environ Microbiol,* 49, 19-23.
WILLIAMS, R. T. & BRIDGES, J. W. (1964) Fluorescence of Solutions: A Review. *J Clin Pathol,* 17, 371-94.
WISTUBA, D. & SCHURIG, V. (2000) Enantiomer separation of chiral pharmaceuticals by capillary electrochromatography. *J Chromatogr A,* 875, 255-76.
WOIWODE, T. F., HAGGERTY, J. E., KATZ, R., GALLOP, M. A., BARRETT, R. W., DOWER, W. J. & CWIRLA, S. E. (2003) Synthetic compound libraries displayed on the surface of encoded bacteriophage. *Chem Biol,* 10, 847-58.
WU, J., CROPEK, D. M., WEST, A. C. & BANTA, S. (2010) Development of a Troponin I Biosensor Using a Peptide Obtained through Phage Display. *Anal Chem,* 82, 8235-43.
WU, Z., TAO, C. A., LIN, C., SHEN, D. & LI, G. (2008) Label-free colorimetric detection of trace atrazine in aqueous solution by using molecularly imprinted photonic polymers. *Chemistry,* 14,

11358-68.
WULFF, G., SARHAN, A. & ZABROCKI, K. (1973) Enzyme-analogue built polymers and their use for the resolution of racemates. *Tetrahedron Letters,* 14, 4329-4332.
YANG, L., LIANG, H., ANGELINI, T. E., BUTLER, J., CORIDAN, R., TANG, J. X. & WONG, G. C. (2004) Self-assembled virus-membrane complexes. *Nat Mater,* 3, 615-9.
YIN, J., YANG, G. & CHEN, Y. (2005) Rapid and efficient chiral separation of nateglinide and its L-enantiomer on monolithic molecularly imprinted polymers. *J Chromatogr A,* 1090, 68-75.
YOSHIMATSU, K., LEJEUNE, J., SPIVAK, D. A. & YE, L. (2009) Peptide-imprinted polymer microspheres prepared by precipitation polymerization using a single bi-functional monomer. *Analyst,* 134, 719-24.
YU, T. T. & SHOICHET, M. S. (2005) Guided cell adhesion and outgrowth in peptide-modified channels for neural tissue engineering. *Biomaterials,* 26, 1507-14.
YU, X., ZHAO, P., ZHANG, W., ZHANG, L. & ZHANG, Y. (2007) Screening of phage displayed human liver cDNA library against dexamethasone. *J Pharm Biomed Anal,* 45, 701-5.
ZWICK, M. B., KELLEHER, R., JENSEN, R., LABRIJN, A. F., WANG, M., QUINNAN, G. V., JR., PARREN, P. W. & BURTON, D. R. (2003) A novel human antibody against human immunodeficiency virus type 1 gp120 is V1, V2, and V3 loop dependent and helps delimit the epitope of the broadly neutralizing antibody immunoglobulin G1 b12. *J Virol,* 77, 6965-78.

Appendix 1

Peptide Sequences Isolated from Phage Display Against Propranolol

Peptide 1 - EMTSTRA

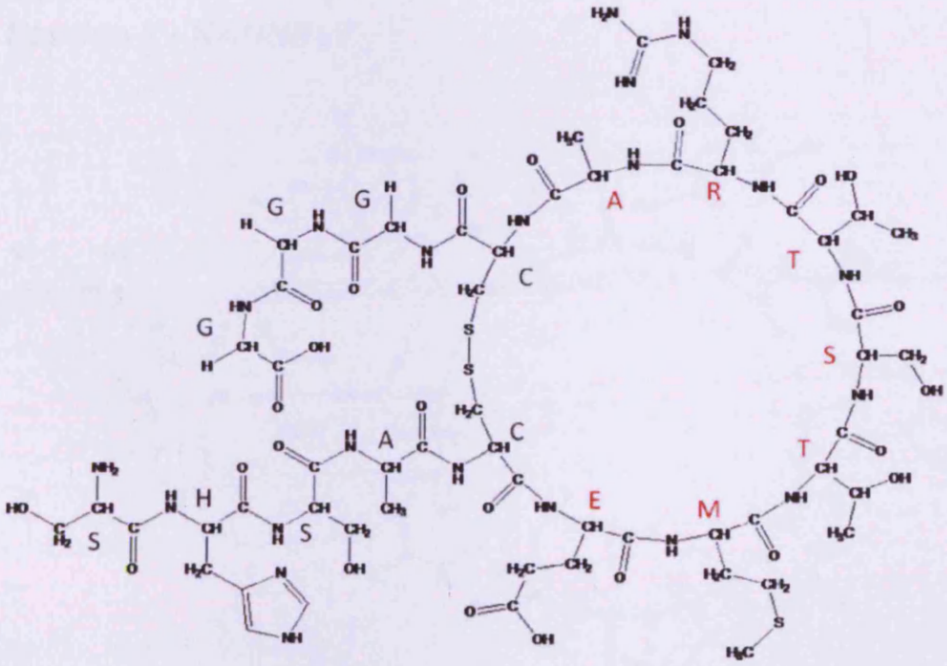

Figure 75: Sequence 1: EMTSTRA (Glutamic acid–Methionine–Threonine–Serine–Threonine–Arginine–Alanine).

Glutamate (E) is polar with a negative charge at physiological pH. Methionine (M) is hydrophobic. Threonine (T) is very small, and whilst a hydroxyl group is present the amino acid is generally hydrophobic. Serine (S) is very small and slightly polar. Arginine (R) is polar and takes a positive charge at physiological pH. Alanine (A) is very small

and slightly hydrophobic.

This clone was present as 14.4% of the successfully sequenced population in the experiment in which the phage library was exposed to propranolol free base as an insoluble complex. It was also present as 8.0% of the successfully sequenced population in the experiment in which the pre-screened phage populous was exposed to propranolol covalently bound to glass beads.

Peptide 2 - NANNRLY

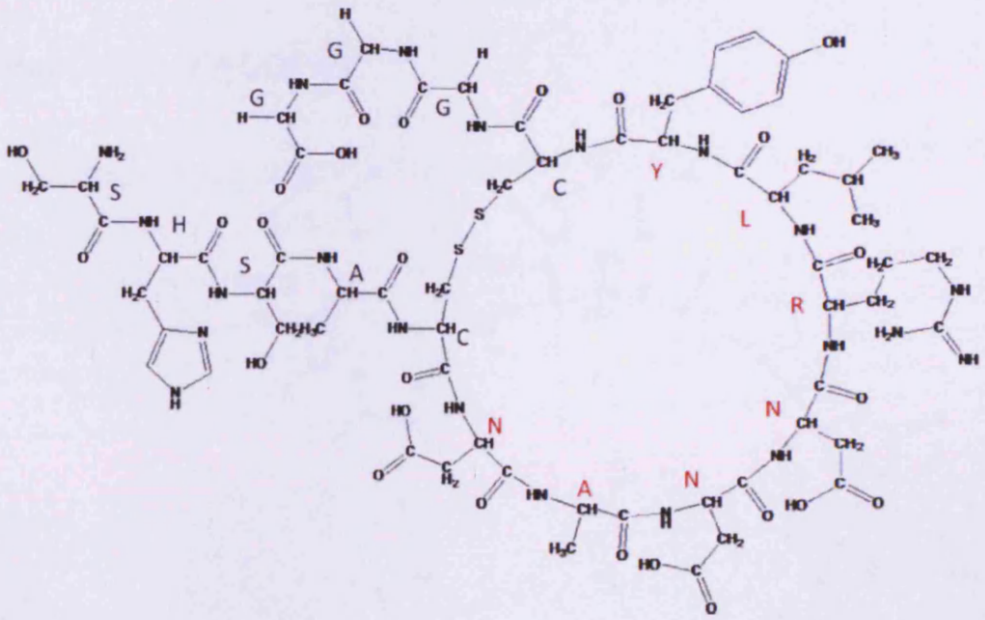

Figure 76: Sequence 2: NANNRLY (Asparagine-Alanine-Asparagine-Asparagine-Arginine-Leucine-Tyrosine).

Asparagine (N) is the predominant amino acid residue in this peptide; it is very small and polar, expressing a slight negative charge at physiological pH. Alanine (A) is very small and slightly hydrophobic.

Arginine (R) is polar and takes a positive charge at physiological pH. Leucine (L) is an aliphatic, hydrophobic residue. Tyrosine (Y) is aromatic and, whilst slightly polar, tends towards hydrophobicity.

This clone was present as 4.1% of the successfully sequenced population in the experiment in which the phage library was exposed to propranolol free base as an insoluble complex. It was not present in the successfully sequenced population in the experiment in which the pre-screened phage populous was exposed to propranolol covalently bound to glass beads.

Peptide 3 - PAQDPRY

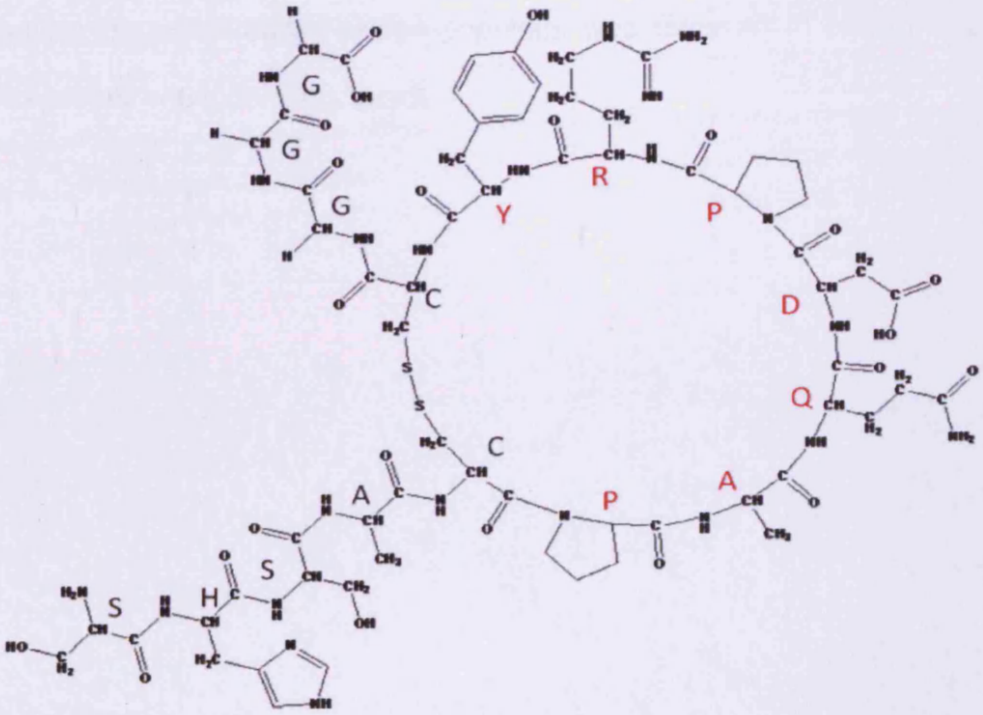

Figure 77: Sequence 3: PAQDPRY (Proline-Alanine-Glutamine-Aspartate-Proline-Arginine-Tyrosine).

Proline (P) is a very small aliphatic residue. Alanine (A) is very small and slightly hydrophobic. Glutamine (Q) is polar and very hydrophilic. Aspartate (D) is polar, expressing a negative charge at physiological pH. Arginine (R) is polar and takes a positive charge at physiological pH. Tyrosine (Y) is aromatic and, whilst slightly polar, tends towards hydrophobicity.

This clone was present as 1.0% of the successfully sequenced population in the experiment in which the phage library was exposed to propranolol free base as an insoluble complex. It was also present as 4.0% of the successfully sequenced population in the experiment in which the pre-screened phage populous was exposed to propranolol covalently bound to glass beads.

Peptide 4 - QIKHRHM

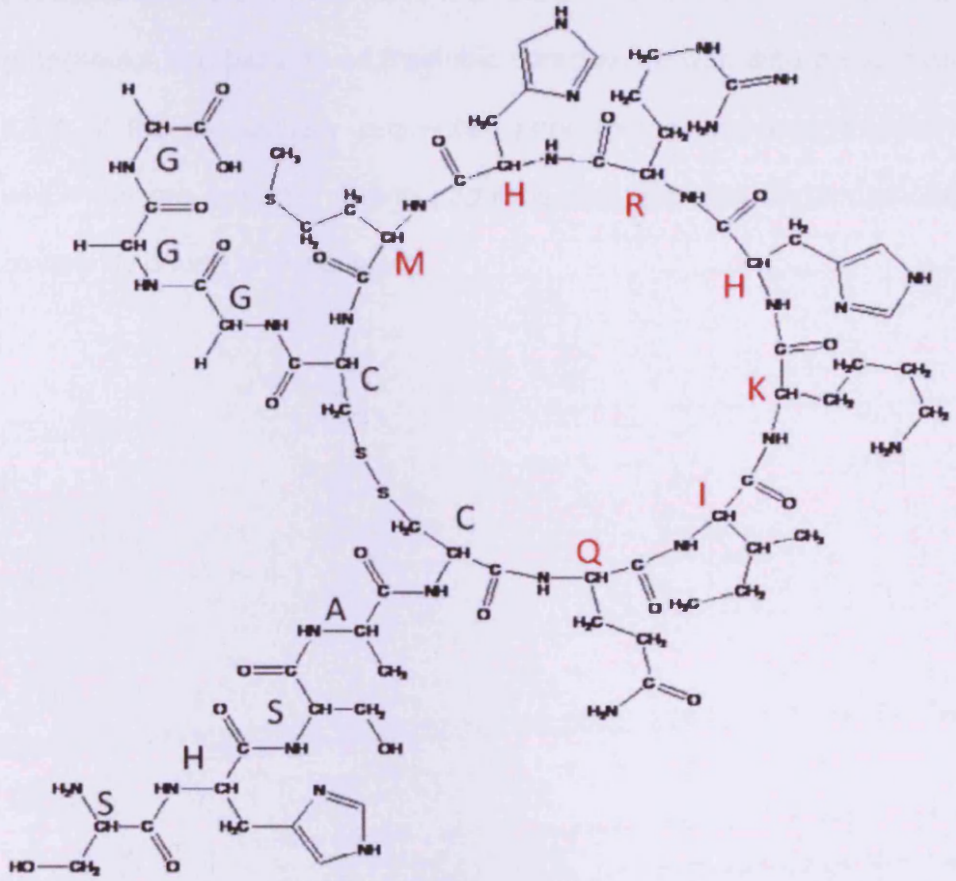

Figure 78: Sequence 4: QIKHRHM (Glutamine-Isoleucine-Lysine-Histidine-Arginine-Histidine-Methionine).

Glutamine (Q) is polar and very hydrophilic. Isoleucine (I) is aliphatic and largely hydrophobic. Lysine (K), whilst expressing a positive charge at physiological pH, is also largely hydrophobic. Histidine (H) has a five-membered nitrogen-containing aromatic ring which can accept a positive charge although the residue remains hydrophobic. Arginine (R) is polar and takes a positive charge at physiological pH. Methionine (M) is hydrophobic.

This clone was present as 4.1% of the successfully sequenced population in the experiment in which the phage library was exposed to propranolol free base as an insoluble complex. It was also present as 4.0% of the successfully sequenced population in the experiment in which the pre-screened phage populous was exposed to propranolol covalently bound to glass beads.

Appendix 2

Fluorescent Properties of Sulforhodamine

A2.1 Introduction

The experiments in this section assessed the alteration of fluorescence filters, together with the material and colour of the plates. Detection limit was assessed alongside the effect of "gain" on linearity of the resulting calibration curve. Incubation with various materials was carried out and the effect upon fluorescence observed. The overall objective was to thoroughly test the fluorescent properties of SR with a view to the construction of suitable assay methodology to allow accurate and consistent quantification of the compound during binding assessments.

A2.2 Methods

A2.2.1 Detection limit of Sulforhodamine 101 using FLUOstar OPTIMA

Standard solutions of SR in distilled water were prepared ranging from 0.001nM to 25nM. Aliquots (200µl) were placed into a black polystyrene 96-well plate (Nunc, Thermo Scientific) and read in the FLUOstar OPTIMA (BMG Labtech, Offenburg, Germany) using an excitation filter at 544nm and emission filter of 590nm. Four replicates of each

concentration were examined.

A2.2.2 Effect of "Gain" on Suiforhodamine Calibration Linearity

Standard solutions of SR in distilled water were prepared ranging from 25nM to 500nM. Aliquots (200µl) were placed into a black polystyrene plate and read in the FLUOstar OPTIMA using an excitation filter at 544nm and emission filter of 590nm. Four replicates of each concentration were examined. The highest concentrations (250nM and 500nM) were then discounted from the plate layout and the sensitivity of the plate-reader was then reset based on the 100nM sample. The lower points were then read again.

A2.2.3 Influence of Plate Colour and Filter

Standard solutions of SR in distilled water were prepared ranging from 10nM to 100nM. Aliquots (200ul) were placed into black or white polystyrene 96-well plates and read in the plate-reader using both 544nm and 580nm excitation filters, and both 590nm and 610nm emission filters.

A2.2.4 Binding of Sulforhodamine to Experimental Materials

Standard solutions of SR in distilled water were prepared ranging from 10nM to 1000nM. Aliquots (300µl) were then placed into polypropylene plates, polystyrene plates or glass multi-dose vials for 24 hours at room

temperature. Samples were then taken (200µl) and transferred to black polystyrene plates and read in the FLUOstar OPTIMA (Ex 544nm; Em 590nm).

A2.2.5 Repeated readings and binding to polystyrene plates

Standard solutions of SR in distilled water were prepared ranging from 20nM to 100nM, and 200µl aliquots were placed into a polystyrene plate such that eight rows contained an identical standard sequence. All readings took place in the FLUOstar OPTIMA (Ex 544nm; Em 590nm). The first row (Row A) was read every time the plate was returned to the instrument, whilst the subsequent rows were only read once after an appropriate period of incubation. Row B was read after 10 minutes, Row C after 20 minutes, Row D after 30 minutes, Row E after 60 minutes, Row F after 120 minutes, Row G after 180 minutes, and Row H after 24 hours.

A2.3 Results

A2.3.1 Detection limit of Suiforhodamine 101 using FluoSTAR OPTIMA

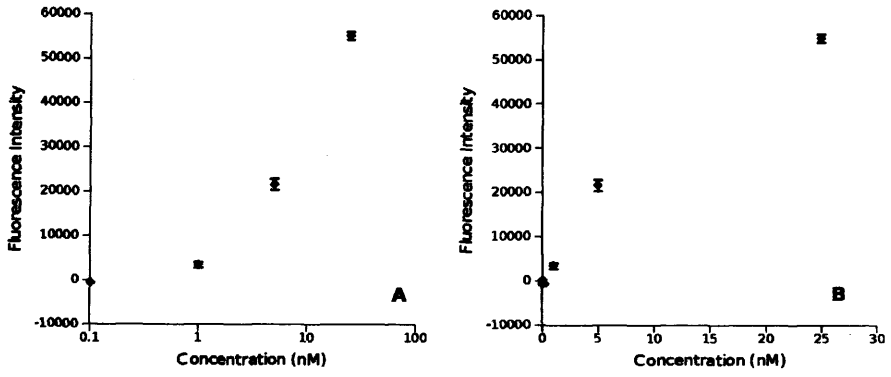

Figure 79: The fluorescence associated with low concentrations of sulforhodamine 101. Mean and standard deviation are shown, n=4. Ex 544nm, Em 590nm.

In Figure 79, "A" depicts a range of concentrations on a log scale. "B" shows a repeated reading of the lower concentrations, with the sensitivity of the plate-reader greatly increased in an effort to distinguish the lower-most points. This demonstrates that, even at high sensitivity, the quantifiable limit (5:1 signal-to-noise ratio) of SR in the FLUOstar OPTIMA is in the region of 10nM, where a sample is 200µl. This equates to approximately 2.0 pmoles per well. Whilst lower amounts can be detected, they are not significantly different from vehicle-only controls or indeed empty wells, so cannot be quantified.

A2.3.2 Effect of "Gain" on Sulforhodamine Calibration Linearity

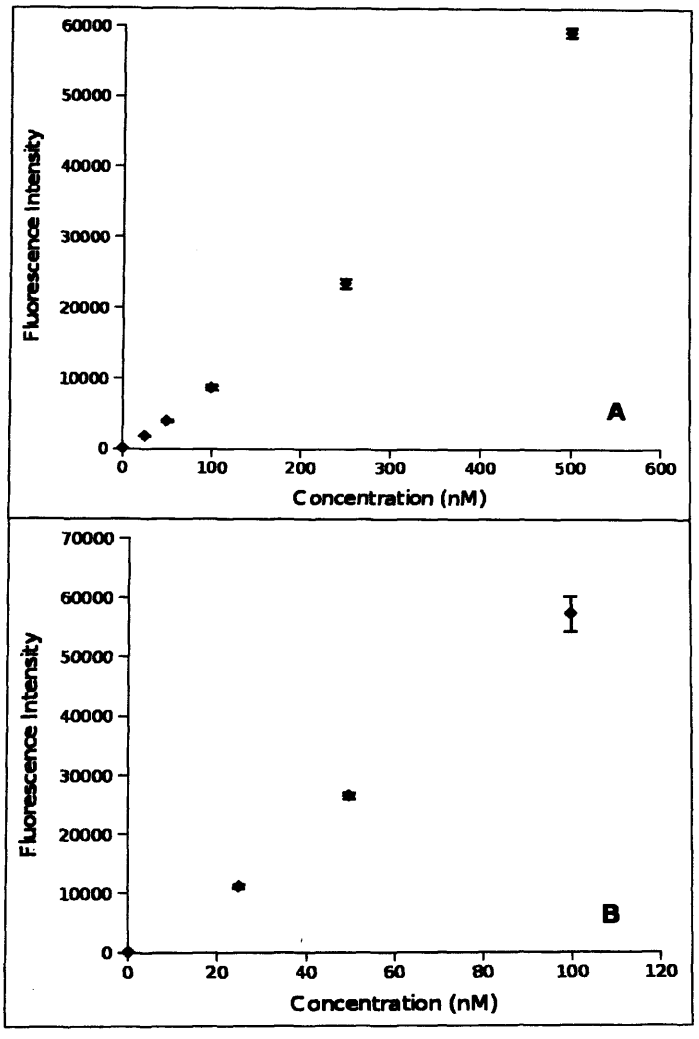

Figure 80: The fluorescence associated with low concentrations of sulforhodamine 101. Mean and standard deviation are shown (n=4). In graph A, the sensitivity of the plate-reader is given as 2476. In graph B, the sensitivity is increased to 3141. In each case the instrument settings were determined automatically to place the highest data point at 90% of the capacity of the instrument.

As illustrated by Figure 80 the sensitivity of the instrument does not appear to have any effect on the distribution of data points in this instance.

A2.3.3 Influence of Plate Colour and Filter

Figure 81 shows SR calibration standards in black plates.

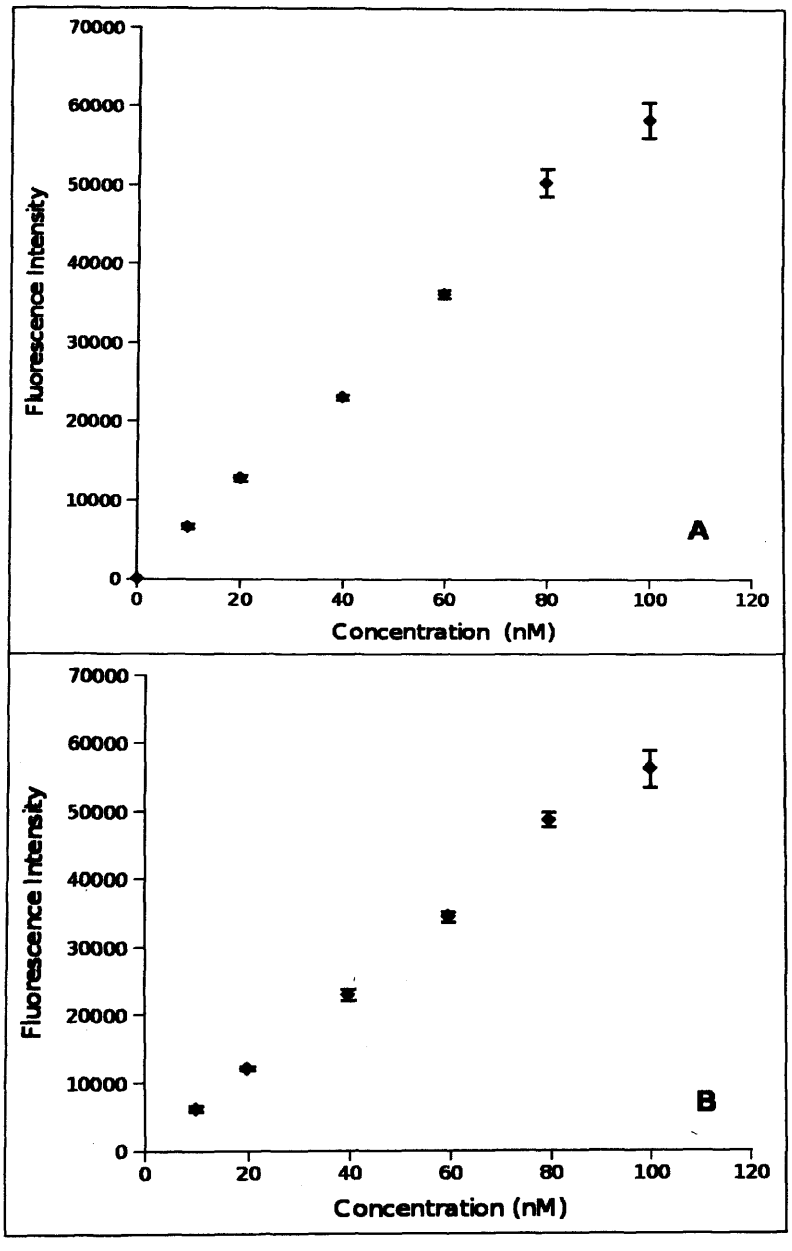

Figure 81: The fluorescence associated with solutions of sulforhodamine 101 in water – in black plates. Filters used were Excitation 544nm and Emission 590nm in A; Excitation 580nm and Emission 610nm in B. Graphs shown mean and standard deviation (n=4).

There appears to be very little difference between the two curves,

although the level of variance is slightly greater when using Excitation at 580nm and Emission at 610nm (graph B above).

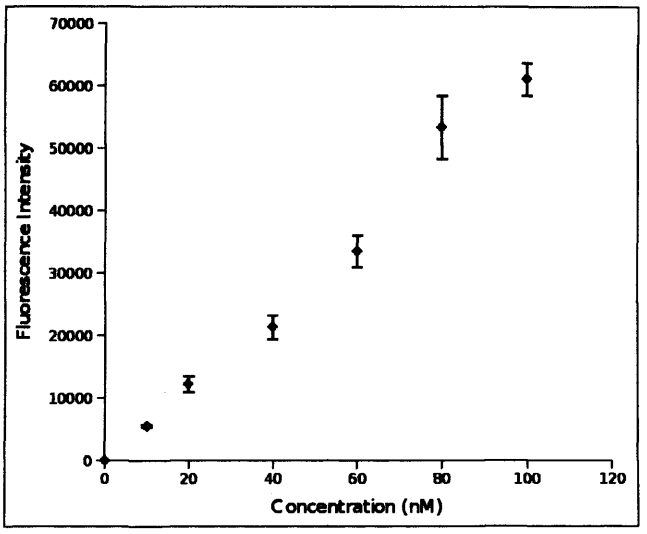

Figure 82: The fluorescence associated with solutions of sulforhodamine 101 in water – in black plates. Filters used were Excitation 544nm and Emission 610nm. Graph shows mean and standard deviation (n=4).

These data are directly comparable with the data obtained from the black plates above. When using excitation of 544nm and reading emission at 610nm the mean fluorescence values stay approximately the same, although far greater variability is seen.

Figure 83 shows SR calibration standards in white plates.

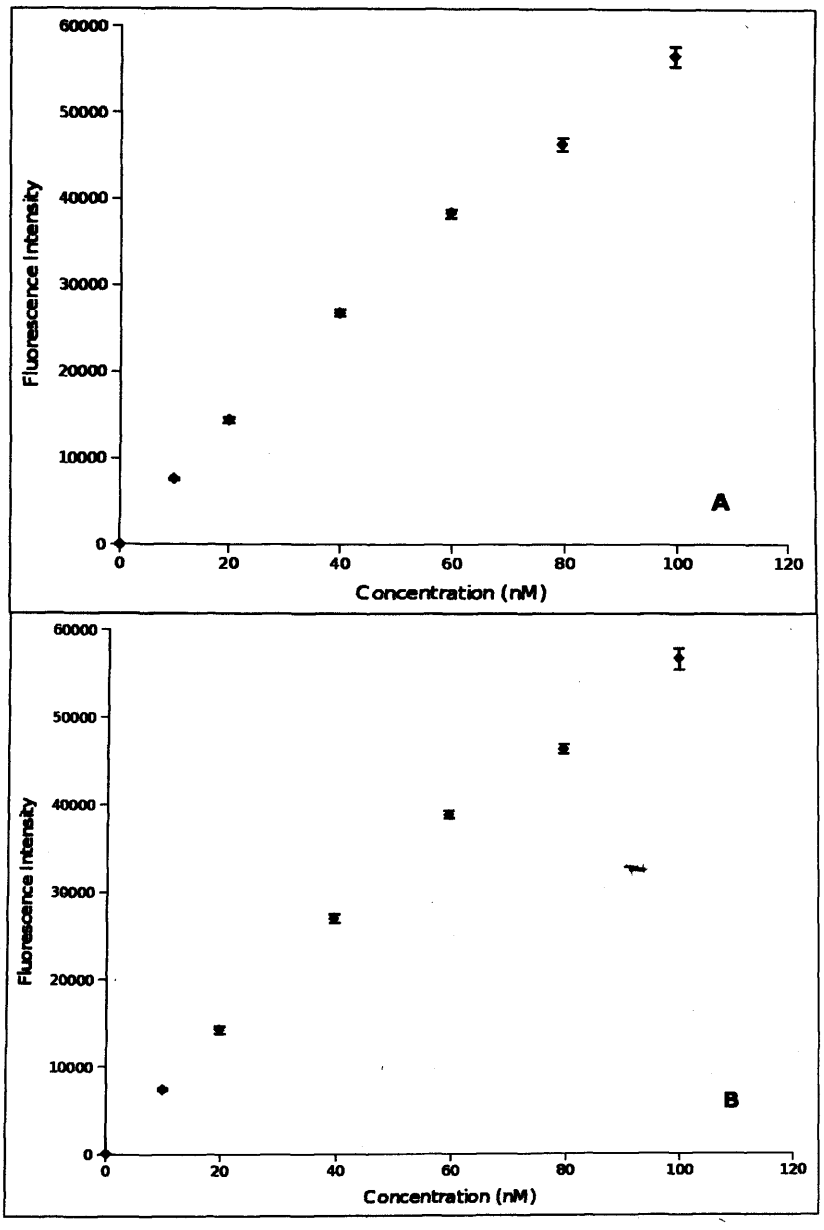

Figure 83: The fluorescence associated with solutions of sulforhodamine 101 in water – in white plates. Filters used were Excitation 544nm and Emission 590nm in A; Excitation 580nm and Emission 610nm in B. Graphs shown mean and standard deviation (n=4).

Again, Figure 83 shows there is little difference between the two filter methods when using the white plates. Although, an interesting observation is that the calibration lines associated with the white plates

appear to curve as if approaching a plateau. The gain was automatically determined by the instrument in each case, based on the well with the greatest fluorescence intensity. The black plates induced a gain of 2844 and 2875 for graphs A and B in Figure 81 respectively, whilst the white plates brought about gain values of 1479 and 1431 for graphs A and B in Figure 83 respectively. This would imply that far greater amounts of light were available when using the white plates as the surface is, of course, more likely to reflect. It is possible that auto-quenching is already being approached at only 100nM.

A2.3.4 Binding to Experimental Materials

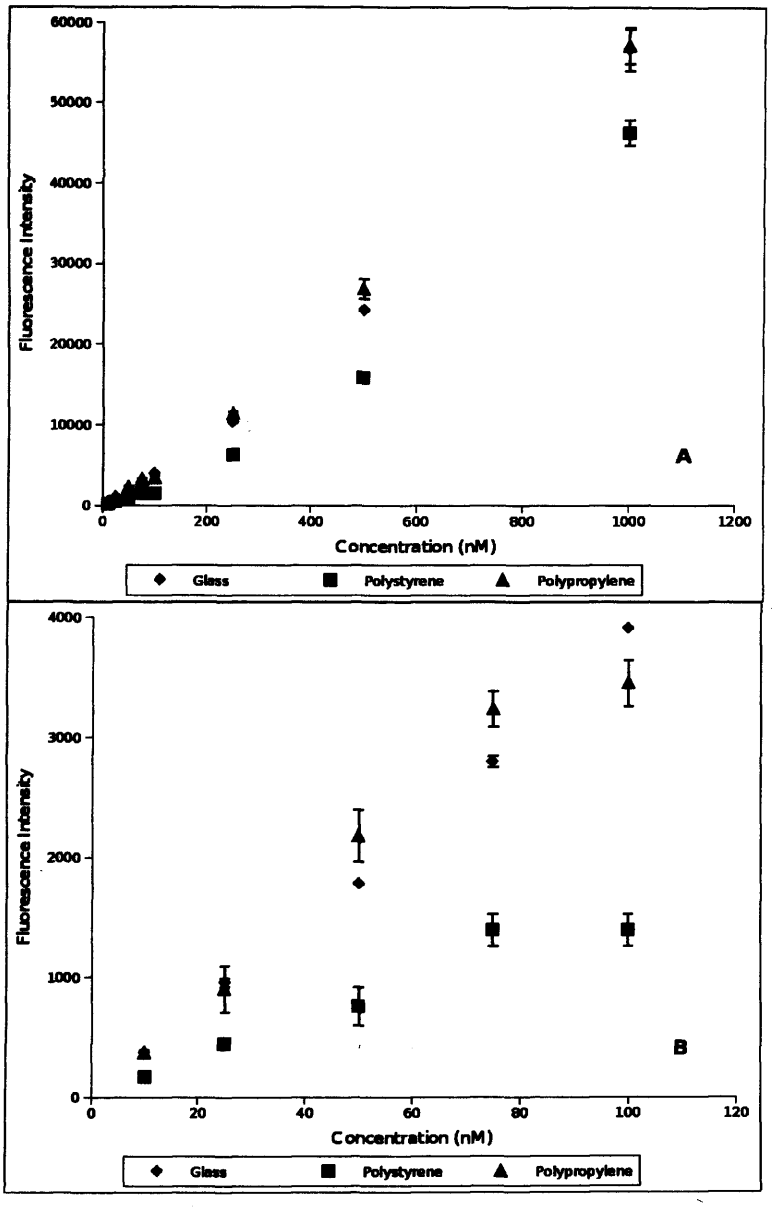

Figure 84: The fluorescence associated with solutions of sulforhodamine 101 in water after incubation with a range of materials. Filters used were Excitation 544nm and Emission 590nm. Graphs shown mean and standard deviation (n=4).

It is evident from Figure 84 that whilst little or no binding occurs with polypropylene in comparison with glass, a large proportion of SR is lost in non-specific binding to polystyrene.

A2.3.5 Repeated readings versus binding to polystyrene plates

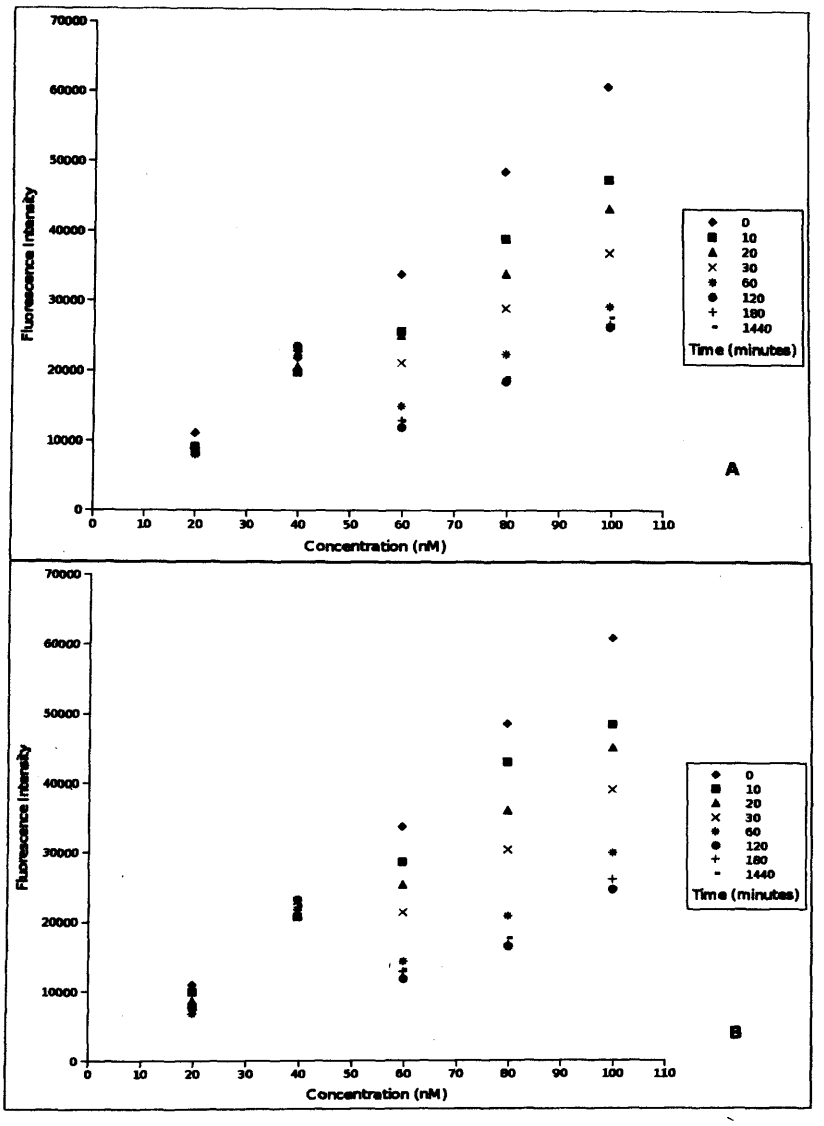

Figure 85: The fluorescence associated with sulforhodamine 101 solutions in water upon repeated reading over time (A) and single readings with incubation time alone (B). Filters used were Excitation 544nm and Emission 590nm.

There appears to be little or no difference between the graphs A and B above, indicating that time spent in the polystyrene plate is the overriding factor in the decrease in fluorescence intensity. This is unsurprising given that SR exhibits a high degree of non-specific

binding to polystyrene. Repeated readings appear to have little or no effect in comparison with regard to photobleaching.

Appendix 3

Preparation of Glass Surfaces Prior to Immobilisation of TR401

A3.1 Introduction

This set of experiments was intended to allow immobilisation of the peptide TR401 via either the N-terminal lysine residue or by the unique sulfhydryl group present on the C-terminal cysteine residue. It was hoped that comparisons could be drawn which would enable a better understanding of the binding event with a view to influencing the peptide orientation in the final polymer product.

A3.2 Methods

A3.2.1 Surface Functionalisation

Glass microscope slide cover slips were cleaned using two sonication steps: 15 minutes in ethanol, followed by 15 minutes in dimethylformamide (DMF). They were then dried under clean, flowing nitrogen. The cover slips were then activated using piranha solution. Briefly, they were placed into a small Petri dish and covered using concentrated sulfuric acid (7ml). Hydrogen peroxide (30% - 3ml) was added dropwise to produce the piranha solution which was kept at

approximately 80°C for 20 minutes, then allowed to cool for a further 10 minutes. The cover slips were then washed three times in distilled water, for 10 minutes each time, then dried under nitrogen.

Evaporation was carried out using a 50%w/w solution of either 3-aminopropyltriethoxysilane (APTES) (Sigma, A3648) or 3-mercaptopropyltriethoxysilane (MPTES) (Fluka, 63797) in paraffin oil (Fisher, P/0320/17) in an upturned lid from a microcentrifuge tube (shown in Figure 86). This was placed in a small Petri dish at room temperature with the cover slips to allow evaporation for five minutes each side. The cover slips were then transferred to acetone and sonicated for 10 minutes, given two further 10 minute washes with acetone without sonication, dried under nitrogen then allowed to cure in a drying oven overnight.

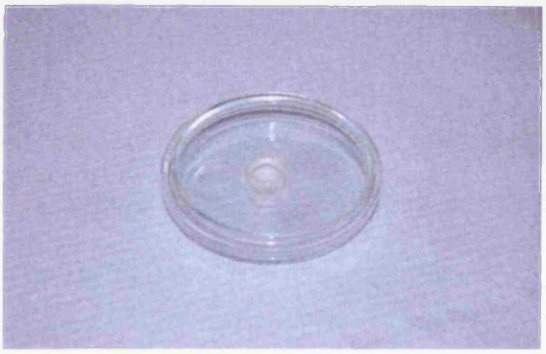

Figure 86: Layout of the evaporation process, showing the glass coverslips arranged around the upturned microcentrifuge tube lid, encased within a Petri dish.

The majority of this linking chemistry is readily transferable to glass beads instead of flat cover slips, with the exception of the initial evaporation steps. This was replaced with a 24 hour reflux in toluene with 2% w/w APTES or MPTES.

A.3.2.2 Confirmation of surface alteration

Atomic Force Microscopy

Treated glass cover slips were incubated in a solution of gold nanoparticles (Sigma, G1527 [~0.75A_{520} units/ml] 10nm diameter) for 24 hours at room temperature in the dark. They were then washed three times in large volumes of distilled water, dried under nitrogen, and the surfaces observed using a Veeco Scanning Probe Microscope 004-130-000.

Contact Angle Observation

The pre-treated glass cover slips were placed on a surface level with the centre of the lens of a camera (Nikon D50 SLR). A small drop of ddH_2O (2µl) was then placed on the surface and a photograph taken.

A3.3 Results

Linking Chemistry – AFM and contact angles

Treatment	Predicted Structure AFM image | Contact Angle	
Piranha solution activated	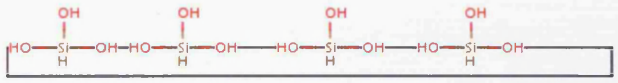	
	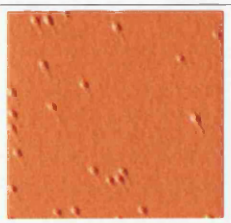	
Evaporation of APTES	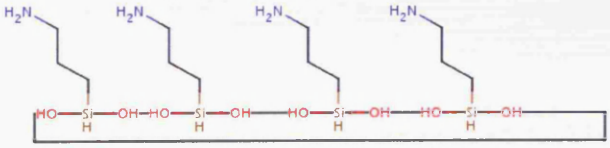	
	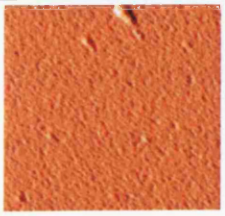	

Sulfo-SMCC linkage	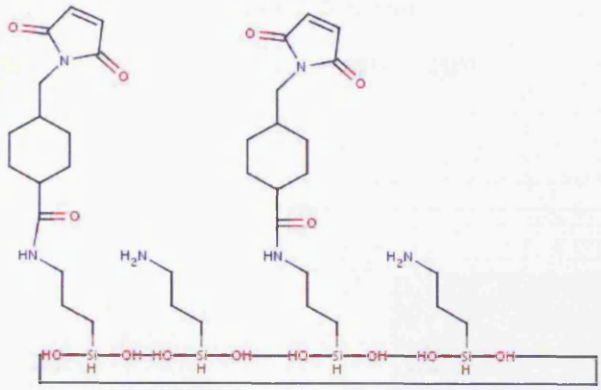	
	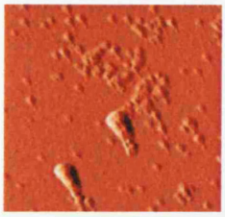	

Table 8: Amine activated surfaces, prepared to connect to the TR401-modified peptide via the sulfhydryl group on the C-terminal cysteine residue.

As shown in Table 8, the piranha solution-activated glass surface is highly hydrophilic and does not attract the gold nanoparticles from suspension, however, once evaporated with APTES, a slight drop in hydrophilicity is seen (water contact angle) and the AFM image shows a surface well-populated with gold nanoparticles. Sulfo-SMCC linkage appears to decrease hydrophilicity further and make the deposition of gold more erratic.

Treatment	Predicted Structure AFM image | Contact Angle	
Piranha solution activated	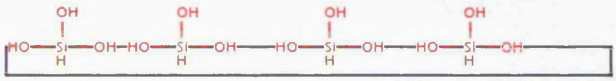	
		
Evaporation of MPTES	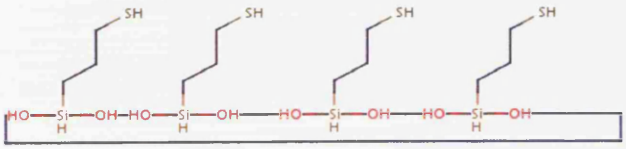	
	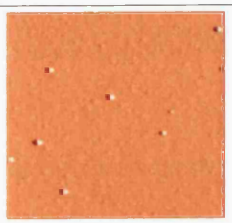	

Sulfo-SMCC linkage	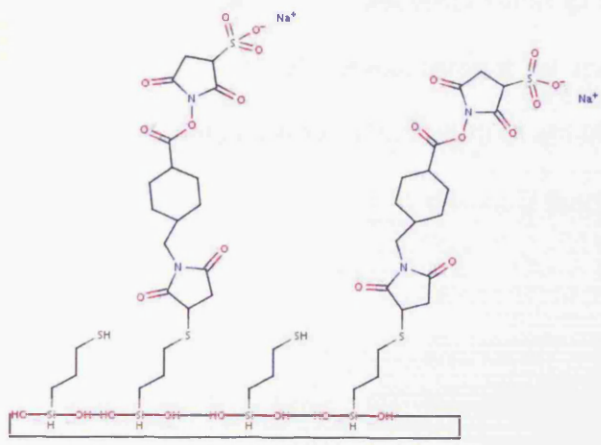	
	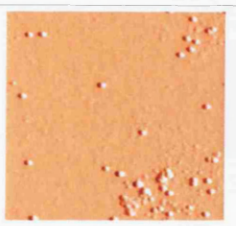	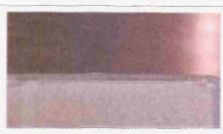

Table 9: Sulfhydryl activated surfaces, prepared to connect to the TR401-modified peptide via the amine group on the N-terminal lysine residue.

Table 9 shows a piranha solution-activated glass surface very similar to that shown in Table 8. However, evaporation of MPTES results in a very hydrophobic surface (water contact angle) and the AFM image shows a surface which still does not attract gold nanoparticles. Sulfo-SMCC linkage appears to increase hydrophilicity once more further and is comparable to the surface seen in Table 8.

Whilst the data presented indicate that successful conjugation of TR401 to glass surfaces is possible, a binding assay using the protocol described in Chapter 3 (3.2.3) showed no significant difference in the amount of sulforhodamine 101 bound by TR401-functionalised glass

beads from controls. This may, in part, be due to decomposition of the peptide-glass linkage throughout the course of the experiment, or, more likely, that the surface area of the glass bead is simply too small to immobilise a sufficient amount of TR401 to be able to detect a binding effect.

Merrifield Resin, with its macroporous structure, provides a far greater surface area upon which to immobilise peptides of interest.

Appendix 4

A4.1 Introduction

Integral to the production of a good quality imprinted polymer is template removal from the finished product. Of course, the binding sites in the finished polymer may have high affinity for their target but if they are still occupied by the template included in the manufacturing process, this binding affinity will never be seen. In this instance, the binding site is not typical of that found in molecular imprinting literature, instead being peptide derived from phage display. Therefore, we turn to phage display protocols for methods of template removal. In their paper (Rozinov and Nolan, 1998), the dye is immobilised to a solid support while the peptide is in situ on the phage particle and the authors elute bound phage from their target with a glycine buffer.

However, it was found that glycine buffer did not disrupt binding when the peptide was immobilised to Merrifield Resin and the dye was free in solution. Arginine buffer is used in protein purification and antibody elution (Ejima et al., 2005, Arakawa et al., 2007). With this in mind, several washing procedures were employed.

A4.2 Methods

TR401-functionalised resin was incubated in a SR solution (16.5μM) and then sonicated in either arginine buffer (1M, pH4.3) or ethanol. Resulting resins were then observed under Leica SP5 confocal laser-scanning microscope equipped with argon and helium/neon laser and a 63×oil-immersion objective. The bright-field and fluorescence frames were then processed as side-by-side images using the Leica LAS AF software. The resins were then re-exposed to SR and observed once more under the microscope in an effort to observe whether rebinding could occur, i.e. whether the washing regimen damages the binding ability of the peptide-functionalised resin.

A4.3 Results

The following series of confocal microscopy images each comprise a fluorescence-only image, a bright-field image, and an overlay.

Table 10: Key to confocal microscopy images presented in Figures 87-90.

Fluorescence Image	Bright-field Image
Overlay	KEY

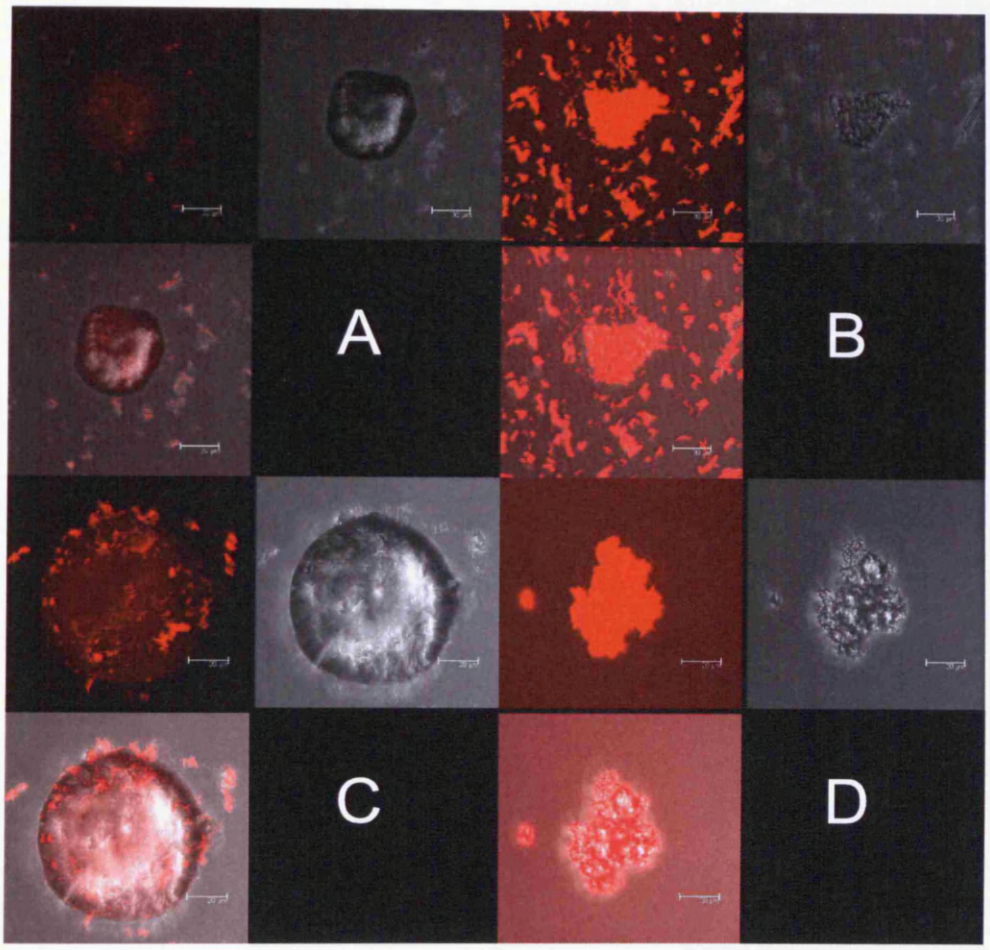

Figure 87: Peptide-functionalised resin: Unexposed resin (A), exposed to sulforhodamine (B), sonicated in arginine buffer (C), re-exposed to sulforhodamine (D) observed under Leica SP5 confocal laser-scanning microscope.

The first experiment in this series observes the washing effect of sonication in arginine buffer (pH 4.3) in an attempt to remove bound SR from peptide-functionalised Merrifield Resin, shown in Figure 87. The first set of images (A) show peptide-functionalised resin that had not been exposed to SR. Some minimal autofluorescence is observed. The second set of images (B) show the same resin after exposure to SR (330nM in water, rinsed twice with distilled water). The third images (C) show the same resin after sonication for 5 minutes in arginine buffer. In

an effort to demonstrate re-binding of SR, the fourth set of images (D) was a re-exposure of this resin to SR solution. Figure 88 shows the same treatments using non-functionalised resin.

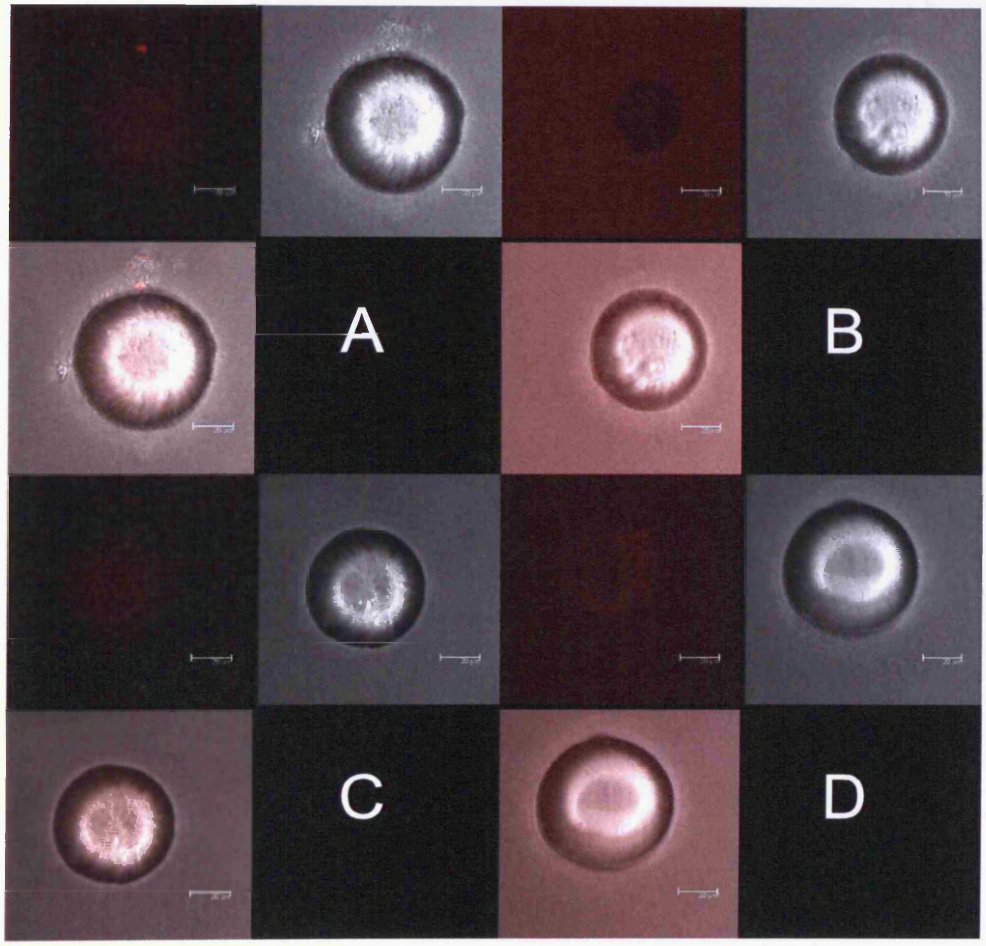

Figure 88: Non-functionalised resin: Unexposed resin (A), exposed to sulforhodamine (B), sonicated in Arginine buffer (C), re-exposed to sulforhodamine (D) observed under Leica SP5 confocal laser-scanning microscope.

Figure 89 and Figure 90 show a repeat of the previous experiment with an ethanol wash in place of arginine.

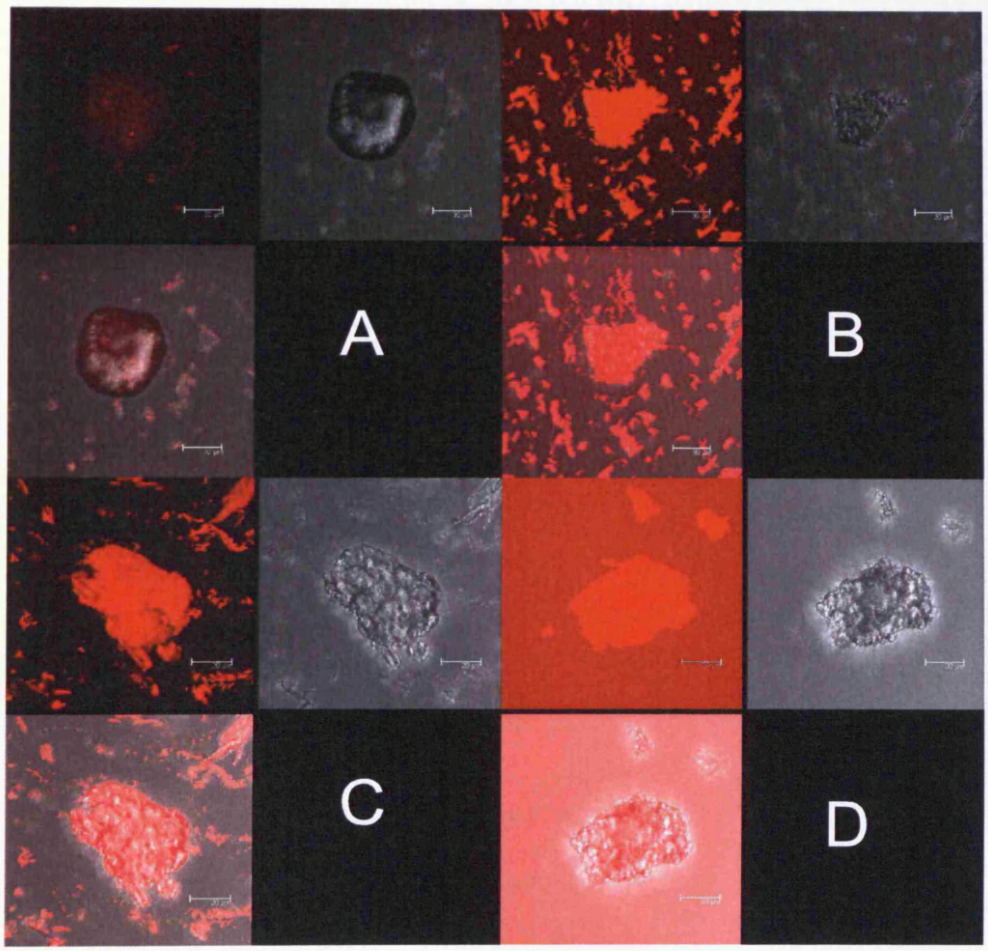

Figure 89: Peptide-functionalised resin: unexposed resin (A), exposed to sulforhodamine (B), sonicated in ethanol (C), re-exposed to sulforhodamine (D) observed under Leica SP5 confocal laser-scanning microscope.

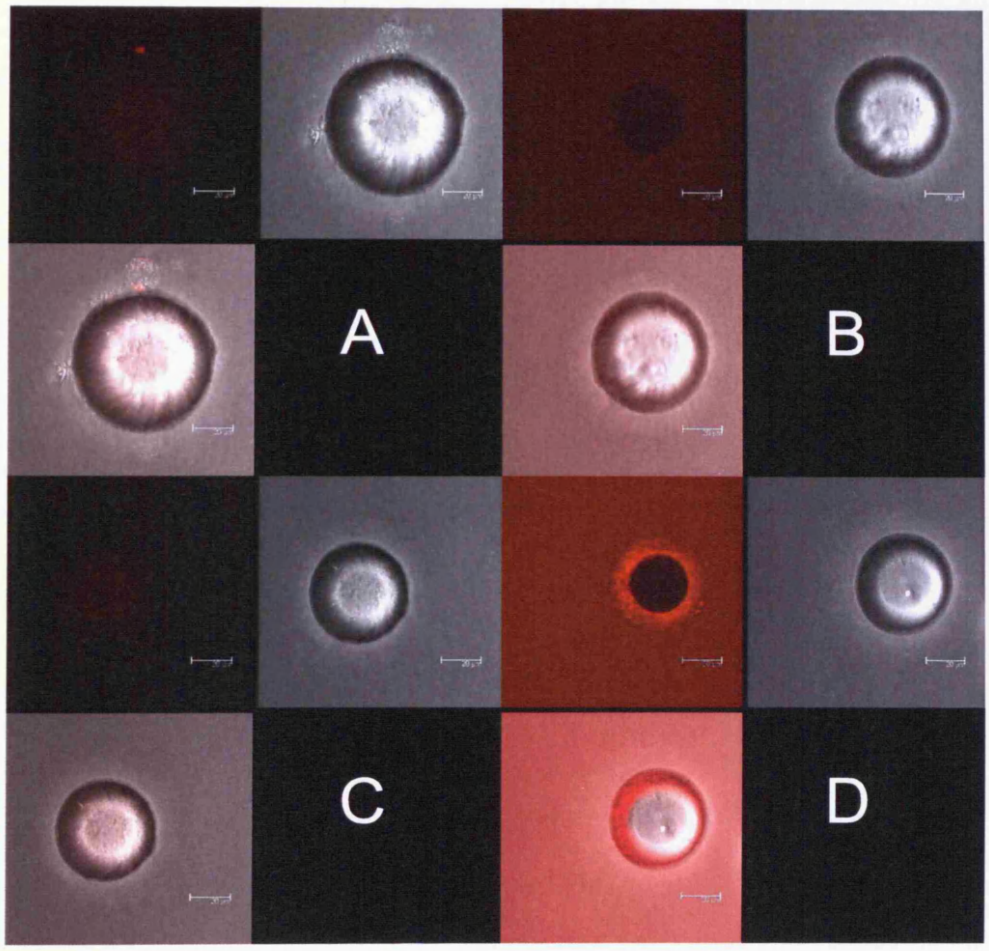

Figure 90: Non-functionalised resin: unexposed resin (A), exposed to sulforhodamine (B), sonicated in ethanol (C), re-exposed to sulforhodamine (D) observed under Leica SP5 confocal laser-scanning microscope.

Appendix 5

Peptide TR401 Stability

Upon receipt of TR401 from manufacture at Severn Biotech, it was assessed using high performance liquid chromatography (HPLC) and Matrix-assisted laser desorption/ionisation-time of flight mass spectrometry (MALDI-TOF MS).

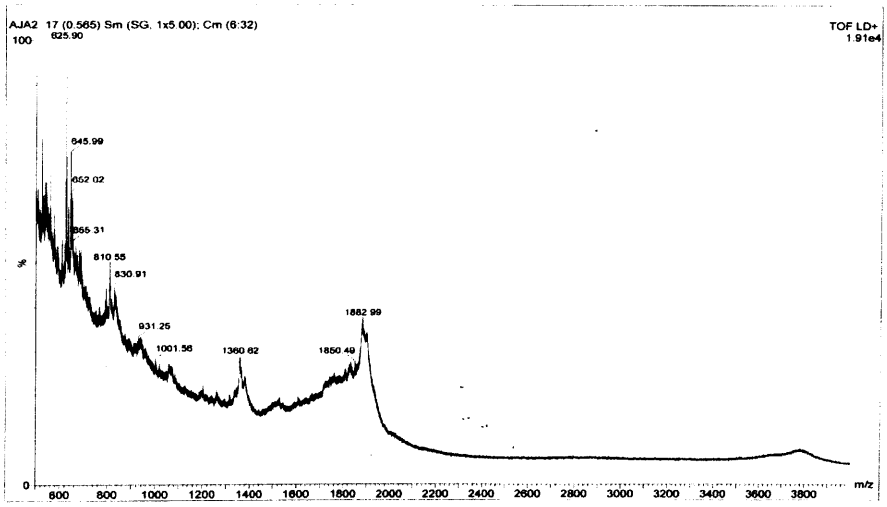

Figure 91: MALDI-TOF scan of TR401 as supplied by Severn Biotech.

Figure 91 shows the mass spectrum of TR401 direct from Severn Biotech, stored at -20°C under desiccation. Figure 92 shows the same sample after being put through three freeze-drying cycles.

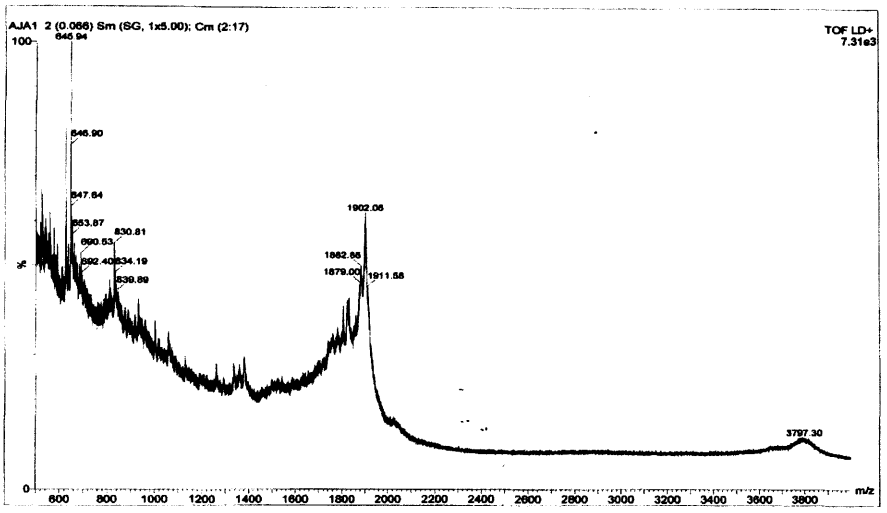

Figure 92: MALDI-TOF scan of TR401 after three freeze-drying cycles.

Figure 91 and 92 indicate that there may already be some fragmentation of the peptide even upon receipt from manufacturer, as the molecular weight of TR401 is approximately 1900Da. There is also some evidence of dimerisation as there is a small peak visible at approximately 3800Da.

TR401, as supplied from Severn Biotech, was dissolved in a range of solvents and assessed using HPLC. The stationary phase consisted of a C18 column, with gradient mobile phase constructed using H_2O + 0.1% trifluoroacetic acid (TFA) and acetonitrile (MeCN) + 0.1%TFA, initially 95:5 for 35 minutes, then 0:100 until 50 minutes. Peptide was detected with UV absorbance at 220nm and 254nm.

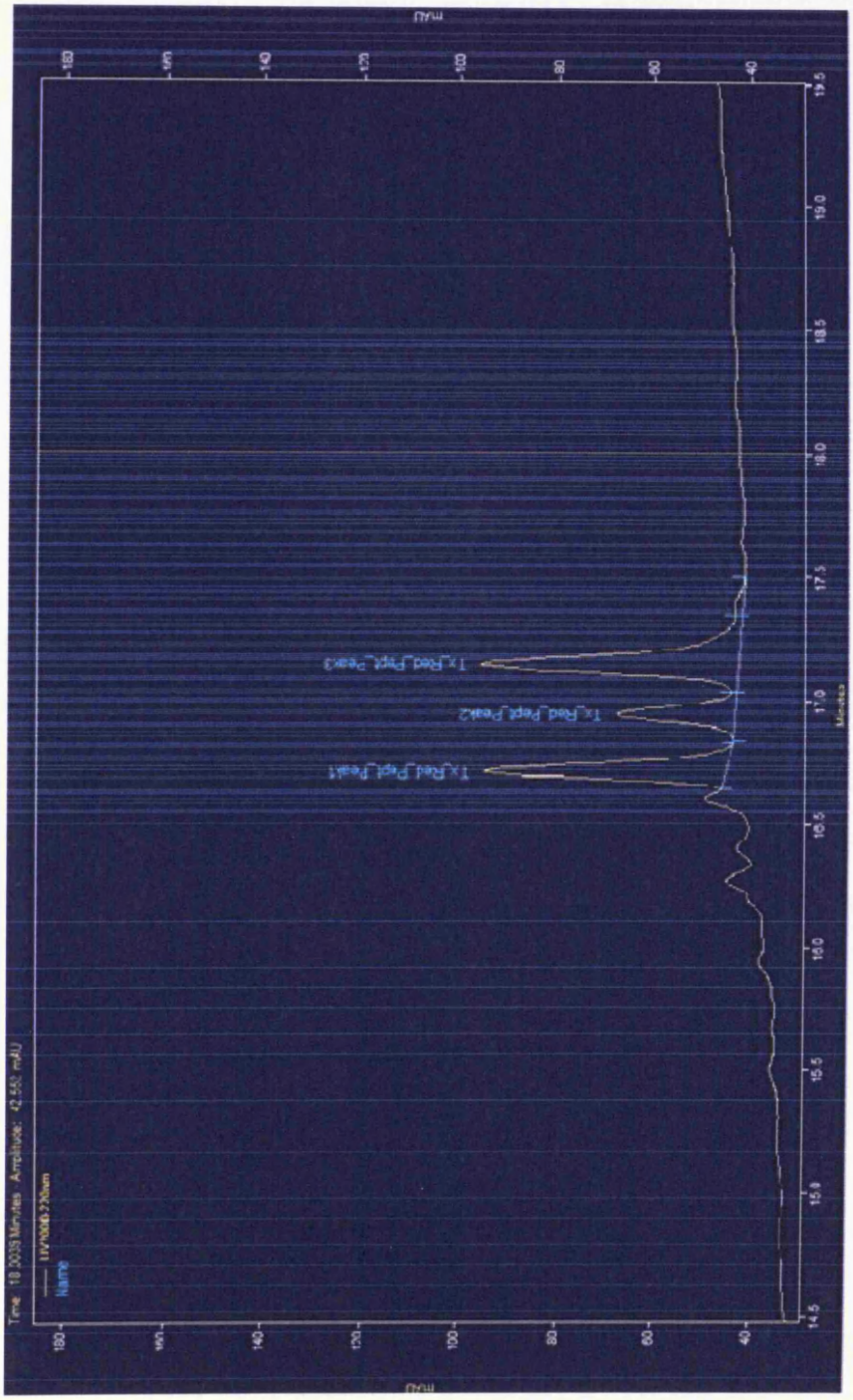

Figure 93: HPLC trace of TR401 from C18 column using gradient mobile phase H_2O + 0.1% trifluoroacetic acid (TFA) and acetonitrile (MeCN) + 0.1%TFA, initially 95:5 for 35 minutes, and then 0:100 until 50 minutes.

Table 11: Peak areas associated with TR401 in a range of solvents as assessed by HPLC.

Treatment	Peak 1 (%)	Peak 2 (%)	Peak 3 (%)
Water	34.7	16.2	44.2
PBS	32.8	18.6	48.1
TBS	48.2	12.3	38.9
Ethanol	45.6	17.1	37.1
Methanol	52.6	19.0	27.8
Methanol/water 50:50	56.5	19.2	23.0

"Peptides containing tryptophan may show some peak splitting on HPLC because this bulky group can affect the secondary structure, causing the peptide to exist in different conformers in solution, which have slightly different retention times on HPLC."

Dr. A. Smithson (Peptide chemist, Severn Biotech)

Personal Communication.

Appendix 6

Polymerisation data

Figures 94-101 show the binding isotherms for which K_D and Bmax are summarised in Chapter 4 (Table 4&5 in Section 4.3.4).

Figure 94 and Figure 95 show the result of the SR binding assays carried out with peptide-functionalised non-imprinted polymer (P-NIP) at varying polymerisation times. Figure 96 and Figure 97 show the equivalent data for the peptide-functionalised molecularly imprinted polymer (P-MIP).

The remaining figures are the result of the non-peptide treatments, both imprinted and non-imprinted.

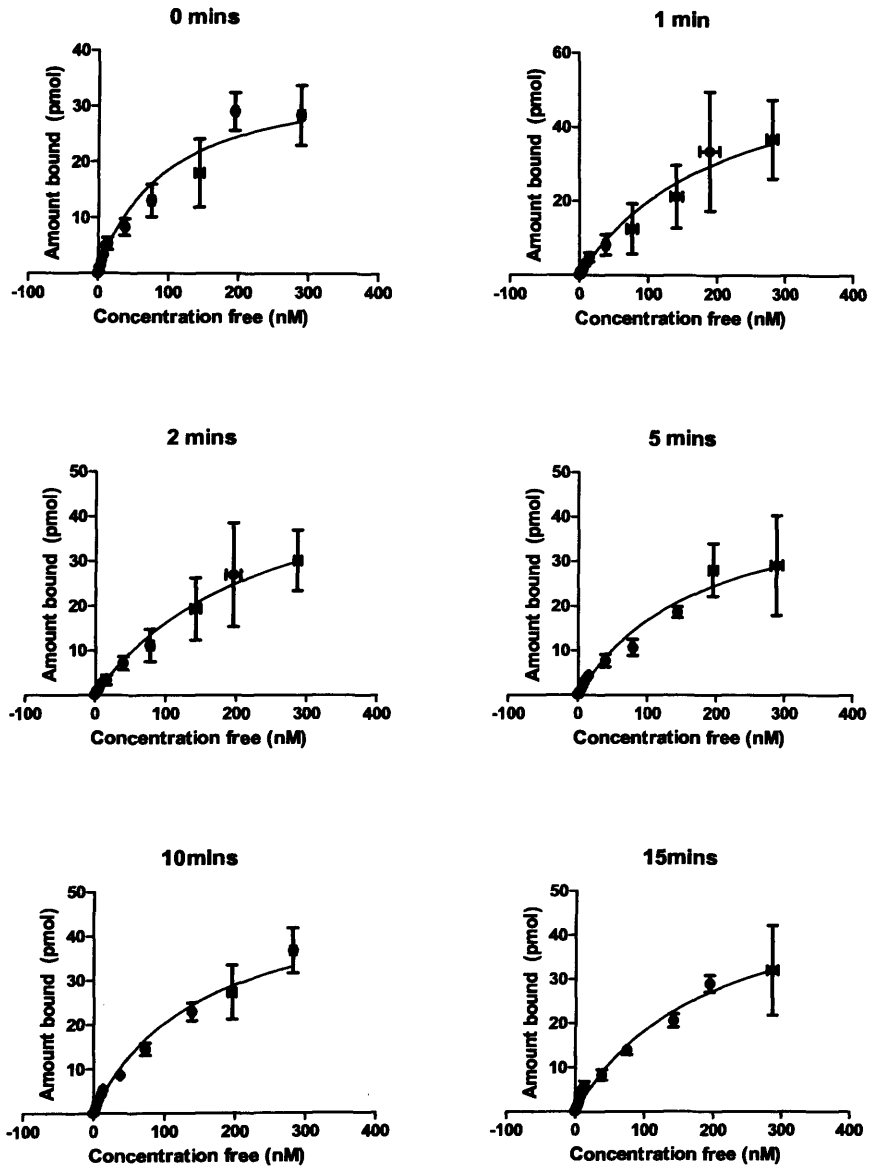

Figure 94: Sulforhodamine-binding assay performed using Peptide-functionalised, non-imprinted polymer (P-NIP) – Polymerisation times ranging from 0 to 15 minutes.

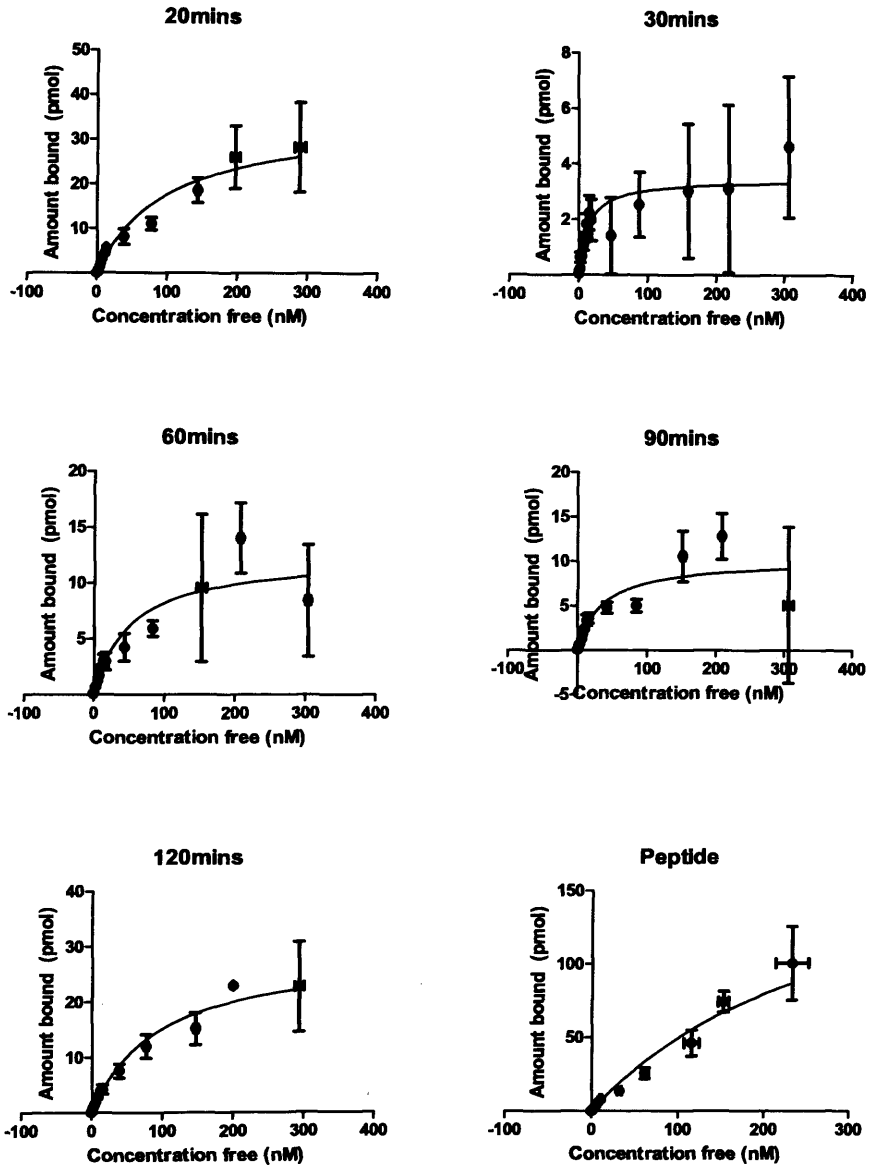

Figure 95: Sulforhodamine-binding assay performed using Peptide-functionalised, non-imprinted polymer (P-NIP) – Polymerisation times ranging from 20 minutes to 120 minutes. TR401-functionalised resin with no polymerisation is included for reference.

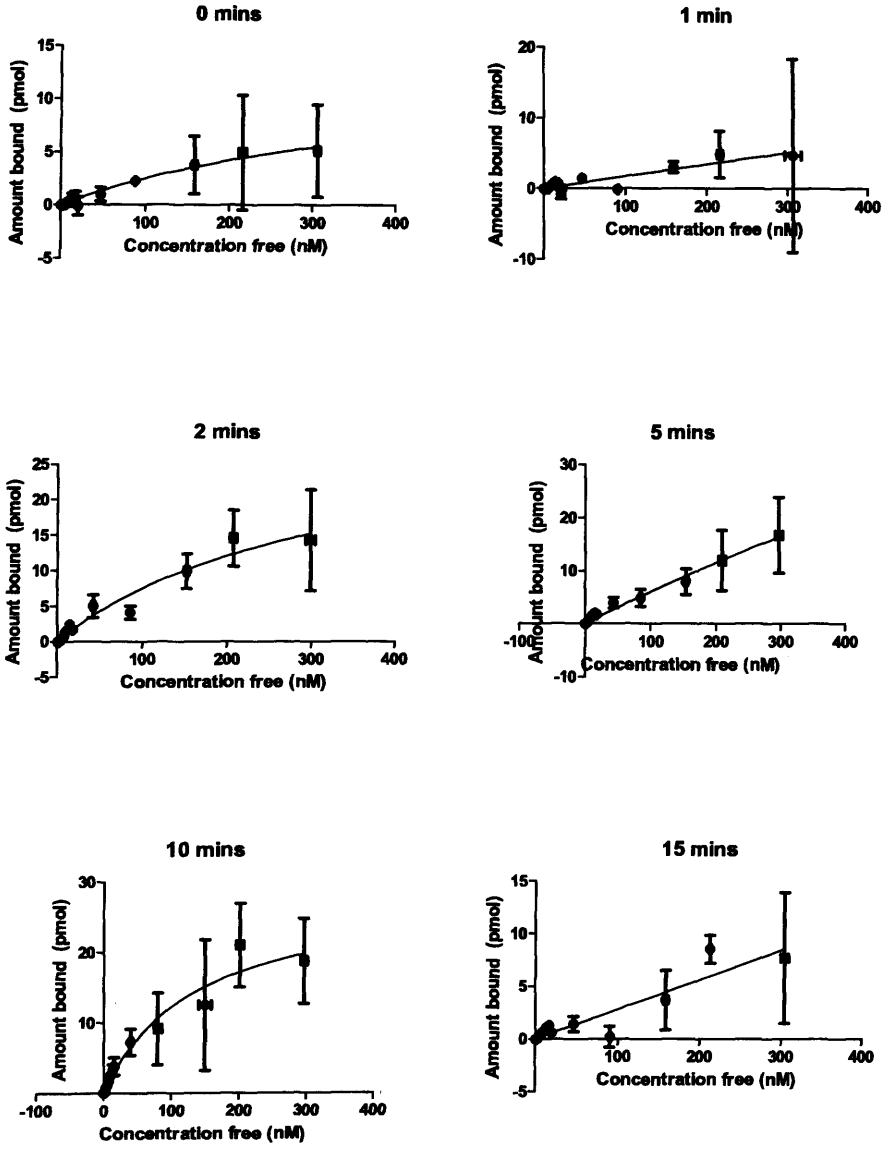

Figure 96: Sulforhodamine-binding assay performed using Peptide-functionalised molecularly imprinted polymer (P-MIP) – Polymerisation times ranging from 0 to 15 minutes.

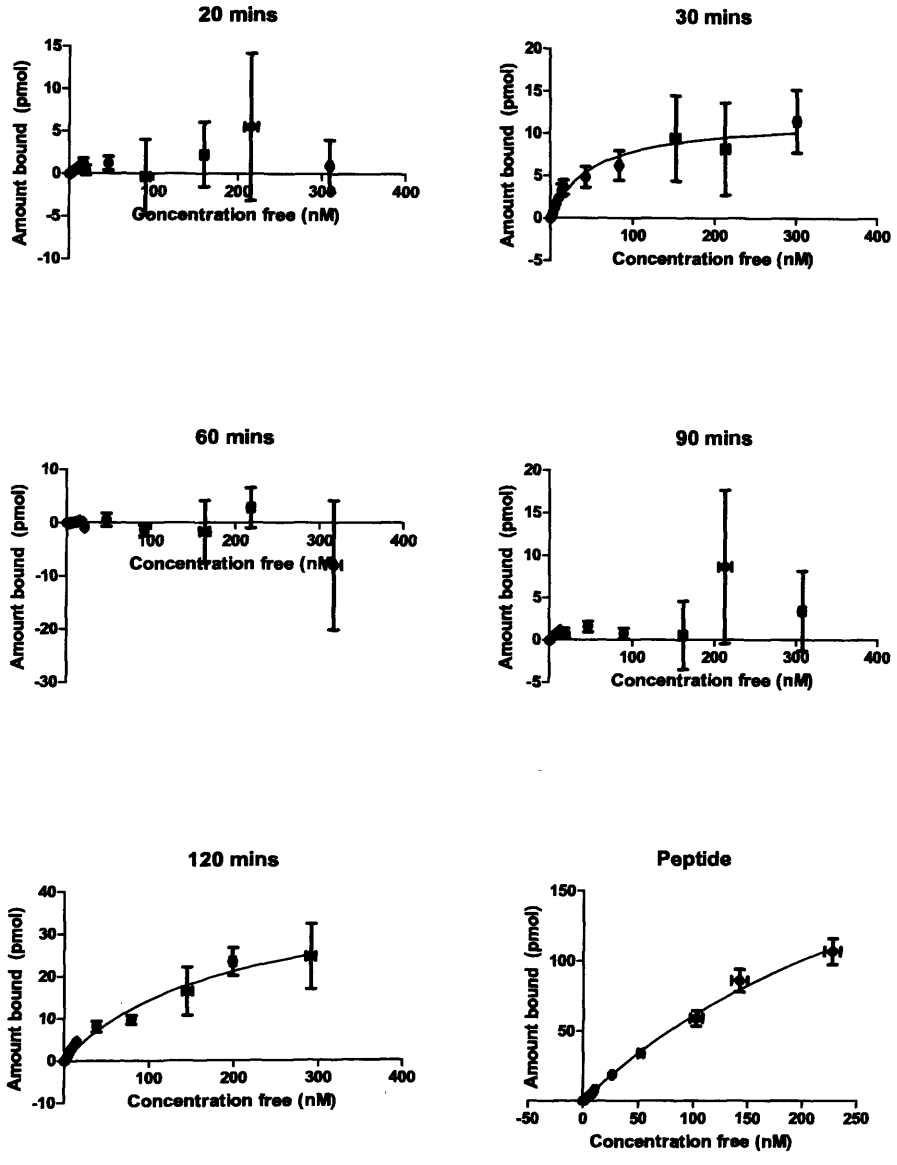

Figure 97: Sulforhodamine-binding assay performed using Peptide-functionalised molecularly imprinted polymer (P-MIP) – Polymerisation times ranging from 20 minutes to 120 minutes. TR401-functionalised resin with no polymerisation is included for reference.

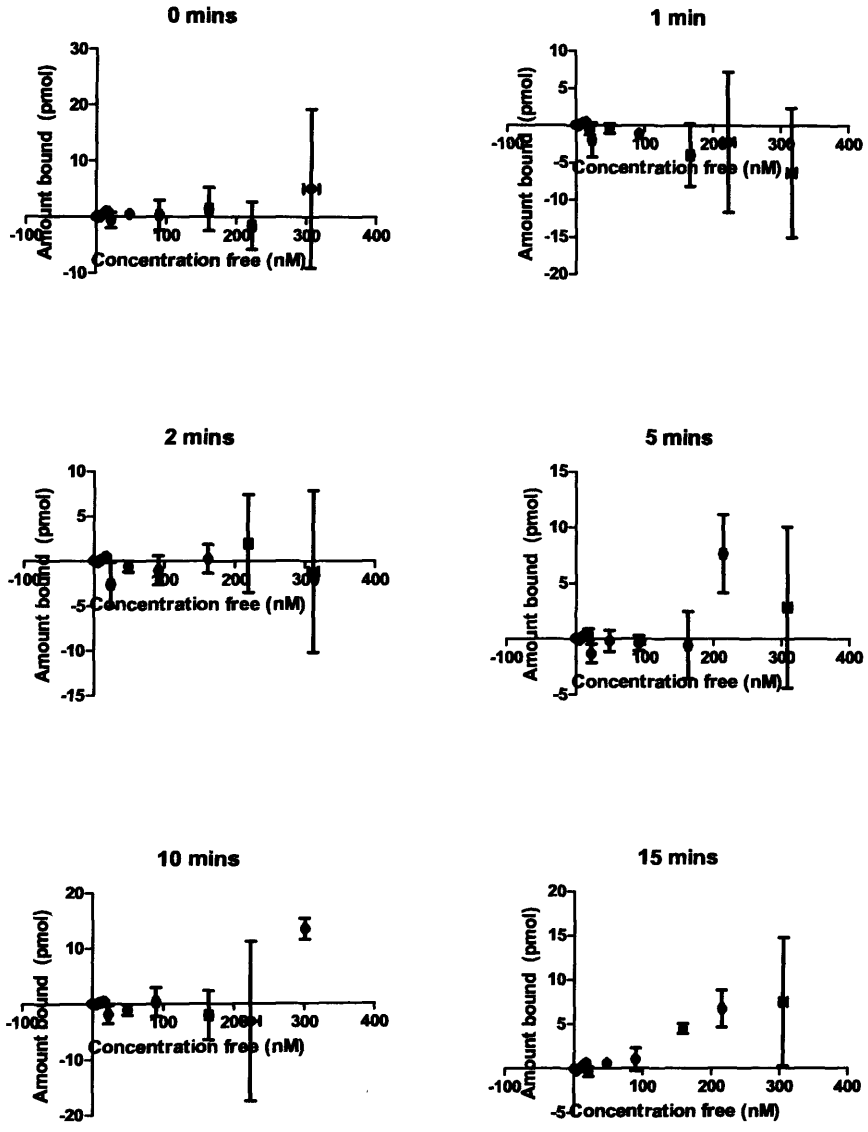

Figure 98: Sulforhodamine-binding assay performed using Molecularly Imprinted Polymer (MIP) *[No peptide]* – Polymerisation times ranging from 0 to 15 minutes.

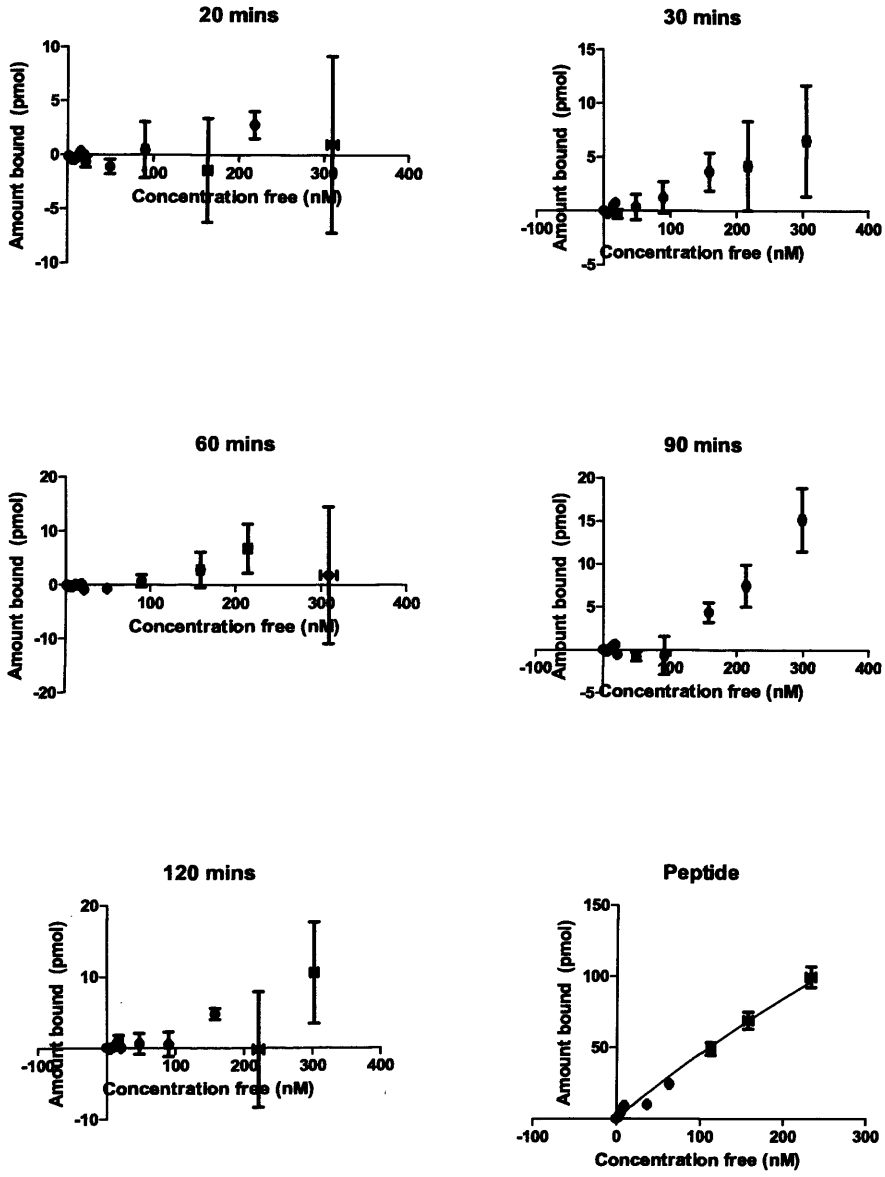

Figure 99: Sulforhodamine-binding assay performed using Molecularly Imprinted Polymer (MIP) *[No peptide]* – Polymerisation times ranging from 20 minutes to 120 minutes. TR401-functionalised resin with no polymerisation is included for reference.

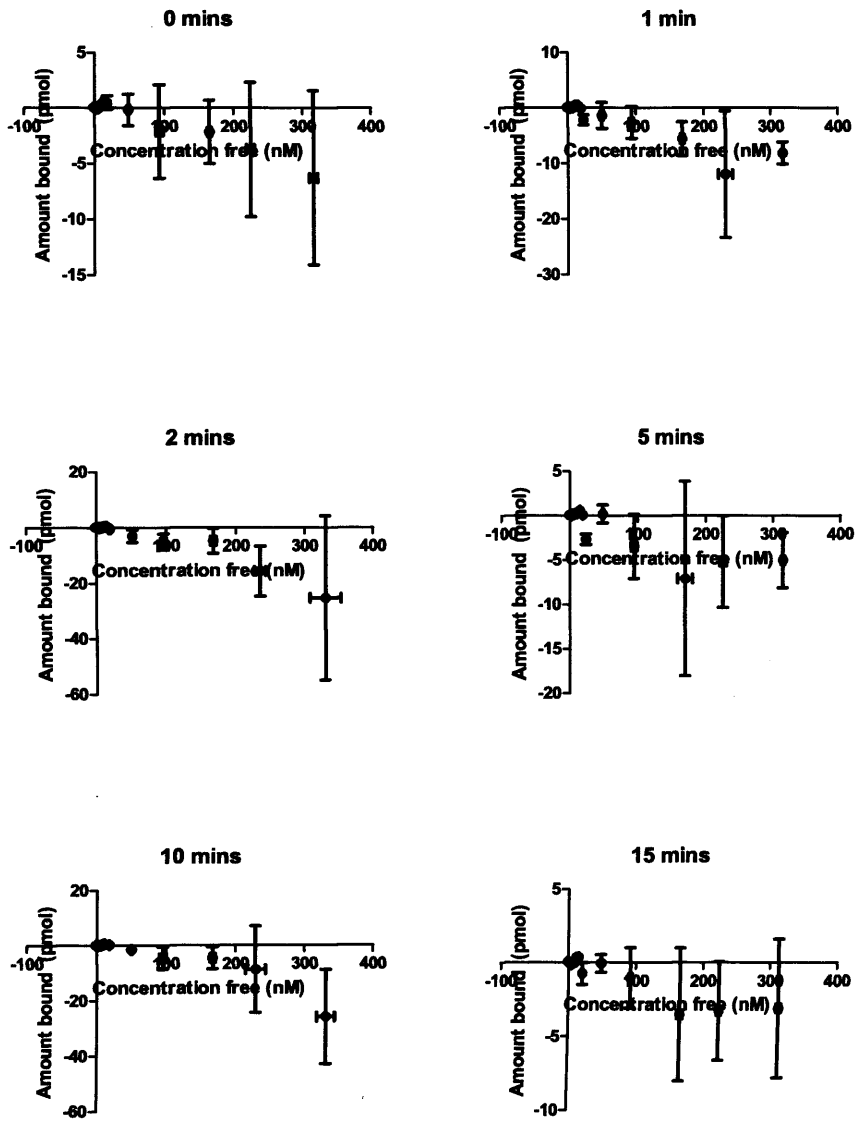

Figure 100: Sulforhodamine-binding assay performed using Non-imprinted Polymer (NIP) *[No peptide, no template]* – Polymerisation times ranging from 0 to 15 minutes.

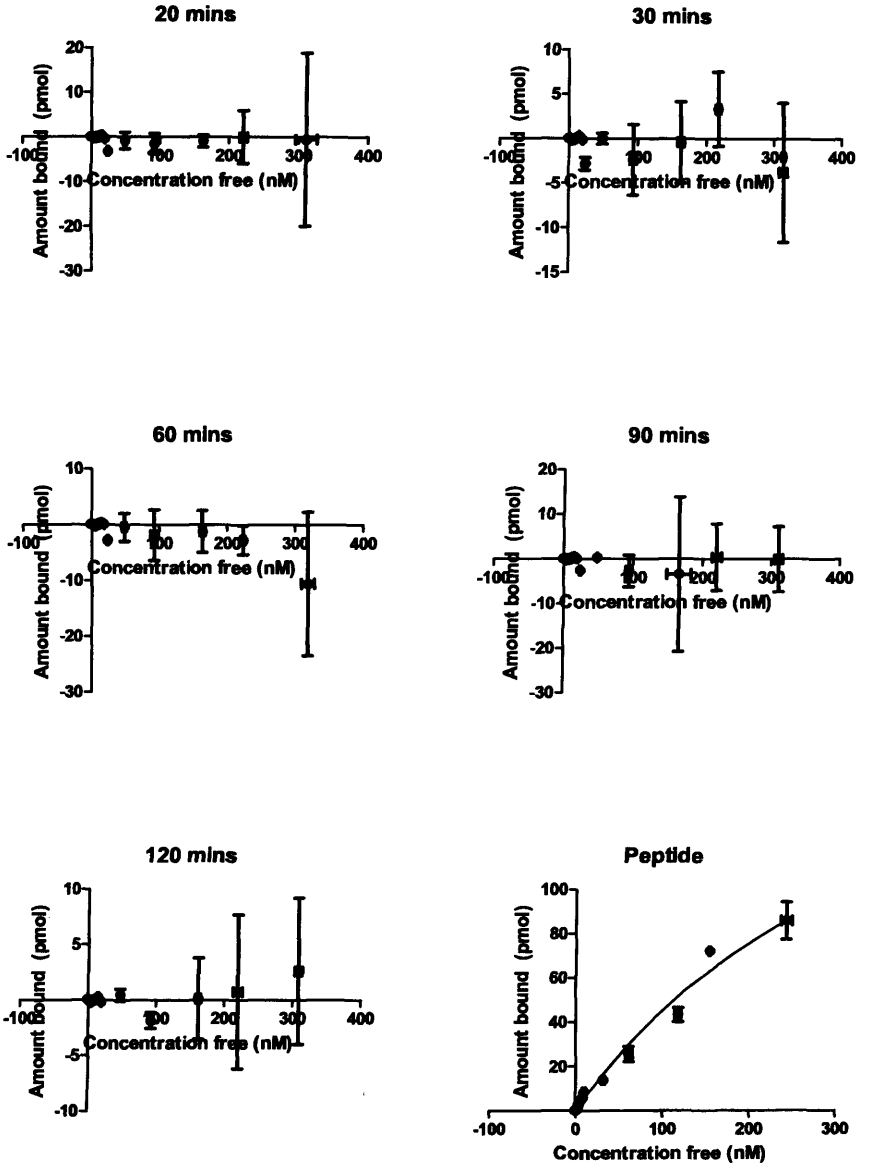

Figure 101: Sulforhodamine-binding assay performed using Non-imprinted Polymer (NIP) [No peptide, no template] – Polymerisation times ranging from 20 minutes to 120 minutes. TR401-functionalised resin with no polymerisation is included for reference.